

# University of Wollongong - Research Online

## Thesis Collection

Title: Numerical modelling of the propagation of ocean waves

Author: Huan-Wen Liu

Year: 2001

Repository DOI:

### Copyright Warning

You may print or download ONE copy of this document for the purpose of your own research or study. The University does not authorise you to copy, communicate or otherwise make available electronically to any other person any copyright material contained on this site.

You are reminded of the following: This work is copyright. Apart from any use permitted under the Copyright Act 1968, no part of this work may be reproduced by any process, nor may any other exclusive right be exercised, without the permission of the author. Copyright owners are entitled to take legal action against persons who infringe their copyright. A reproduction of material that is protected by copyright may be a copyright infringement. A court may impose penalties and award damages in relation to offences and infringements relating to copyright material.

Higher penalties may apply, and higher damages may be awarded, for offences and infringements involving the conversion of material into digital or electronic form.

**Unless otherwise indicated, the views expressed in this thesis are those of the author and do not necessarily represent the views of the University of Wollongong.**

Research Online is the open access repository for the University of Wollongong. For further information contact the UOW Library: [research-pubs@uow.edu.au](mailto:research-pubs@uow.edu.au)

*University of Wollongong Thesis Collections*

*University of Wollongong Thesis Collection*

---

*University of Wollongong*

*Year 2001*

---

# Numerical modelling of the propagation of ocean waves

Huan-Wen Liu  
University of Wollongong

Liu, Huan-Wen, Numerical modelling of the propagation of ocean waves, Doctor of Philosophy thesis, School of Mathematics and Applied Statistics - Faculty of Informatics, University of Wollongong, 2001. <http://ro.uow.edu.au/theses/2053>

This paper is posted at Research Online.

## **NOTE**

This online version of the thesis may have different page formatting and pagination from the paper copy held in the University of Wollongong Library.

## **UNIVERSITY OF WOLLONGONG**

### **COPYRIGHT WARNING**

You may print or download ONE copy of this document for the purpose of your own research or study. The University does not authorise you to copy, communicate or otherwise make available electronically to any other person any copyright material contained on this site. You are reminded of the following:

Copyright owners are entitled to take legal action against persons who infringe their copyright. A reproduction of material that is protected by copyright may be a copyright infringement. A court may impose penalties and award damages in relation to offences and infringements relating to copyright material. Higher penalties may apply, and higher damages may be awarded, for offences and infringements involving the conversion of material into digital or electronic form.

# Numerical Modelling of the Propagation of Ocean Waves

A thesis submitted in partial fulfilment of the requirements  
for the award of the degree

DOCTOR OF PHILOSOPHY

from

UNIVERSITY OF WOLLONGONG

by

Huan-Wen Liu  
BSc, MSc

School of Mathematics and Applied Statistics  
2001

# Declaration

In accordance with the regulations of the University of Wollongong, I hereby state that the work described herein is my own original work, except where due references are made, and has not been submitted for a degree at any other universities or institutions.

Huan-Wen Liu

Date:

# Table of Contents

Table of Contents	iii
Abstract	iv
Acknowledgements	vi
Symbols and abbreviations	vii
<b>1 Introduction</b>	<b>1</b>
<b>2 Basic theory</b>	<b>10</b>
2.1 Wave shoaling, diffraction and refraction . . . . .	10
2.2 Governing equations . . . . .	12
2.3 The mild-slope equation . . . . .	15
2.4 The Boussinesq equations . . . . .	17
<b>3 The dual reciprocity boundary element method</b>	<b>19</b>
3.1 Conventional BEM . . . . .	19
3.2 Domain integral . . . . .	23
3.3 Computing particular solutions . . . . .	24
3.4 The choice of interpolation functions . . . . .	26
3.5 Multiple reciprocity boundary element method . . . . .	27
3.6 Approximation to internal partial derivatives . . . . .	28
<b>4 A linear wave model: GDRBEM</b>	<b>30</b>
4.1 Introduction . . . . .	31
4.2 DRBEM and integral equations . . . . .	32
4.3 Numerical examples . . . . .	36
4.3.1 Homma's island . . . . .	37
4.3.2 Conical islands . . . . .	42

<b>5</b>	<b>A weakly nonlinear wave model: PDRBEM</b>	<b>59</b>
5.1	Governing equations . . . . .	59
5.2	Formation of integral equations . . . . .	67
5.3	Run-ups of nonlinear waves . . . . .	69
5.4	Numerical examples . . . . .	72
5.4.1	Diffraction around a vertical cylinder . . . . .	73
5.4.2	Combined refraction and diffraction on a conical island . . . .	75
<b>6</b>	<b>Conclusions</b>	<b>98</b>
<b>A</b>	<b>Numerical discretization</b>	<b>100</b>
<b>B</b>	<b><math>G(x, y)</math> and its derivatives for nonzero water depth</b>	<b>105</b>
<b>C</b>	<b><math>G(x, y)</math> and its derivatives for zero water depth</b>	<b>110</b>
<b>D</b>	<b>Particular solutions used in DRBEM</b>	<b>112</b>
<b>E</b>	<b>Publications of the author</b>	<b>114</b>
	<b>Bibliography</b>	<b>119</b>

# Abstract

This thesis considers the refraction and diffraction of both linear and nonlinear waves. In the first part, a linear numerical model based on the dual reciprocity boundary element method (DRBEM) is presented for the study of combined diffraction and refraction of linear waves. This model is more general than that presented by Zhu (1993a) in the sense that areas or coastlines where the water depth is zero can be successfully dealt with. Our comparison study shows that the new model is very accurate for the propagation of long waves such as tsunamis. Moreover, it is numerically very efficient in comparison with models based on finite elements or differences. Using the new model, the interaction between the diffractive and refractive effects is examined.

In the second part, a numerical model is developed by expanding the Boussinesq equations using a perturbation method and the DRBEM. Based on the assumption that the incident waves are harmonic, the time-dependent nonlinear Boussinesq equations are transformed into three time-independent linear equations, where no approximation for the seabed slope is made. Then the first-order solution  $\eta_0$  is found as the solution of the linear shallow-water equation. The first-order solution is then used in the governing equations at second-order. By employing a transformation, all the third-order and the fourth-order partial derivatives of  $\eta_0$  in the right-hand sides are



removed, resulting in the minimization of any errors which occur in approximating these derivatives. To validate the new model, the wave run-ups of weakly-nonlinear waves scattered by islands are found. Thirteen cases of run-ups around a vertical cylindrical island are considered and it is found that the nonlinear and dispersive contributions of the new model are significant and a much better comparison with experimental results is obtained than for the linear diffraction theory. The combined wave diffraction and refraction by a conical island is also modelled and discussed. Our model is found to be more accurate than other nonlinear models as the dispersive effects have been included, but is also more computationally efficient since there is no time marching and the spatial dimensionality of the numerical calculation has been reduced by one with the adoption of the DRBEM.

# Acknowledgements

I would like to express sincere gratitude to Associate Professor Song-Ping Zhu and Dr. Timothy R. Marchant, my supervisors, for leading me to the fields of dual reciprocity boundary element method and ocean waves which were totally new to me a few years ago. Without their many valuable suggestions and constant support this thesis would never have come into existence.

Special thanks must go to Dr. Ahmed El-Feki who taught me how to write Fortran codes when I started this research project. I would like to thank Dr. Anna Maria Milan, Dr. Qiyin Wang and Mr. Weiliang Wu who gave me much help in using Latex to prepare the thesis.

My indebtedness must be expressed to the financial support from a Australian Government Overseas Postgraduate Research Scholarship and from a University of Wollongong Postgraduate Award. The support from the Industry and Applied Mathematics Group in the School of Mathematics and Applied Statistics, University of Wollongong is also appreciated.

# Symbols and abbreviations

$\alpha$	coefficient vector
$\alpha_j$	coefficients
$\alpha(\xi)$	internal angle of the boundary at point $\xi$
$\gamma$	Euler's constant $\approx 0.57721$
$\Gamma$	boundary
$\Gamma_i$	coastline of an island
$\Gamma_o$	toe of a conical island
$\Gamma_B$	artificial boundary
$\delta$	Dirac delta function
$\epsilon$	wave nonlinearity, small parameter in the perturbation solution
$\eta$	free surface elevation without time-dependence
$\eta^I$	free surface elevation of incident waves without time-dependence
$\eta_0$	free surface elevation of 1st-order without time-dependence
$\eta_1$	free surface elevation of 2nd-order fundamental frequency without time-dependence
$\eta_2$	free surface elevation of 2nd-order double frequency without time-dependence

$\eta_0^s$	free surface elevation of 1st-order scattered waves without time-dependence
$\eta_1^s$	free surface elevation of 2nd-order scattered waves at fundamental frequency without time-dependence
$\eta_2^s$	free surface elevation of 2nd-order scattered waves at double frequency without time-dependence
$\phi$	velocity potential without time-dependence
$\phi^I$	velocity potential of incident waves without time-dependence
$\phi^s$	velocity potential of scattered waves without time-dependence
$\phi^*$	$= H_0^{(1)}$ , Hankel function of first kind and order zero
$\phi_\beta$	$= (c^2 + \ \mathbf{x} - \mathbf{x}_j\ ^2)^{\beta/2}$ , the family of multiquadrics
$\hat{\phi}_j$	particular solution of inhomogenous Helmholtz equation
$\Phi$	velocity potential with time-dependence
$\theta$	polar coordinate
$\omega$	wave frequency
$\Omega$	two-dimensional domain
$\xi$	source point
$\zeta$	free surface elevation with time-dependence
$\zeta^s$	free surface elevation of scattered waves with time-dependence
$\zeta_{inc}$	free surface elevation of incident waves with time-dependence
$\zeta_{phys}$	physical surface elevation, real part of $\zeta$
$a$	radius of shoreline circle
$A$	amplitude of incident waves

$b$	radius of island toe
$C$	phase velocity of waves
$C_o$	phase velocity of waves in outer region $\Omega_o$
$C_g$	group velocity of waves
$C_{g,o}$	group velocity of waves in outer region $\Omega_o$
$f_j$	radial basis function, interpolation function
$g$	gravitational acceleration
$h$	water depth (varying)
$h_i$	shoreline water depth
$h_o$	constant water depth in outer regin
$H$	wave height
$H_0^{(1)}$	Hankel function of first kind and order zero
$i$	imaginary unit, subscript
$J_n$	Bessel function of the first kind and order $n$
$k$	wave number, $k = 2\pi/L$
$l$	number of collocation points in domain
$L$	wave length
$m$	number of points on $\Gamma_o$
$n$	number of points on $\Gamma_i$
$\mathbf{n}$	outward normal unit vector of the inner domain $\Omega_i$
$\mathbf{n}'$	outward normal unit vector of the inner domain $\Omega_o$

$p$	nonuniform pressure distribution applied to the free surface
$P$	pressure
$q$	directional derivatives of $\eta$ along the direction $\mathbf{n}$
$r, \theta, z$	cylindrical coordinates with origin at the centre of a cylinder
$Re$	real part of a complex quantity
$t$	time
$T$	wave period
$\bar{\mathbf{u}}$	depth-averaged horizontal velocity vector
$\bar{\mathbf{u}}_0$	1st-order depth-averaged horizontal velocity vector
$\bar{\mathbf{u}}_1$	depth-averaged horizontal velocity vector of 2nd-order at fundamental frequency
$\bar{\mathbf{u}}_2$	depth-averaged horizontal velocity vector of 2nd-order at double frequency
$x, y, z$	rectangular coordinates
$\mathbf{x}$	$= (x, y)$
ATPS	augmented thin plate spline
BEM	boundary element method
DRBEM	dual reciprocity boundary element model
GDRBEM	general dual reciprocity boundary elements model
MSL	mean surface level
MSWE	the mild-slope wave equation

PDRBEM	perturbation dual reciprocity boundary elements model
RBF	radial basis function
TPS	thin plate spline

# Chapter 1

## Introduction

Tsunamis are long waves generated by earthquakes, the eruption of volcanoes and any other kind of land movement on the bottom of oceans. While in the deep ocean, these waves have an amplitude of about half a metre, however the amplitude of the tsunami waves increase significantly when an island is approached, due to diffraction, refraction, reflection and shoaling. The recorded amplitude of the tsunamis in Okushiri Island of Japan (Hokkaido Tsunami Survey Group 1993) is 15.25 metres at the front side and about 10 metres at the lee side. Consequently, tsunamis often result in extensive property damages and death. For example, from 1992 to 1994, submarine earthquakes around the Pacific basin generated six large tsunamis: the Nicaragua tsunami on September 2, 1992; the Flores Island tsunami on December 12, 1992; the Hokkaido Island tsunami on July 12, 1993; the East Java tsunami of June 2, 1994; the Kuril Islands tsunami of October 4, 1994; and the Mindoro Island tsunami of November 15, 1994. They all caused extensive property damages and death of at least 1640 people (Liu *et al.* 1995). The most recent tsunami attack took place on August 17, 1998 at Papua New Guinea; more than 2,200 local residents were killed while many houses and roads were completely destroyed (see González 1999).



Because of the undoubted practical importance in understanding the propagation of tsunami waves, their run-ups on coasts, and their impact on coastal facilities, there have been many research and modelling activities in this area. Due to the problem's complexity, the governing equations, which consist of the Euler water wave equations, are simplified or approximated. Linear model equations include the Helmholtz equation, the linear shallow-water equation and the mild-slope wave equation (MSWE) (Berkhoff 1972, 1976 and Smith & Sprinks 1975). In the nonlinear regime, the nonlinear shallow-water equation, the nonlinear MSWE (Beji & Nadaoka 1997), the Airy equation (see Mei 1989), the conventional Boussinesq equations (Peregrine 1967) and various improved Boussinesq equations (Madsen & Sørensen 1992, Witting 1984 and Nwogu 1993) are used.

Despite these simplifications, only a few analytical models have been obtained based on some very simple linear equations. Examples include MacCamy & Fuchs' (1954) solution of the Helmholtz equation for a cylindrical island standing in the middle of an open ocean with constant water depth, Homma's (1950) solution of the linear shallow-water equation for a circular island mounted on a paraboloidal shoal, Zhang & Zhu's (1994b) and Zhu & Zhang's (1995) solution of the shallow-water equation for conical and circular islands. However, all these solution techniques, which exploit the combination of simple boundary geometry and relatively simple form of the governing differential equation, fail when one has to face either non-constant water depth, any nonlinearity, or a nonsymmetric geometry. Numerical solutions must be used to solve any nonlinear equation or the MSWE for a problem with variable water depth and bottom topography in general.

Various numerical models therefore have been developed, which range from the numerical integration (Vastano & Reid 1967 and Lautenbacher 1970), finite difference (Liu *et al.* 1994, 1995), finite elements (Bettess & Zienkiewicz 1977 and Houston 1981), the orthogonal collocation (Jonsson *et al.* 1976), the conventional boundary elements (Au & Brebbia 1983) to the dual reciprocity boundary elements (Zhu 1993a and Poulin 1997). All these models, each focusing on a specific aspect of the problem, contribute to our understanding and modelling capability of this extraordinary phenomenon.

In the linear region, the MSWE, as the starting point of many wave refraction and diffraction models, was independently derived by Berkhoff (1972) and Smith & Sprinks (1975). With the assumption that the bottom slope is mild and thus the mean water depth variation is moderate, they demonstrated how a three-dimensional problem can be well approximated by a two-dimensional one, using the perturbation expansion. This two dimensional equation, which describes the long wave propagation, is later referred to as the mild-slope wave equation (MSWE) by many researchers (see Jonsson & Skovgaard 1979). In Chapter 2 of this thesis, the derivation of the MSWE by Smith & Sprinks (1975) will be briefly presented.

The MSWE has proved a useful model for a wide range of water wave problems, as both refractive and diffractive effects have been included in this single equation. It is also an equation that takes many others as its special cases. For instance, the MSWE not only leads to the eikonal equation (giving the ‘rays’), but also to a ‘transport equation’ (giving the amplitudes), see Jonsson (1979). In deep or constant depth water, it reduces to the Helmholtz equation. And in a shallow water case, it reduces to the linear shallow-water equation. According to Jonsson (1981), the MSWE is

also less restrictive hence more convenient than ray approximation and parabolic approximation.

The limitation of the MSWE is the assumption of the 'mild-slope' which restricts its application to seabed geometry of first order in bottom slope. However, Tsay & Liu (1983) showed that the MSWE can produce accurate results even for bottom slope as large as one in one. Booij (1983) further revealed that Tsay & Liu's (1983) discovery is correct for waves propagating parallel to the contours of a sloping bed, but for waves propagating normal to the contours of a sloping bed, the MSWE produces accurate results provided that the slope is less than one in three.

Various extensions of the MSWE have been made in recent years. For example, Booij (1981) tried to extend the MSWE to include the effect of a current, but his extended MSWE actually contains an error as pointed out by Kirby (1984). Employing the Galerkin-eigenfunction method, Massel (1993) also extended the MSWE for the case where the bottom slope is not necessarily 'mild'. Kirby (1986), responding to the failure of the MSWE to approximate adequately wave scattering by singly and doubly periodic ripple beds, gave an extended MSWE. By keeping all the terms to second order, Chamberlain & Porter (1995) produced a modified MSWE which contains the original MSWE and Kirby's (1986) extended version as special cases. More recently, using some interfacial jump conditions at locations where the bed slope is discontinuous to ensure continuity of mass flow there, Porter & Staziker (1995) obtained an extension of the MSWE, the application of this new version revised Booij's (1983) estimate of the maximum slope gradient from one in three to one in one.

Because of its advantages, the MSWE has become a popular basis for calculating surface waves on slowly varying depth. Several numerical approaches have been

developed to solve the MSWE. For example, following Chen & Mei's (1974) work in solving the Helmholtz equation in a constant depth region, Bettess & Zienkiewicz (1977) and Houston (1981) developed the so-called hybrid method for the MSWE, in which an infinite computational domain is divided into two: an outer region where infinite elements (Bettess & Zienkiewicz 1977) or eigenfunctions (Houston 1981) can be adopted and an inner region where finite element or difference techniques can be used to obtain solutions. Excellent results were reported for problems concerning wave scattering by islands as well as harbour oscillations. Most of the subsequent work differs only on the treatment of the outer domain. Tsay & Liu (1983) also used eigenfunctions in the outer domain to calculate wave forces and moments acting on a floating dock. However, as the MSWE is of the elliptical type, the amount of data and hence the size of the coefficient matrix become very large when finite element and hybrid element methods are used, therefore the computation becomes very expensive as shown by Houston (1981).

The boundary element method (BEM) only requires a discretization on the boundary of a computational domain and it is popular to solve wave propagation problems with constant water depth (see Hwang & Tuck 1970, Au & Brebbia 1983 and Zhu & Moule 1994). However, when the water depth becomes a variable, the conventional BEM seems to be powerless because that a domain integral arises and the domain has to be discretized, which destroys the computational advantage of the conventional BEM.

The most powerful approach to convert domain integral to boundary integral is the so-called dual reciprocity boundary element method (DRBEM) which was first proposed by Nardini & Brebbia (1982) and later improved by many others such as

Partridge & Brebbia (1989) and Zhang & Zhu (1994b). By expanding the right-hand side in the governing equation as a series of interpolation functions, the particular solution of the governing equation is approximated by a series. Then Green's reciprocity theorem can be used twice in the right-hand side and the domain integral is successfully converted into a boundary integral. For the completeness of this thesis, we shall briefly introduce the DRBEM and some related topics in Chapter 3.

Having realized the great potential of the DRBEM, Zhu (1993a) first applied it to wave diffraction and refraction problems. He argued that the DRBEM model showed a great advantage in numerical efficiency over hybrid element models, in terms of both computational time and computer memory required. For example, for the case of Homma's island (Homma 1950) with incident wave of period  $T = 120$  sec, Houston (1981) had to carry out his calculation with 10,560 elements on the half of a symmetrical domain. For a general domain without symmetry to be utilized, he would have to use 21,120 elements which would lead to a linear system with 21,600 real equations. However, using only 60 quadratic boundary elements (with 120 boundary nodes) and 192 internal collocation points for all the calculations covering the full domain, Zhu (1993a) has obtained a very accurate result comparing with the results presented by Jonsson *et al.* (1976) and Houston (1981).

Recently, another DRBEM model for wave diffraction and refraction was proposed by Poulin (1997). Following the idea of Rangogni (1988), varying water depth is approximated with a perturbed constant depth in the MSWE, thus the domain integral which is a result of the varying depth is no longer a function of the unknown wave potential but only a function of position and the constant depth wave potential. She

argued that this leads to significant reduction of the number of unknowns in the resulting system. It is shown that the accuracy of the solution increases with increasing wave period and with decreasing the depth ratio, as is expected for a perturbation method. However, since the equation solved by Poulin (1997) is only an approximate form of the MSWE, the accuracy of the solutions, as shown in the verification of the model for Homma's island, is satisfactory only for seabed geometry with a depth ratio not greater than 3. For Homma's original island with a depth ratio of 9, the accuracy is acceptable only for long waves. Hence, Poulin's (1997) perturbation DRBEM model is not as accurate as Zhu's (1993a) DRBEM model.

Unfortunately, in Zhu's DRBEM model, there is a restriction that the water depth is always nonzero. This assumption narrows the range of application of the DRBEM model in comparison with its hybrid counterparts. In Chapter 4 (see also Zhu *et al.* 2000), as the first objective of this thesis, a general DRBEM model (GDRBEM) is presented, which is an extension of Zhu's DRBEM model to cases where zero-water-depth coastlines are allowed. The generalization involves some special treatment on the limiting values of the product of wave velocity and group velocity. To test our new model, wave refraction and diffraction scattered by both paraboloidal island and conical island are calculated. It is shown that the GDRBEM model is very accurate and computationally efficient.

Although many numerical models have been developed for the problem of wave diffraction and refraction, the range of water waves that can be treated by most of these models is very restricted, being essentially limited to small-amplitude waves, described by linearized shallow-water wave equations, such as the Helmholtz equation, the linear shallow-water equation or the MSWE. Although the results of these models

based on linear governing equations may often provide some good approximation to the wave diffraction and refraction process, in reality, the experimental results suggest that the linearized theories give quite large errors in many practical situations. In fact, tsunamis are dramatically nonlinear in their final run-up stage.

Based on the Boussinesq equations, a time-marching finite-difference method was developed by Abbott *et al.* (1978), and further extended and tested by Abbott *et al.* (1984) and Madsen & Warren (1984). Rygg (1988) proposed a line by line iterative method for nonlinear Boussinesq equations. Based on Nwogu's (1993) improved Boussinesq equations, Wei & Kirby (1995) developed a high-order numerical model where they used a fourth-order predictor-corrector scheme for time stepping and discretized the first-order spatial derivatives to fourth-order accuracy. Recently, based on the nonlinear shallow-water equations, a time-marching finite-difference method was proposed by Liu *et al.* (1994, 1995), who studied the run-ups of both solitary waves and periodic waves around a conical island and compared numerical and experimental results. However, clearly, all these kinds of time-marching finite-difference schemes require significant computational effort.

As the second object of this thesis, in Chapter 5, the linear DRBEM model is further extended to apply to weakly-nonlinear shallow-water waves. A weakly-nonlinear wave model, called the perturbation dual reciprocity boundary element method (PDRBEM) wave model, will be developed to solve the Boussinesq equations for periodical incident waves. By using the perturbation method and the assumption of harmonic waves, the time-dependent nonlinear Boussinesq equations are transformed into three time-independent linear equations, which greatly improves the computational efficiency. Moreover, the three linear equations are sequentially solved

by means of the linear GDRBEM method. In order to validate our new model, thirteen different cases of wave run-ups around a vertical cylinder for are calculated and compared with experimental data, linear diffraction theoretical solutions (MacCamy & Fuchs 1954) and the second order diffraction theoretical solutions (Kriebel 1990, 1992a). It is shown that the nonlinear and dispersive contributions of the new model are very significant and that the new model provides a much better comparison with experimental results than does the linear diffraction theory. And in some cases, the PDRBEM solutions are even better than the second order diffraction theoretical solutions (Kriebel 1990, 1992a). Furthermore, four cases of combined wave diffraction and refraction by a conical island are also tested. The run-ups from the PDRBEM are compared with experimental data, the linear theoretical solutions (Zhang & Zhu, 1994a) and numerical solutions based on the nonlinear shallow-water equation (Liu *et al.* 1994). It is shown the agreement between the PDRBEM solutions and experimental data is satisfactory.



# Chapter 2

## Basic theory

### 2.1 Wave shoaling, diffraction and refraction

As shown in Figure 2.1, water waves are characterized by their height,  $H$ , their length,  $L$  and their period,  $T$ . The wave height  $H$  is the distance between the trough (lowest part) and crest (highest part) of the wave. The wavelength  $L$  is the distance between two consecutive wave crests (or troughs). And the wave period  $T$  is the time for two consecutive crests to pass a point. In addition, phase velocity  $C$  of the waves is defined as the wavelength  $L$  divided by the wave period  $T$  since the waves have to travel one wavelength every wave period.

During the propagation of water waves, three main phenomena, shoaling, refraction and diffraction can occur. Generally, if the ratio of water-depth to wavelength is less than  $1/20$ , then the waves are considered to be in shallow water. In the deep ocean, tsunamis (earthquake-generated waves) are also considered shallow water waves (Bascom 1964) due to their long wavelength. When waves move over shallow water, shoaling occurs. In shoaling there is first a slight decrease in wave height (corresponding to a maximum in group velocity), then the wave height increases and the wave period remains the same when the waves propagate in smaller water depth.

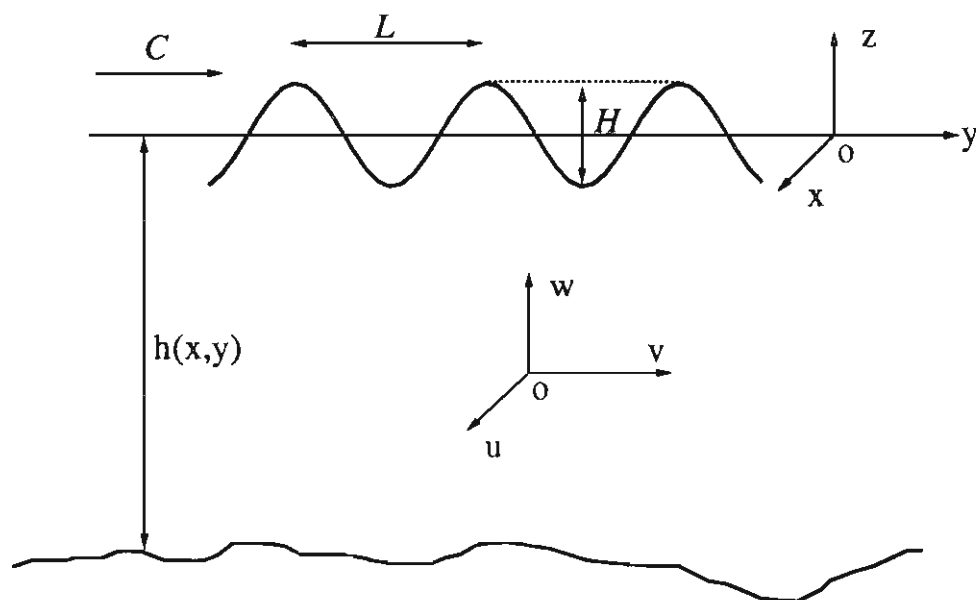


Figure 2.1: Coordinate system and definitions.

Also, the waves begin to feel the bottom of the ocean, which also contributes to the decrease of the wave speed  $C$  and wavelength  $L$ . When the wave crest becomes too steep, it becomes unstable, curling forward and breaking. This usually happens when the height of the wave becomes about the same order as the local water depth. That is, a 10 cm high wave usually breaks in about 10 cm of water.

Wave refraction is the bending of crests of waves because of varying water depths underneath. The part of a wave in shallow water moves slower than the part of a wave in deeper water. So when the depth under a wave crest varies along the crest, the crest bends and wave direction changes. An example of refraction is when waves approach a straight shoreline at an angle. The part of the wave crest closer to shore is in shallower water and moving slower than the part away from the shore in deeper water. The wave crest in deeper water catches up so that the wave crest tends to become parallel to the shore. See Fig. 27 in Bascom (1964). Wave refraction also occurs around a circular island. A wave approaching from one direction will wrap

around the island and the wave crest will approach the beach parallel to all tangents of the boundary of the island. See Fig. 28 in Bascom (1964).

Diffraction usually happens when waves suddenly encounter a steep-sided obstacle such as a breakwater or an island rising abruptly from the depth. It seems that on the lee side of the island, the water would be perfectly calm. However this is not true. As the waves pass the obstacle, some of their energy is propagated sideways as the wave crest extends itself into the so-called 'shadow zone' (Fig. 26, Bascom 1964). The turning of the waves into the sheltered region is due to the changes in wave height (say along the crest) in the same wave. If the sides of the obstacle are sloping under the water, then refraction would also be present.

## 2.2 Governing equations

Consider now the problem where a fixed surface-piercing island of some kind is placed on an uneven ocean bed and periodic surface water waves are propagating with phase velocity  $C$  toward the island, as shown in Figure 2.2-2.3. The instantaneous surface elevation is denoted by  $\zeta(x, y, t)$ , which is measured positive upwards with zero at the mean surface level (MSL). The water depth is denoted by  $h(x, y)$ . For convenience, the coordinate system is chosen so that the incident waves propagate in the positive  $x$ -direction. Then, with the assumption that the fluid is incompressible and flow is irrotational, the governing equation for the wave field  $\Phi(x, y, z, t)$  is the Laplace equation

$$\nabla^2 \Phi + \frac{\partial^2 \Phi}{\partial z^2} = 0, \quad \nabla = \left( \frac{\partial}{\partial x}, \frac{\partial}{\partial y} \right). \quad (2.2.1)$$

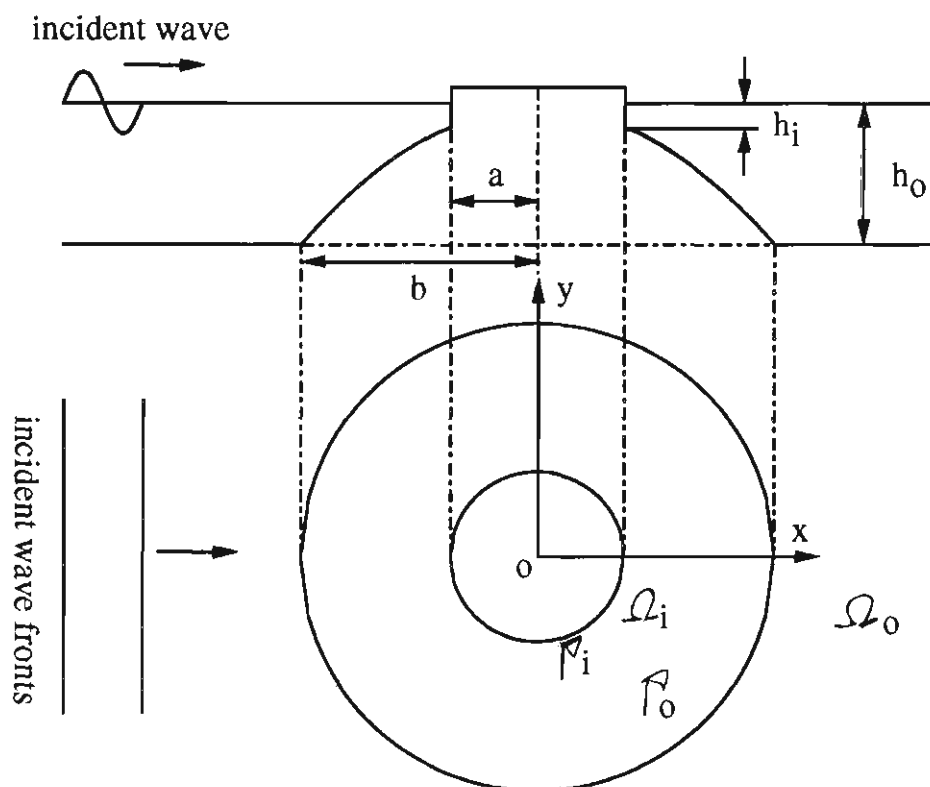


Figure 2.2: Periodical waves scattered by a circular island with a paraboloidal shoal ( $a = 10,000m$ ,  $b = 30,000m$ ,  $h_o = 4,000m$  and  $h_i = 444m$ ).

The Laplace equation is an elliptic-type differential equation and therefore to solve it we need the following conditions on all the boundaries of the domain:

$$\frac{\partial \Phi}{\partial z} + \nabla \Phi \cdot \nabla h = 0, \quad z = -h(x, y), \quad (2.2.2)$$

$$\frac{\partial \zeta}{\partial t} + \nabla \Phi \cdot \nabla \zeta = \frac{\partial \Phi}{\partial z}, \quad z = \zeta(x, y, t), \quad (2.2.3)$$

$$\frac{\partial \Phi}{\partial t} + \frac{1}{2} \left[ |\nabla \Phi|^2 + \left( \frac{\partial \Phi}{\partial z} \right)^2 \right] + g\zeta = 0, \quad z = \zeta(x, y, t), \quad (2.2.4)$$

where  $g$  is the acceleration due to gravity. Other conditions satisfied by  $\Phi$  and  $\zeta$ , such as those to be applied on lateral boundaries or asymptotically if the fluid extends to infinity, do not immediately concern us in this chapter and will be discussed later.

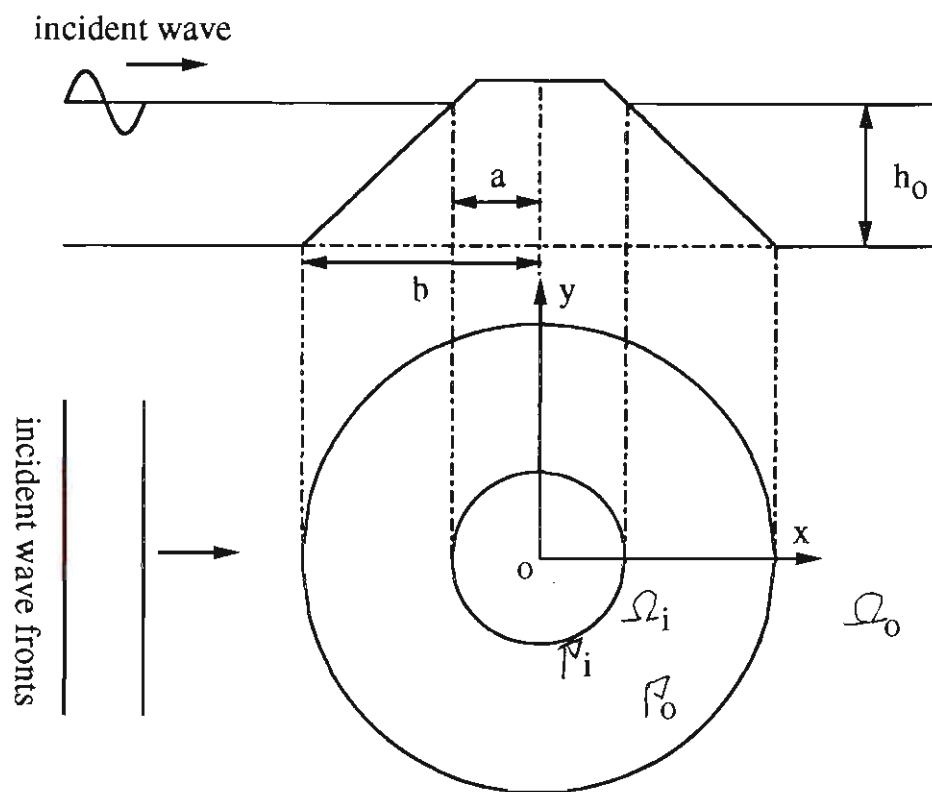


Figure 2.3: Periodical waves scattered by a conical island.

The above system of differential equations has nonlinear free surface boundary conditions, so it is impossible to find an analytical solution. Therefore, numerical solutions are usually resorted to. However, because the Laplace equation (2.2.1) is three-dimensional and elliptic, the computational effort is very high. Therefore many two-dimensional approximation versions have been developed. In linear regime, the most powerful one is the so-called mild-slope wave equation (MSWE), and in nonlinear regime, the most popular one is the Boussinesq equations.

## 2.3 The mild-slope equation

The MSWE, in which refractive and diffractive effects are combined, was originally proposed by Eckart (1952) with a shallow-water restriction. Later, the equation was rederived independently by Svendsen (1967) in one dimension and by Berkhoff (1972, 1976) in two dimensions without restriction on the water depth. But according to Houston (1981), the two-dimensional wave equation derived by Eckart (1952) does not reduce to the linear shallow-water equations derived by Svendsen (1967) and by Berkhoff (1972, 1976). Other derivations are given by Smith and Sprinks (1975) and by Lozano & Meyer (1976). The MSWE was also derived by Booij (1981) using Luke's variational principle. Here we introduce the main steps of the derivation by Smith and Sprinks (1975).

According to Mei (1989), the assumptions that the wave slope  $\epsilon = kA$  is small, i.e.,  $\epsilon \ll 1$  and the separation of the harmonic time dependence  $e^{-i\omega t}$  from  $\zeta(x, y, t)$  and  $\Phi(x, y, z, t)$ , i.e.,

$$\zeta(x, y, t) = \eta(x, y)e^{-i\omega t}, \quad \Phi(x, y, z, t) = \phi(x, y, z)e^{-i\omega t}, \quad (2.3.1)$$

lead the nonlinear equations (2.2.1)-(2.2.4) to be simplified into

$$\frac{\partial^2 \phi}{\partial z^2} + \nabla^2 \phi = 0, \quad -h(x, y) \leq z \leq 0, \quad (2.3.2)$$

$$\frac{\partial \phi}{\partial z} + \nabla \phi \cdot \nabla h = 0, \quad z = -h(x, y), \quad (2.3.3)$$

$$\frac{\partial \phi}{\partial z} - \frac{\omega^2}{g} \phi = 0, \quad z = 0. \quad (2.3.4)$$

The MSWE of Berkhoff (1972, 1976) is a depth-integrated version of the Laplace equation (2.3.2). By assuming that the water depth variation is moderate, i.e.,

$|\nabla h|/(kh) \ll 1$ , the velocity potential may be written as

$$\phi(x, y, z) = \frac{ig\eta(x, y)}{\omega} f(z, h), \quad (2.3.5)$$

where

$$f(z, h) = \frac{\cosh k(z + h)}{\cosh kh}, \quad \omega^2 = gk \tanh kh, \quad (2.3.6)$$

with  $f$  satisfying

$$\frac{\partial^2 f}{\partial z^2} + k^2 f = 0, \quad -h(x, y) \leq z \leq 0, \quad (2.3.7)$$

$$\frac{\partial f}{\partial z} = 0, \quad z = -h(x, y), \quad (2.3.8)$$

$$\frac{\partial f}{\partial z} - \frac{\omega^2}{g} f = 0, \quad z = 0, \quad (2.3.9)$$

and  $k$  and  $h$  referring to their local values.

Employing the formula of integration by parts, i.e.,

$$\int_{-h}^0 \left[ f \left( \frac{\partial^2 \phi}{\partial z^2} - k^2 \phi \right) - \phi \left( \frac{\partial^2 f}{\partial z^2} - k^2 f \right) \right] dz = \left[ f \frac{\partial \phi}{\partial z} - \phi \frac{\partial f}{\partial z} \right]_{-h}^0, \quad (2.3.10)$$

we have

$$\int_{-h}^0 f(k^2 \phi + \nabla^2 \phi) dz = -[f \nabla h \cdot \nabla \phi]|_{-h}. \quad (2.3.11)$$

By calculating  $\nabla \phi$  and  $\nabla^2 \phi$  from (2.3.5) and inserting into (2.3.11), we have

$$\begin{aligned} & \int_{-h}^0 \left[ f^2 \nabla^2 \eta + 2f \frac{\partial f}{\partial h} \nabla \eta \cdot \nabla h + \eta f \frac{\partial^2 f}{\partial h^2} (\nabla h)^2 + \eta f \frac{\partial f}{\partial h} \nabla^2 h + k^2 \eta f^2 \right] dz \\ &= -\nabla h \cdot \nabla \eta f^2|_{-h} - \eta (\nabla h)^2 f \frac{\partial f}{\partial h}|_{-h}. \end{aligned} \quad (2.3.12)$$

Note that  $\nabla h/(kh) \ll 1$ , we can ignore all the terms of order  $(\nabla h)^2$  and  $\nabla^2 h$  and rewrite (2.3.12) as

$$\nabla \cdot \left[ \left( \int_{-h}^0 f^2 dz \right) \nabla \eta \right] + k^2 \left( \int_{-h}^0 f^2 dz \right) \eta = 0. \quad (2.3.13)$$

That is the MSWE

$$\nabla \cdot (CC_g \nabla \eta) + k^2 CC_g \eta = 0, \quad (2.3.14)$$

where

$$C = \sqrt{\frac{g}{k} \tanh kh}, \quad (2.3.15)$$

$$C_g = \frac{C}{2} \left( 1 + \frac{2kh}{\sinh 2kh} \right), \quad (2.3.16)$$

are the phase velocity and the group velocity, respectively.

It is easy to see that  $C = C_g \approx \sqrt{gh}$  and  $\omega^2 \approx k^2 gh$  in shallow water, the MSWE (2.3.14) becomes to the linear shallow-water equation

$$\nabla \cdot (h \nabla \eta) + \frac{\omega^2}{g} \eta = 0. \quad (2.3.17)$$

On the other hand, in constant-depth water or in deep water,  $C \approx \sqrt{g/k}$ ,  $C_g = \frac{1}{2}C$  and  $\omega \approx \sqrt{gk}$ , the MSWE (2.3.14) reduces to the Helmholtz equation

$$\nabla^2 \eta + k^2 \eta = 0. \quad (2.3.18)$$

## 2.4 The Boussinesq equations

Due to strong interactions with bottom topography, waves observed in the nearshore zone are almost always nonlinear and, as it is obvious from the frequent occurrence of whitecapping and breaking, nonlinearity is usually quite high. Realistic modelling of these waves must therefore account for these nonlinear interactions. Among many weakly-nonlinear shallow-water equations, the most powerful one is the Boussinesq equations.

Originally, the Boussinesq equations are derived by Boussinesq (1872) which is valid for a constant water depth. Mei & LeMehaute (1966) extended it to a varying



water depth. Peregrine (1967) derived the equations by using perturbation method. Based on the assumption that the scale of the water depth is small in comparison with the horizontal length scale, the wave amplitude is small compared with the water depth, i.e.,

$$\epsilon = A/h_o \ll 1, \quad \mu^2 = (h_o/L)^2 \ll 1, \quad (2.4.1)$$

and  $\mu^2 = O(\epsilon)$ , the Boussinesq equations of Peregrine (1967) take the following dimensional forms:

$$\begin{cases} \bar{\mathbf{u}}_t + g\nabla\zeta + (\bar{\mathbf{u}} \cdot \nabla)\bar{\mathbf{u}} = \frac{h}{2}\nabla[\nabla \cdot (h\bar{\mathbf{u}}_t)] - \frac{h^2}{6}\nabla(\nabla \cdot \bar{\mathbf{u}}_t), \\ \zeta_t + \nabla \cdot [(h + \zeta)\bar{\mathbf{u}}] = 0. \end{cases} \quad (2.4.2)$$

where  $\zeta(x, y, t)$  is the free-surface elevation and  $\bar{\mathbf{u}}(x, y, t)$  the depth-averaged horizontal velocity vector.

## Chapter 3

# The dual reciprocity boundary element method

The dual reciprocity boundary element method (DRBEM) was first proposed by Nardini & Brebbia (1982) and was further extended by many authors such as Nardini & Brebbia (1986), Partridge & Brebbia (1989) and Zhang & Zhu (1994b). A great advantage in using DRBEM is that the elegance of the traditional BEM, i.e., only boundary integrals need to be carried out, is well preserved. The fundamental mathematical theories of DRBEM have been explained in detail by Partridge *et al.* (1992). Only its main points are therefore outlined here.

### 3.1 Conventional BEM

Consider the general inhomogeneous Helmholtz equation

$$\nabla^2 u + \lambda^2 u = R(x, y, u, u_x, u_y) \quad (x, y) \in \Omega, \quad (3.1.1)$$

where  $\Omega \in \mathbf{R}^d$  is the domain to be considered with boundary  $\Gamma$ . Here we only consider two dimensional case  $d = 2$ .

Let  $\mathbf{x} = (x, y)$ . It is well-known that the fundamental solution of the Helmholtz equation

$$\nabla^2 u + \lambda^2 u = -\delta(\mathbf{x} - \xi) \quad (3.1.2)$$

is the Hankel function of the first kind of zero order:

$$u^*(\xi, \mathbf{x}) = \frac{i}{4} H_0^{(1)}(\lambda \rho)$$

with  $\rho = \|\mathbf{x} - \xi\|$  being the distance between a source point  $\xi$  and a field point  $\mathbf{x}$ .

For any fixed source point  $\xi$ , multiplying both sides of equation (3.1.1) by the weighting function  $u^*(\xi, \mathbf{x})$  and using the Green's second identity, i.e.,

$$\int_{\Omega} (u^* \nabla^2 u - u \nabla^2 u^*) d\Omega = \int_{\Gamma} \left( \frac{\partial u}{\partial \mathbf{n}} u^* - u \frac{\partial u^*}{\partial \mathbf{n}} \right) d\Gamma, \quad (3.1.3)$$

we can rewrite equation (3.1.1) as

$$-\int_{\Omega} u(\mathbf{x}) \delta(\mathbf{x} - \xi) d\Omega + \int_{\Gamma} (qu^* - uq^*) d\Gamma = \int_{\Omega} Ru^* d\Omega, \quad (3.1.4)$$

where  $q(\xi, \mathbf{x}) = \frac{\partial u(\xi, \mathbf{x})}{\partial \mathbf{n}}$  and  $q^*(\xi, \mathbf{x}) = \frac{\partial u^*(\xi, \mathbf{x})}{\partial \mathbf{n}}$  with  $\mathbf{n}$  being outward normal unit vector along the boundary  $\Gamma$  of the domain  $\Omega$ .

For the source point  $\xi$  inside the domain  $\Omega$ , equation (3.1.4) now becomes

$$-u(\xi) + \int_{\Gamma} (qu^* - uq^*) d\Gamma = \int_{\Omega} Ru^* d\Omega. \quad (3.1.5)$$

For the source point  $\xi$  is on the boundary  $\Gamma$  (see Figure 3.1), equation (3.1.4) can be easily modified as

$$\begin{aligned} & -u(\xi) + \lim_{\epsilon \rightarrow 0} \int_{\Gamma - A\xi - \xi B} (qu^* - uq^*) d\Gamma + \lim_{\epsilon \rightarrow 0} \int_{\Gamma_{\epsilon}} (qu^* - uq^*) d\Gamma \\ & = \int_{\Omega} Ru^* d\Omega, \end{aligned} \quad (3.1.6)$$

where, as shown in Figure 3.1,  $\Gamma_\epsilon$  is the circular arc from point  $A$  to  $B$  with the radius  $\rho = \epsilon$  and the centre being located at the source point  $\xi$ . The limit for the first integral in (3.1.6) is

$$\lim_{\epsilon \rightarrow 0} \int_{\Gamma - A\xi - \xi B} (qu^* - uq^*) d\Gamma = \int_{\Gamma} (qu^* - uq^*) d\Gamma. \quad (3.1.7)$$

While the limit for the second integral can be written as

$$\lim_{\epsilon \rightarrow 0} \int_{\Gamma_\epsilon} (qu^* - uq^*) d\Gamma = q(\xi) \lim_{\epsilon \rightarrow 0} \int_{\Gamma_\epsilon} u^* d\Gamma - u(\xi) \lim_{\epsilon \rightarrow 0} \int_{\Gamma_\epsilon} q^* d\Gamma. \quad (3.1.8)$$

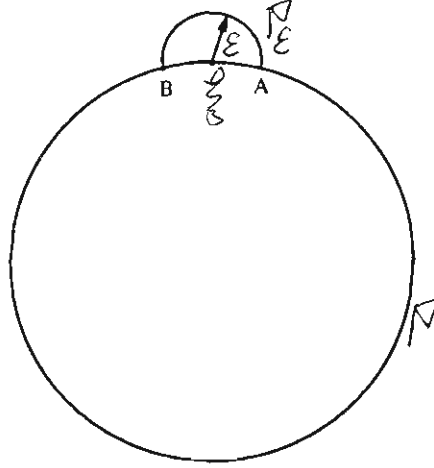


Figure 3.1: The source point  $\xi$  on boundary.

In order to calculate the two limits in the right-hand side in equation (3.1.8), we expand the Hankel function up to the order  $(k\rho)^2$ , which is given by

$$u^*(\xi, \mathbf{x}) \approx -\frac{1}{2\pi} \left[ \gamma + \ln \left( \frac{k\rho}{2} \right) \right] + \frac{i}{4} \quad (3.1.9)$$

where  $\gamma$  is the Euler's constant ( $\gamma = 0.577216\dots$ ) and hence

$$q^*(\xi, \mathbf{x}) = \frac{\partial u^*}{\partial \mathbf{n}} = \frac{\partial u^*}{\partial \rho} = -\frac{1}{2\pi\rho}. \quad (3.1.10)$$

Substituting (3.1.9)-(3.1.10) into (3.1.8) which gives

$$\begin{aligned}
 & \lim_{\epsilon \rightarrow 0} \int_{\Gamma_\epsilon} (qu^* - uq^*) d\Gamma \\
 &= q(\xi) \lim_{\epsilon \rightarrow 0} \int_0^\alpha \left\{ -\frac{1}{2\pi} \left( \gamma + \ln \frac{k\epsilon}{2} \right) + \frac{i}{4} \right\} \epsilon d\theta - u(\xi) \lim_{\epsilon \rightarrow 0} \int_0^\alpha \frac{-1}{2\pi\epsilon} \epsilon d\theta \\
 &= \frac{\alpha}{2\pi} u(\xi),
 \end{aligned} \tag{3.1.11}$$

where  $\alpha = \alpha(\xi)$  is the internal angle of the boundary at point  $\xi$ .

Hence for the point  $\xi$  inside the domain  $\Omega$  or on the boundary  $\Gamma$ , the boundary integral formulation can be uniformly written as

$$-c_\xi u(\xi) + \int_\Gamma (qu^* - uq^*) d\Gamma = \int_\Omega Ru^* d\Omega, \tag{3.1.12}$$

with

$$c_\xi = \begin{cases} \frac{\alpha(\xi)}{2\pi}, & \text{if } \xi \in \Gamma, \\ 1, & \text{if } \xi \in \Omega. \end{cases}$$

Equation (3.1.12) contains domain integral on the right-hand side if  $R \neq 0$ . For some special cases such as a particular solution  $\hat{u}$  to equation (3.1.1) has been found (a particular solution to (3.1.1) is a solution which does not necessarily satisfy the given boundary conditions), the domain integral can be directly transformed into equivalent boundary integrals by using the Green's second identity again. Since for general  $R$  the particular solution  $\hat{u}$  is difficult to find, the calculation of the domain integral becomes unavoidable. To overcome this, Nardini & Brebbia (1982) proposed the powerful DRBEM, which will be briefly described in next section.

## 3.2 Domain integral

The main idea of DRBEM is using a linear combination of a series of particular solutions to approximate the particular solution  $\hat{u}$  to equation (3.1.1). To achieve this, the right-hand side function  $R$  in (3.1.1) is expanded to a series of interpolation functions  $f_j(\mathbf{x})$ , that is,

$$R \approx \sum_{j=1}^{n+l} \alpha_j f_j(\mathbf{x}), \quad (3.2.1)$$

where  $\alpha_j$  are the coefficients to be determined with the collocation method by demanding the satisfaction of  $n + l$  equations

$$R(\mathbf{x})|_{\mathbf{x}_i} = \sum_{j=1}^{n+l} \alpha_j f_j(\mathbf{x}_i), \quad i = 1, \dots, n + l, \quad (3.2.2)$$

at  $n$  collocation points on the boundary  $\Gamma$  and  $l$  interior nodes within the domain  $\Omega$ .

System (3.2.2) can also be expressed in matrix form:

$$\begin{bmatrix} R(\mathbf{x}_1) \\ R(\mathbf{x}_2) \\ \vdots \\ R(\mathbf{x}_N) \end{bmatrix} = \begin{bmatrix} f_{11} & f_{12} & \cdots & f_{1N} \\ f_{21} & f_{22} & \cdots & f_{2N} \\ \vdots & \vdots & \ddots & \vdots \\ f_{N1} & f_{N2} & \cdots & f_{NN} \end{bmatrix} \begin{bmatrix} \alpha_1 \\ \alpha_2 \\ \vdots \\ \alpha_N \end{bmatrix}, \quad (3.2.3)$$

where  $N = n + l$  and

$$f_{ij} = f_j(\mathbf{x}_i), \quad i, j = 1, \dots, N.$$

Simply, we denote the equation (3.2.3) as

$$\mathbf{R} = \mathbf{F}\alpha, \quad (3.2.4)$$

and therefore, if the collocation matrix  $\mathbf{F}$  is invertible,  $\alpha$  can be expressed in terms of  $\mathbf{F}^{-1}$  and  $\mathbf{R}$  as

$$\alpha = \mathbf{F}^{-1}\mathbf{R}. \quad (3.2.5)$$

Assume that a particular solution to every equation

$$\nabla^2 \hat{u}_j + \lambda^2 \hat{u}_j = f_j, \quad (3.2.6)$$

for  $j = 1, \dots, n + l$  can be found. Then by using Green's second identity (3.1.3), the domain integral in the right-hand side of equation (3.1.12) becomes

$$\begin{aligned} \int_{\Omega} R u^* d\Omega &\approx \sum_{j=1}^{n+l} \alpha_j \int_{\Omega} f_j(\mathbf{x}) u^* d\Omega \\ &= \sum_{j=1}^{n+l} \alpha_j \int_{\Omega} [\nabla^2 \hat{u}_j + \lambda^2 \hat{u}_j] u^* d\Omega \\ &= \sum_{j=1}^{n+l} \alpha_j \left[ -c_{\xi} \hat{u}_j(\xi) + \int_{\Gamma} (\hat{q}_j u^* - \hat{u}_j q^*) d\Gamma \right], \end{aligned} \quad (3.2.7)$$

which involves boundary integrals only. Substituting (3.2.7) into (3.1.12) yields

$$c_{\xi} u(\xi) - \int_{\Gamma} (q u^* - u q^*) d\Gamma = \sum_{j=1}^{n+l} \alpha_j \left[ c_{\xi} \hat{u}_j(\xi) - \int_{\Gamma} (\hat{q}_j u^* - \hat{u}_j q^*) d\Gamma \right]. \quad (3.2.8)$$

### 3.3 Computing particular solutions

In DRBEM, in order to reduce the interpolation error to a minimum, it is preferable that the right-hand side  $f$  of a governing equation be kept as simple as possible. At the same time, the simplicity of the main differential operator should be taken into account in order to obtain the corresponding particular solution analytically. As a result, most of the main differential operators used in the DRBEM were restricted in Laplacian operator and particular solutions related to  $f_j$  being radial basis functions (RBFs) such as  $1 + r_j$ , thin plate splines (TPS)  $r_j^2 \log r_j$  or multiquadrics  $\sqrt{r_j^2 + c^2}$  can be obtained by repeated integration (Partridge *et al.* 1992 and Golberg & Chen 1997), where  $r_j = \|\mathbf{x} - \mathbf{x}_j\|$ .

However, if the main differential operator is different from Laplace operator, such as Helmholtz-type operators, this has proven difficult. The first significant result along this line was given by Zhu (1993b) where a constructive scheme of evaluating particular solutions associated with Helmholtz equation was given for  $f_j$  being polynomial RBFs, see Appendix D. Then, analytical formulae of particular solutions associated with Helmholtz-type operators were given by Chen & Rashed (1998) for  $f_j$  being thin plate splines (TPS). Recently, in order to improve the convergence rate of TPS, Muleshkov *et al.* (1999) chose  $f_j$  to be the so-called higher order polyharmonic splines  $r_j^{2k} \log r_j$ ,  $k=1,2,\dots$ , and particular solutions associated with Helmholtz-type operators were obtained.

Golberg (1995) gave an excellent review paper on evaluating particular solutions. According to Golberg (1995), if the governing operator is rotationally symmetric, then it is natural to use RBFs as interpolation functions so that the particular solution can be obtained by solving an ordinary differential equation. If the governing operator is not rotationally symmetric, other approaches need to be taken. For example, if the governing operator is  $a^2 \partial^2 / \partial x^2 + b^2 \partial^2 / \partial y^2$ , then choose a modified RBFs with  $r'_j = \sqrt{(x - x_j)^2 / a^2 + (y - y_j)^2 / b^2}$  as interpolation functions so that a corresponding particular solution may be found.

For a general operator where one can not find the particular solution, one may also look for a numerical approximation to the particular solution. For example, Alessandri & Tralli (1991) proposed a bicubic spline approximation method.



### 3.4 The choice of interpolation functions

There are no limitations to choose interpolation functions  $f_j, j = 1, \dots, n + l$  provided that the collocation matrix  $\mathbf{F}$  is invertible and particular solutions can be found. However the accuracy of the DRBEM strongly depends on the choice of interpolation functions. The main source of error in the DRBEM is the approximation of the right-hand side. Hence, the choice of interpolation functions have always been a hot research topics related to the DRBEM.

Among various interpolation functions, the most popular one is the so-called RBFs which are functions with the form of  $f_j(\mathbf{x}) = f(r_j)$ . Partridge & Brebbia (1989) showed that satisfactory results can usually be obtained if  $f_j(\mathbf{x})$  takes the form  $\sum_{m=0}^s r_j^m$ . Moreover, they also pointed out that the use of  $s = 1$  giving  $f_j = 1 + r_j$  is generally sufficient.

Then Duchon (1977) demonstrated that the so-called augmented thin plate splines (ATPS), which are a combination of the TPS and some augmented linear terms  $1, \mathbf{x}$  in  $\mathbf{R}^2$  ( $1, \mathbf{x}, z$  in  $\mathbf{R}^3$ ), are the optimal interpolation functions in two and three dimensional spaces respectively in the sense that they interpolate  $R$  in  $\mathbf{R}^d$  ( $d=2, 3$ ) with a minimized rotation-invariant seminorm. This theoretical work has been strongly supported by some numerical results (Golberg 1994, Bridges & Wrobel 1996 and Zhu *et al.* 1998). However, despite their optimal properties, ATPS have some drawbacks. For example, they are only  $C^1$  in  $\mathbf{R}^2$  and nondifferentiable in  $\mathbf{R}^3$  and their convergence rate is slow (Powell 1993).

Some researchers such as Golberg *et al.* (1996) suggested that the family of multiquadrics  $\varphi_\beta(r_j) = (c^2 + r_j^2)^{\beta/2}$  can overcome the above drawbacks of ATPS, where  $\beta$  is an odd integer and  $c$  is a shape parameter to be determined by the

collocation method. For Poisson equation, Golberg *et al.* (1996) have shown that considerable improvement can be obtained (up to three orders of magnitude) by using multiquadrics. For time-dependent nonlinear diffusion equation, Zhu & Liu (1998) also show the superiority of the multiquadrics to the linear RBF  $1+r_j$ . However, there are difficult and unresolved problems concerning the choice of the shape parameter  $c$  which can affect the accuracy of the solution by several order of magnitude (Golberg *et al.* 1996) and analytical particular solutions are known only for Laplacian operator.

Very recently, Muleshkov *et al.* (1999) demonstrated that an  $n$ th order polyharmonic splines  $r_j^{2^n} \log r_j$  can achieve  $L_2$  convergence rates of  $O(h^n)$  and the related particular solutions can be analytically obtained. It is shown that numerical solutions using the higher order polyharmonic splines are much more accurate than those using TPS.

### 3.5 Multiple reciprocity boundary element method

In DRBEM, there are  $n + l$  collocation points, including  $n$  boundary points of BEM method and  $l$  internal nodes. To ensure the accuracy of the DRBEM solution, some internal nodes are normally have to be included. Recently a new technique without any internal collocation point, called the Multiple Reciprocity Boundary Element Method (MRBEM), has been developed by Nowak & Brebbia (1989a,1989b) and applied it to solve Poisson equation and Helmholtz equation with the Laplacian form. Then, using this new technique, Neves & Brebbia (1991) solved the Navier equations of elasticity, Nowak & Brebbia (1992) solved the linear potential problems with body forces and Itagaki & Brebbia (1993) extended it to solve the modified Helmholtz

equations. The MRBEM consists of a repeated application of Green's second identity and can be thought of as an extension of the idea of the DRBEM. However, instead of approximating the source term by the set of radial basis functions, a sequence of functions related to the fundamental solution is introduced. These constitute a set of higher order fundamental solutions which permit the Green's second identity to be applied to each term of the sequence. As a result, the MRBEM leads in the limit to the exact boundary only formulation of the domain integrals and therefore no internal collocation node is needed. The related theory has been given in detail by Nowak & Neves (1994).

However the governing equations which will be used in the wave models presented in this thesis are Helmholtz equation (rearranged from the MSWE) and the Boussinesq equations, which could not be solved by adopting the MRBEM thus should not be used in this thesis.

### 3.6 Approximation to internal partial derivatives

The right-hand side in (3.1.1) may contain partial derivatives  $u_x$  and  $u_y$ . This is the case that we will study later in this thesis, see (4.2.1). Sometimes it is difficult to evaluate these partial derivatives at internal nodes due to the presence of domain integrals. In fact, by differentiating (3.1.12) with respect to  $\xi_1$  and  $\xi_2$ , we have

$$\begin{cases} \frac{\partial u}{\partial \xi_1} = \int_{\Gamma} \left( q \frac{\partial u^*}{\partial \xi_1} - u \frac{\partial q^*}{\partial \xi_1} \right) d\Gamma - \int_{\Omega} R \frac{\partial u^*}{\partial \xi_1} d\Omega, \\ \frac{\partial u}{\partial \xi_2} = \int_{\Gamma} \left( q \frac{\partial u^*}{\partial \xi_2} - u \frac{\partial q^*}{\partial \xi_2} \right) d\Gamma - \int_{\Omega} R \frac{\partial u^*}{\partial \xi_2} d\Omega. \end{cases} \quad (3.6.1)$$

However, the use of the DRBEM provides a very simple alternative to (3.6.1).

Assume that  $\mathbf{u} = (u_1, u_2, \dots, u_N)^T$  has an expansion similar to (3.2.4):

$$\mathbf{u} \approx \mathbf{F}\beta. \quad (3.6.2)$$

Differentiating the above produces

$$\mathbf{u}_x \approx \mathbf{F}_x \beta, \quad (3.6.3)$$

where

$$\mathbf{u}_x = \left( \frac{\partial u_1}{\partial x}, \frac{\partial u_2}{\partial x}, \dots, \frac{\partial u_N}{\partial x} \right)^T, \quad (3.6.4)$$

$$\mathbf{F}_x = \begin{bmatrix} \frac{\partial f_1}{\partial x}(\mathbf{x}_1) & \frac{\partial f_2}{\partial x}(\mathbf{x}_1) & \dots & \frac{\partial f_N}{\partial x}(\mathbf{x}_1) \\ \frac{\partial f_1}{\partial x}(\mathbf{x}_2) & \frac{\partial f_2}{\partial x}(\mathbf{x}_2) & \dots & \frac{\partial f_N}{\partial x}(\mathbf{x}_2) \\ \vdots & \vdots & \ddots & \vdots \\ \frac{\partial f_1}{\partial x}(\mathbf{x}_N) & \frac{\partial f_2}{\partial x}(\mathbf{x}_N) & \dots & \frac{\partial f_N}{\partial x}(\mathbf{x}_N) \end{bmatrix}. \quad (3.6.5)$$

Inverting (3.6.2) and substituting into (3.6.3) produces

$$\mathbf{u}_x \approx \mathbf{F}_x \mathbf{F}^{-1} \mathbf{u}. \quad (3.6.6)$$

Thus, the nodal values of the partial derivative are approximated by the nodal values of the problem variable  $u$ . A similar equation can be deduced for the partial derivatives with respect to  $y$ .

Care should be taken to chose the interpolation functions again. Zhang & Zhu (1994b) showed that the choice of linear RBF  $1 + r_j$  results in the creation of singularities on all the collocation points because the diagonal elements of  $\mathbf{F}_x$  and  $\mathbf{F}_y$  are undefined. Further, Zhang & Zhu (1994b) showed that the choices of  $1 + r_j^2 + r_j^3$  and  $1 + r_j^3$  do not creat any singularity for the case where the right-hand side contains the first order partial derivatives. In this thesis, we chose  $1 + r_j^2 + r_j^3$  as the interpolation functions.

## Chapter 4

### A linear wave model: GDRBEM

Based on the DRBEM, Zhu (1993a) first proposed a DRBEM wave model to solve the wave diffraction and refraction problem. It is shown that the DRBEM wave model is as accurate as a finite-element method (Houston 1981) but it is much more efficient than the latter. However, in Zhu's model, there is a so-called vertical-wall assumption along the coastline of the island, which requires that the water depth is always finite along the boundary of the island. Because of this restriction, the wave diffraction and refraction problem related to an island with a zero-water-depth coastline has, so far, not been dealt with by the DRBEM model. In this chapter, a general DRBEM (GDRBEM) model is presented and wave run-ups around islands with zero and nonzero water-depth coastlines are calculated and compared with other numerical solutions.

## 4.1 Introduction

The mean free-surface elevation of a train of monochromatic waves propagating over a seabed of variable water depth  $h(\mathbf{x}) = h(x, y)$  can be expressed as

$$\eta^I(x, y) = Ae^{ik_o r \cos \theta} = A \sum_{n=0}^{\infty} \epsilon_n i^n J_n(k_o r) \cos n\theta, \quad (4.1.1)$$

with  $A$  being the incident wave amplitude,  $\omega$  the angular frequency,  $k_o$  the wave number in constant-depth ( $h_o$ ) water and  $\epsilon_n$  the Jacobi symbol ( $\epsilon_n = 1$  for  $n = 0$  and  $\epsilon_n = 2$  for  $n > 0$ ).

The waves may be diffracted and reflected by an island or a finite number of isolated islands. They may also be refracted because of the change of water depth as they approach these islands. According to the linearized mild-slope theory (Berkhoff 1972, 1976 and Smith & Sprinks, 1975),  $\eta(\mathbf{x})$  should satisfy the MSWE (2.3.8), i.e.,

$$\nabla \cdot (CC_g \nabla \eta) + k^2 CC_g \eta = 0, \quad (4.1.2)$$

together with boundary condition (Tsay & Liu 1983 and Chen & Mei 1974) along the coastline  $\Gamma_i$ :

$$CC_g \frac{\partial \eta}{\partial \mathbf{n}}|_{\Gamma_i} = 0, \quad (4.1.3)$$

and the Sommerfeld radiation condition (Sommerfeld 1949) at infinity

$$\lim_{r \rightarrow \infty} \sqrt{r} \left( \frac{\partial \eta_s}{\partial r} - ik_o \eta_s \right) = 0, \quad r = \sqrt{x^2 + y^2}, \quad (4.1.4)$$

where  $k = k(\mathbf{x})$  is the wave number, which is determined by the implicit dispersion relation

$$\omega^2 = gk \tanh(kh). \quad (4.1.5)$$

## 4.2 DRBEM and integral equations

The differential system (4.1.2)-(4.1.4) is usually defined on an infinite or a semi-infinite computational domain, with incident waves coming along the  $x$ -axis from the infinity. Such a computational domain is usually divided into two subdomains  $\Omega_i$  and  $\Omega_o$  with  $\Omega_i$  denoting a finite inner region with variable water depth and  $\Omega_o$  denoting an infinite outer region in which there is a constant water depth.

The governing differential equations in these regions are of different forms and they will be discussed separately. For simplicity, we only discuss constant boundary elements in this section.

*In the inner region  $\Omega_i$ :* Let  $G = CC_g$ . Since  $G(\mathbf{x})$  is weakly singular with its limit being zero (see Appendix C) as the water depth  $h(\mathbf{x})$  approaches zero along the coastline, Zhu's method (Zhu 1993a) which requires both sides of equation (4.1.2) be divided by  $G(\mathbf{x})$  is no longer valid. Instead, equation (4.1.2) should be rewritten as

$$\nabla^2(G\eta) + k_o^2(G\eta) = R(\mathbf{x}), \quad (4.2.1)$$

where

$$\begin{aligned} R(\mathbf{x}) &= (k_o^2 - k^2)G\eta + \nabla \cdot (\eta \nabla G) \\ &= (k_o^2 - k^2)G\eta + \nabla G \cdot \nabla \eta + \eta \nabla^2 G. \end{aligned} \quad (4.2.2)$$

Let  $\eta^*(\xi, \mathbf{x}) = \frac{i}{4} H_0^{(1)}(k_o \rho)$ . By using the conventional BEM as shown in section 3.1, equation (4.2.1) can be written as

$$c_\xi^{(i)} G(\xi) \eta(\xi) - \int_{\Gamma_o + \Gamma_i} \frac{\partial G}{\partial \mathbf{n}} \eta \eta^* d\Gamma + \int_{\Gamma_o + \Gamma_i} G(\eta q^* - q \eta^*) d\Gamma = - \int_{\Omega_i} R \eta^* d\Omega, \quad (4.2.3)$$

where  $q(\xi, \mathbf{x}) = \frac{\partial \eta(\xi, \mathbf{x})}{\partial \mathbf{n}}$ ,  $q^*(\xi, \mathbf{x}) = \frac{\partial \eta^*(\xi, \mathbf{x})}{\partial \mathbf{n}}$  and

$$c_\xi^{(i)} = \begin{cases} \frac{1}{2}, & \text{if } \xi \in \Gamma_o + \Gamma_i, \\ 1, & \text{if } \xi \in \Omega_i. \end{cases}$$

In the outer region  $\Omega_o$ : Since the water depth is assumed to be constant in this region, it is easy to see that the scattered wave  $\eta_s$  should satisfy the Helmholtz equation

$$\nabla^2 \eta_s + k_o^2 \eta_s = 0. \quad (4.2.4)$$

Using BEM, we can rewrite equation (4.2.4) as

$$-c_\xi^{(o)} \eta_s(\xi) + \int_{\Gamma_o} \left( \frac{\partial \eta_s}{\partial \mathbf{n}'} \eta^* - \eta_s \frac{\partial \eta^*}{\partial \mathbf{n}'} \right) d\Gamma + \int_{\Gamma_\infty} \left( \frac{\partial \eta_s}{\partial \mathbf{n}} \eta^* - \eta_s \frac{\partial \eta^*}{\partial \mathbf{n}} \right) d\Gamma = 0, \quad (4.2.5)$$

where  $\mathbf{n}'$  is the outward normal unit vector of the outer domain  $\Omega_o$  and

$$c_\xi^{(o)} = \begin{cases} \frac{1}{2} & \text{if } \xi \in \Gamma_o, \\ 0 & \text{if } \xi \in \Omega_i + \Gamma_i. \end{cases}$$

By using the Sommerfeld radiation condition at infinity, the last term in equation (4.2.5) becomes

$$\int_{\Gamma_\infty} \left( \frac{\partial \eta_s}{\partial \mathbf{n}} \eta^* - \eta_s \frac{\partial \eta^*}{\partial \mathbf{n}} \right) d\Gamma = \int_{\Gamma_\infty} \left( ik\eta^* - \frac{\partial \eta^*}{\partial \mathbf{n}} \right) \eta_s d\Gamma. \quad (4.2.6)$$

Notice that we can write the fundamental solution when  $r \rightarrow \infty$  as (see Watson 1962)

$$\eta^* \approx \frac{i}{4} \sqrt{\frac{2}{\pi k \rho}} e^{i(k\rho - \frac{\pi}{4})}, \quad (4.2.7)$$

which gives

$$\frac{\partial \eta^*}{\partial \mathbf{n}} = \frac{\partial \eta^*}{\partial \rho} \approx -\frac{k}{4} \sqrt{\frac{2}{\pi k \rho}} e^{i(k\rho - \frac{\pi}{4})}. \quad (4.2.8)$$

So the last term in equation (4.2.5) vanishes.



The continuity of the wave potential and flux across the common boundary  $\Gamma_o$  shared by  $\Omega_o$  and  $\Omega_i$  demands

$$\begin{cases} \eta = \eta_s + \eta^I, \\ q = -(\frac{\partial \eta_s}{\partial \mathbf{n}'} + \frac{\partial \eta^I}{\partial \mathbf{n}'}), \end{cases}$$

be satisfied on  $\Gamma_o$ . Therefore, equation (4.2.5) can be rewritten as

$$\int_{\Gamma_o} (\eta q^* - q \eta^*) d\Gamma = c_\xi^{(o)} \eta(\xi) - c_\xi^{(o)} \eta^I(\xi) + \int_{\Gamma_o} (\eta^I q^* - q^I \eta^*) d\Gamma, \quad (4.2.9)$$

where  $q^I = \frac{\partial \eta^I}{\partial \mathbf{n}}$ .

*Final integral equation:* For simplicity, the two integral equations (4.2.3) and (4.2.9) can now be merged into one

$$\begin{aligned} & c_\xi G(\xi) \eta(\xi) - \int_{\Gamma_o + \Gamma_i} \frac{\partial G}{\partial \mathbf{n}} \eta \eta^* d\Gamma + G_i \int_{\Gamma_i} (\eta q^* - q \eta^*) d\Gamma \\ &= c_\xi^{(o)} G_o \eta^I(\xi) - G_o \int_{\Gamma_o} (\eta^I q^* - q^I \eta^*) d\Gamma - \int_{\Omega_i} R \eta^* d\Omega \end{aligned} \quad (4.2.10)$$

with  $G_o = G(\mathbf{x})|_{\Gamma_o}$ ,  $G_i = G(\mathbf{x})|_{\Gamma_i}$  and

$$c_\xi = \begin{cases} \frac{1}{2} & \text{if } \xi \in \Gamma_i, \\ 1 & \text{if } \xi \in \Gamma_o, \\ 1 & \text{if } \xi \in \Omega_i. \end{cases}$$

Using DRBEM, we have

$$\int_{\Omega_i} R(\mathbf{x}) \eta^* d\Omega \approx \sum_{j=1}^{n+m+l} \alpha_j \left[ -c_\xi^{(i)} \hat{\eta}_j(\xi) + \int_{\Gamma_o + \Gamma_i} (\hat{q}_j \eta^* - \hat{\eta}_j q^*) d\Gamma \right],$$

where  $n$  and  $m$  are the number of the collocation points on the boundary  $\Gamma_i$  and  $\Gamma_o$ , and  $l$  is the number of the collocation points inside the domain  $\Omega$ . Consequently

equation (4.2.10) can be rewritten as

$$\begin{aligned}
& c_\xi G(\xi) \eta(\xi) - \int_{\Gamma_o + \Gamma_i} \frac{\partial G}{\partial \mathbf{n}} \eta \eta^* d\Gamma + G_i \int_{\Gamma_i} (\eta q^* - q \eta^*) d\Gamma \\
&= \sum_{j=1}^{n+m+l} \alpha_j \left[ c_\xi^{(i)} \hat{\eta}_j(\xi) + \int_{\Gamma_o + \Gamma_i} (\hat{\eta}_j q^* - \hat{q}_j \eta^*) d\Gamma \right] - \\
&+ G_o \left[ c_\xi^{(o)} \eta^I(\xi) - \int_{\Gamma_o} (\eta^I q^* - q^I \eta^*) d\Gamma \right]. \tag{4.2.11}
\end{aligned}$$

Equation (4.2.11) involves boundary integrals only and after appropriate discretization, a linear system of algebraic equations involving the unknown function  $\eta(\mathbf{x})$  on  $\Gamma_i + \Gamma_o$  can be established (see Appendix A for details). To solve equation (4.2.11) numerically with the DRBEM, a discretization process involving dividing the boundary curves  $\Gamma_o$  and  $\Gamma_i$  into a number of small elements and replacing the unknown function by an interpolation function, would convert equation (4.2.11) into a system of algebraic equations. Depending of the interpolation functions one adopts to approximate the unknown function within each boundary element, the final form of these algebraic equations will be different. We have adopted both constant elements and quadratic elements in the numerical examples presented in the next section. See Appendix A for details of the final matrix equation with constant elements. In equation (4.2.11), one also needs to calculate  $\partial G / \partial x$ ,  $\partial G / \partial y$ ,  $\partial G / \partial \mathbf{n}$  and  $\nabla^2 G$ . Since  $k(\mathbf{x})$  is implicitly defined through the dispersion relation (4.1.5), the calculation was quite involved and tedious, particularly when the possibility of zero water depth needs to be taken into consideration. Therefore, we have listed the results of these calculations respectively in Appendix B for the case of nonzero water depth and in Appendix C for the zero water depth case.

Once  $\eta(\mathbf{x})$  is solved numerically, the total (complex) instantaneous surface elevation can be found, through the definition:

$$\begin{aligned}\zeta(\mathbf{x}, t) &= \eta(\mathbf{x})e^{-i\omega t} = [a_0(\mathbf{x}) \sin \omega t - b_0(\mathbf{x}) \cos \omega t] \\ &\quad + i[a_0(\mathbf{x}) \cos \omega t + b_0(\mathbf{x}) \sin \omega t].\end{aligned}\tag{4.2.12}$$

where  $a_0(\mathbf{x})$  and  $b_0(\mathbf{x})$  are the real and imaginary parts of  $\eta(\mathbf{x})$  respectively. Hence the physical surface elevation is the real part of this expression, that is

$$\zeta_{phys}(\mathbf{x}, t) = a_0(\mathbf{x}) \sin \omega t - b_0(\mathbf{x}) \cos \omega t,\tag{4.2.13}$$

and the run-up is the maximum of  $\zeta_{phys}(\mathbf{x}, t)$ , this is,  $\sqrt{[a_0(\mathbf{x})]^2 + [b_0(\mathbf{x})]^2}$ .

### 4.3 Numerical examples

As a generalization of Zhu's DRBEM model (Zhu 1993a) for nonzero water depth, the GDRBEM model presented in this thesis includes both nonzero and zero water depth cases. In order to test the new model for these two different cases, in this section we shall present the calculated results of the wave amplification (relative run-up) around coastlines for both Homma's (1950) paraboloidal island with a vertical wall (see Figure 2.3) and three conical islands, Hawaii, Oahu and Small, without a vertical wall (see Figure 2.2). Although Homma's island has been used as a test example by Zhu (1993a) for his DRBEM model, here we will test it again considering that the GDRBEM model is slightly different from Zhu's model in the formulation of the integral equation system. In addition, to investigate the change of wave amplification from nonzero water depth to zero water depth, a new group of conical islands stemming from

Hawaii with various water depths along the coastline is designed and test results are compared with zero-water-depth results of Hawaii.

Figure 4.1 shows the boundary element nodes and internal collocation points used in the present GDRBEM method. We performed our numerical calculation with both constant and quadratic elements and found that for long waves constant elements are sufficient. For very short waves, results obtained with quadratic elements are far better. Thus, we shall only present those results obtained with quadratic elements here in this section. For both types of islands, 60 quadratic elements (with 120 boundary nodes) are always used except in one case with the period  $T = 60$  sec for Homma's island. In addition, 360 internal collocation points are always evenly distributed on six inner circles where their radius are  $r_i = a + c_i(b - a)$  with  $c_i$  being 0.10, 0.25, 0.40, 0.55, 0.65 and 0.80 for  $i = 1, \dots, 6$ .

### 4.3.1 Homma's island

As shown in Figure 2.2, an idealized island of circular cylindrical shape is surrounded by an infinite ocean of constant depth everywhere except on the paraboloidal shoal, at the centre of which the island stands. Plane monochromatic waves are incident, and are diffracted and refracted by the island-shoal structure. Homma (1950) presented an analytical solution of the shallow-water equation for this problem, which has been employed by many authors as a comparison with various numerical solutions. For example, based on the shallow-water equation, there are Vastano and Reid's (1967) finite difference model, Berkhoff's (1972) finite element model coupled with a boundary integral method and Bettess & Zienkiewicz's (1977) hybrid finite element model. On the other hand, based on the MSWE, there are Jonsson *et al.*'s (1976) orthogonal

collocation model, Houston's (1981) finite element model, Tsay & Liu's (1983) hybrid finite element model, Zhu's (1993a) DRBEM model and Poulin's (1997) perturbation DRBEM model.

Shown in Figure 4.2 is a comparison of the wave amplification around the coastline of the island between Homma's (1950) analytical solution and our GDRBEM solution for incident waves with four different periods. As we can see, there is hardly any noticeable difference between Homma's analytical solution and the GDRBEM solution for 1440 sec and 720 sec. This is because when the periods are large, the water depth becomes relatively small in comparison with the wavelength and consequently the MSWE can be well approximated by the shallow-water equation, which is what Homma's solution is based on. As the period decreases, the difference between the two solutions gradually increases. For 410 sec. incident waves, the difference between two solutions has reached about 4%. For period  $T = 240$  sec, Figure 4.3 shows the comparison among Homma's (1950) solution, Jonsson *et al.*'s (1976) orthogonal-collocation solution, Tsay & Liu's (1983) hybrid-element solution and the present GDRBEM solution. The comparison shows that the agreement among the GDRBEM results, Jonsson *et al.*'s (1976) results and Tsay & Liu's (1983) results is very good. However, all these three numerical solutions exhibit considerable differences with Homma's (1950) solution. That is because Homma's (1950) solution is based on the shallow-water equation and others are based on the MSWE.

Generally speaking, cases with periods of incident waves being less than 160 sec. are regarded as very severe tests for any numerical model since they are short waves with high frequency. For incident wave with period  $T = 120$  sec, the ratio of wavelength to water depth is approximately 11. In order to achieve necessary accuracy,

Houston (1981) not only had to carry out his calculation with 10,560 fine finite elements on a CRAY-1 super computer, but also had to make use of the symmetry property of this rather particular geometry and distributed those elements only on half of the domain. For a general domain without symmetry to be utilized, he would have to use 21,120 finite elements which would lead to a linear system with 21,600 real equations. In this thesis, we merely used 60 quadratic boundary elements (with 120 boundary nodes) and 360 internal collocation points for all the calculations covering the full domain. The total number of real equations is only 960. But as we can see in Figure 4.4, our GDRBEM solution agrees excellently with Jonsson *et al.*'s (1976) solution. This excellent agreement among Jonsson *et al.*'s (1976) orthogonal collocation, Houston's (1981) hybrid element and our GDRBEM shows the present GDRBEM method is not only highly accurate but also very efficient. On the other hand, we can see again that Homma's (1950) solution, which is based on the shallow-water equation without frequency dispersion, becomes increasingly inaccurate for this short wave case. This reflects, as suggested by Jonsson *et al.* (1976), that the long-wave solution should not be used for incident waves of period less than 300 sec.

Recently, Homma's island was also calculated by using the DRBEM by Poulin (1997). Following Rangogni's (1988) original idea, Poulin (1997) solved the MSWE with the following perturbation form

$$\nabla^2 \phi_o + k_o^2 \phi_o = 0, \quad (4.3.1)$$

$$\nabla^2 \phi + k_o^2 \phi = 2k_o^2 \phi_o \left( \frac{C}{C_o} - 1 \right) - \nabla \phi_o \cdot \left( \frac{\nabla C_g}{C_{g,o}} + \frac{\nabla C}{C_o} \right), \quad (4.3.2)$$

where wave potential  $\phi_o$ , phase velocity  $C_o$  and group velocity  $C_{g,o}$  are corresponding to the constant water depth  $h_o$  and  $\phi$  is corresponding to the real water depth  $h$ .

Equation (4.3.2) is similar to the equation solved by Zhu (1993a), i.e.,

$$\nabla^2 \phi + k_o^2 \phi = (k_o^2 - k^2) \phi - \nabla \phi \cdot \left( \frac{\nabla C_g}{C_g} + \frac{\nabla C}{C} \right), \quad (4.3.3)$$

but with a different right-hand side which is known after the equation (4.3.1) is solved for constant water depth. Poulin thoroughly verified the perturbation method with various geometries in Homma's island. As a product of the depth approximation made in the perturbation method, the accuracy of the results strongly depends on both depth ratio  $h_i/h_o$  and wave period  $T$ . It is shown that the accuracy of the perturbation method is overall satisfactory only for depth ratio not greater than 3 (see Figure 9.1-9.18, Poulin 1997). For Homma's original island with depth ratio being 9, which is the case tested here and in Zhu's (1993a) model, the accuracy of the perturbation solutions is acceptable only for relatively long waves with  $T = 1440$  sec and  $T = 720$  sec. Comparatively, the accuracy of Zhu's DRBEM model and the present generalization version is excellent for all the wave periods.

Furthermore, although there is no other known solution to compare with, the wave amplifications around the coastline of the island for two very short incident waves with their periods only being 90 sec and 60 sec were also calculated using the present GDRBEM method. Considering the higher frequency of the incident wave with  $T = 60$  sec, we doubled the number of quadratic elements on the boundary while keeping the number of internal collocation nodes unchanged. Wave amplification factors for these two periods are graphed in Figure 4.5. This shows that the wave amplification factor, where the wave train is directly incident on the island ( $\theta = 180^\circ$ ), varies dramatically for  $T = 90$  sec and 60 sec, between 3.5 and 0.97, respectively. We note that for  $T=120$ , a perfect comparison is obtained with Houston's (1981) solution and Jonsson *et al.*'s (1976) solution and the amplification factor is 2, the theoretical

short wave limit. This implies that the results for  $T = 90$  sec and 60 sec are inaccurate, as our model is only valid for long waves.

As one can see in Figure 4.5, when the wavelength of the incident waves is very short, say for the case of  $T = 60$  sec, the calculated results show that wave amplification factor never exceeds 2. Near the front side, the amplification is even less than 1. On one hand, it is well-known that the wave amplification should be theoretically approaching 2 in the front side for pure reflection when the period  $T$  reached the limit 0. If this theoretical limit result is really true even for the case  $T = 60$  sec, it means that the case of  $T = 60$  sec is out of the validity of our model as the waves are too short to be modelled by our GDRBEM and too much error might have been produced. However, on the other hand, we can still argue that the period of 60 sec is still far from the limit 0 and the corresponding wave amplification may not have to achieve the amplification limit of pure reflection so early. Considering that this case have not been calculated by any other wave model and there is no known result to compare with, we leave it open and at this stage we assume that our numerical result is correct. Then it shows that when short waves being diffracted by an island whose diameter is of the same order as the wavelength, the diffraction becomes very much a “localized” effect; short waves are not amplified as much as long incident waves. Furthermore, we should notice that the maximum amplification now has shifted from the front side of the island (the side that faces the incident waves) to the half way between the front and lee side of the island. This information is useful in predicting the location of the “worse hit” of a tsunami wave on an island.



4.3.2 Conical islands

Conical islands were first studied by Lautenbacher (1970). In his paper, three individual Hawaiian islands (Hawaii, Oahu and Small) were assumed to be conical (see Figure 2.3) and are separately attacked by three different monochromatic, plane incident waves. The geometrical parameters of the three islands and the parameters of incident waves are tabulated in Table 4.1. Lautenbacher transformed the linear long-wave equation into an integral equation and then solved it numerically. Smith & Sprinks (1975) also used the same example to demonstrate the MSWE but only presented the results for the shallow-water equation. Using a hybrid finite element method, Tsay & Liu (1983) solved the MSWE for conical islands but only presented two numerical solutions for Hawaii. Recently, an analytical solution of the shallow-water equation for axisymmetrical conical island was worked out by Zhang & Zhu (1994a).

Table 4.1 Parameters for Hawaiian islands and incident waves.

Islands	$b(m)$	$b : a$	$h_o(m)$	$L : b$			$L : h_o$			$T(min)$		
Hawaii	115781	1.67	5487	2	4	8	42.2	84.4	169	17	34	69
Oahu	92625	4.00	4573	2	4	8	40.5	81.0	162	14	28	57
Small	46313	4.65	5487	1.57	6.7	15.7	13.3	56.6	133	5	22	50

In this thesis, using the present GDRBEM method, both the MSWE and the shallow-water equation are solved for three Hawaiian islands and various incident waves. In Figure 4.6-4.8, wave amplification distributions along coastlines of three islands are plotted. In Figure 4.6, an excellent agreement among our two numerical solutions and Zhang & Zhu’s (1994a) analytical solution is obtained for all three

incident waves with their wavelengths being  $2b$ ,  $4b$  and  $8b$ , respectively. In Figure 4.7-4.8, excellent agreement among our two numerical solutions and Zhang & Zhu's (1994a) analytical solution is obtained for longer wave length cases, i.e.,  $L = 4b$  and  $L = 8b$  for Oahu and  $L = 6.7b$  and  $L = 15.7b$  for Small.

As pointed out by Jonsson *et al.* (1976), the usually accepted shallow-water limit in terms of wavelength to water-depth ratio is 20. In the case of Small, this gives a limiting period of 410 sec or about 7 min. In the case of  $L = 1.57b$  for Small, the ratio of the wavelength to the water depth is 13.3 (see Table 4.1) and the period is 5 min; the incident wave is very short already. Therefore significant discrepancy between the solution with frequency dispersion and that without frequency dispersion shown in Figure 4.8 can be well explained. In the case of Oahu, the ratio of the wavelength to the water depth when  $L = 2b$  is about 40.5, which is larger than 20, and this explains why the circles fall right on the solid line in Figure 4.7.

On the other hand, some differences between the dotted line and circles, i.e., between Zhang & Zhu's (1994a) analytical solution and the present GDRBEM solution without frequency dispersion, can be noticed in the cases of  $L = 2b$  for Oahu (see Figure 4.7) and  $L = 1.57b$  for Small (see Figure 4.8). Such differences can not be explained by the ratio of the wavelength to water depth. We then investigated the convergence of the numerical solutions in terms of the number of internal nodes as well as the number of boundary elements. Shown in Figure 4.9-4.10 are convergence test results for the Oahu Island. For quadratic elements, when the number of elements is increased from 60 to 90, some improvement is indeed observed as shown in Figure 4.9. However, when we further increased the number of boundary elements and/or the number of internal nodes to 120 and 540 respectively, accuracy started to worsen

off again as shown by the dash-dotted line in Figure 4.9, this is probably because the accumulation of round-off errors start to increase dramatically when the number of internal collocation points and boundary elements increases to a level that the accuracy of the machine is reached or the collocation matrix  $F$  in (3.2.4) is singular or ill-conditioned. A similar behaviour has been observed for constant elements as well as shown in Figure 4.10. Therefore, we had to conclude that the numerical solutions did converge for the case of the Oahu Island. For the Small Island, our convergence test results lead to the same conclusion.

Then the only plausible explanation of this discrepancy may be made when we notice the fact that one of the integral equations in equation (4.2.11) becomes a Fredholm integral equation of the first kind when the water depth becomes zero uniformly on the coastlines for the cases presented in Figure 4.6-4.8. As pointed out by Golberg (1978) and Power & Wrobel (1995) (also see Poulin 1997), in contrast to the integral equation of the second kind, the troublesome feature of dealing with integral equation of the first kind is that the problem is ill-posed, which means that there is a lower bound for the size of boundary discretization. However, with the same first-kind integral equation for the case of Hawaii, the problem doesn't seem to appear at all. Therefore, the intrinsic reason for such discrepancies in the cases of Oahu and Small deserves a further investigation, which is currently undertaken and the results will be reported upon its completion.

It is quite interesting to notice that for the case of Small, the solution from the MSWE with the frequency dispersion exhibits the wave amplitude in the lee of the island exceeding that in the front of the island. Although this rather unusual phenomenon has been already observed by Jonsson *et al.* (1976) and by Houston (1981)

for nonzero water depth, it has never been mentioned before for zero-water-depth case.

Finally, to investigate the change of the wave amplification from nonzero-depth water to zero-depth water around coastlines, we designed a new island stemming from Hawaii with a circular cylindrical shape situated on a conical shoal as shown in Figure 4.11. Clearly, when  $h_i = h_o$ , this new island is actually a circular cylinder, which is the case to which MacCamy & Fuchs' (1954) analytical solution is applicable. On the other hand, when  $h_i = 0$ , this is the case with zero water depth on the coastline and Zhang & Zhu's (1994a) analytical solution becomes applicable if we keep the water depth shallow enough. The relative run-ups are calculated using the present GDRBEM method for the water depth  $h_i$  along the coastline being 0,  $0.01h_o$ ,  $0.02h_o$ ,  $0.05h_o$ ,  $0.1h_o$ ,  $0.2h_o$ ,  $0.3h_o$ ,  $0.5h_o$  and  $h_o$ . The solutions for  $L = 2b$  in all these cases are presented in Figure 4.12 together with Zhang & Zhu's (1994a) analytical solution based on the shallow-water equation for the case of  $h_i = 0$  and MacCamy & Fuchs' (1954) analytical solution based on the Helmholtz equation for the case of  $h_i = h_o$ . It can be seen that all the numerical solutions with different  $h_i$  values are nicely bounded between the two analytical solutions with the numerical solution agreeing perfectly with that of MacCamy and Fuchs' analytical solution at one end and agreeing well again with that of Zhang and Zhu's analytical solution at the other. Most significantly, what is exhibited in Figure 4.12 is the interaction between the diffraction and refraction effects. When the total water depth as well as the incident wavelength are held constant, the diffraction effects are significantly enhanced as the slope of the shoal is increased. As one can clearly see from Figure 4.12, when there is no shoal ( $h_i = h_o$ ), there is no refraction and the maximum wave amplification is

only about 2. The maximum wave amplification increases as the bottom slope does, because of the 'convergence of rays' at the island front. As  $h_i$  decreases from  $h_o$  to zero, i.e., as the slope of the bottom shoal increases, not only does the maximum wave amplification increase, but also the variation of wave amplification along the coastline is significantly enhanced. Finally when  $h_i = 0$ , the maximum wave amplification reaches more than 5; the wave amplitude at the front side of an island will suffer the worst effects of a tsunami wave. Results shown in Figure 4.12 have also verified that our model correctly takes the zero-water solution as the limit of the nonzero water depth solution.

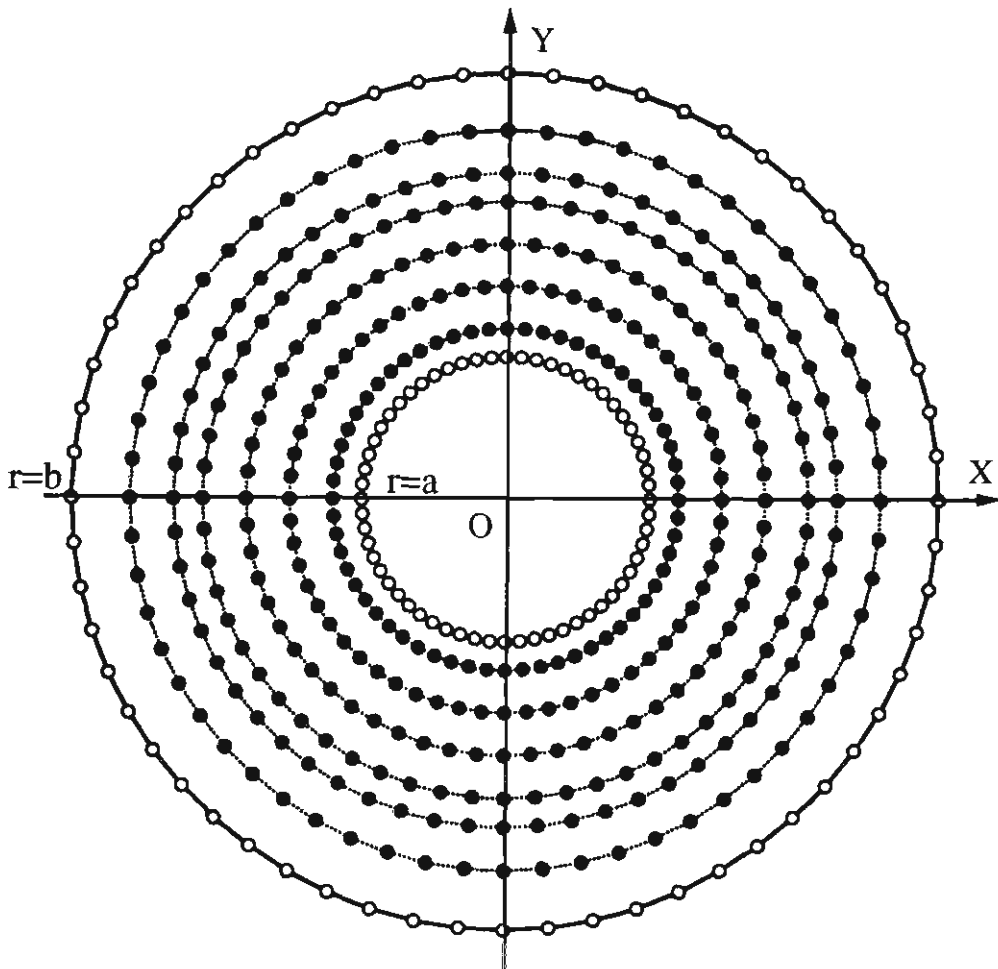


Figure 4.1: Nodes of quadratic boundary elements and internal collocation points used in the GDRBEM.

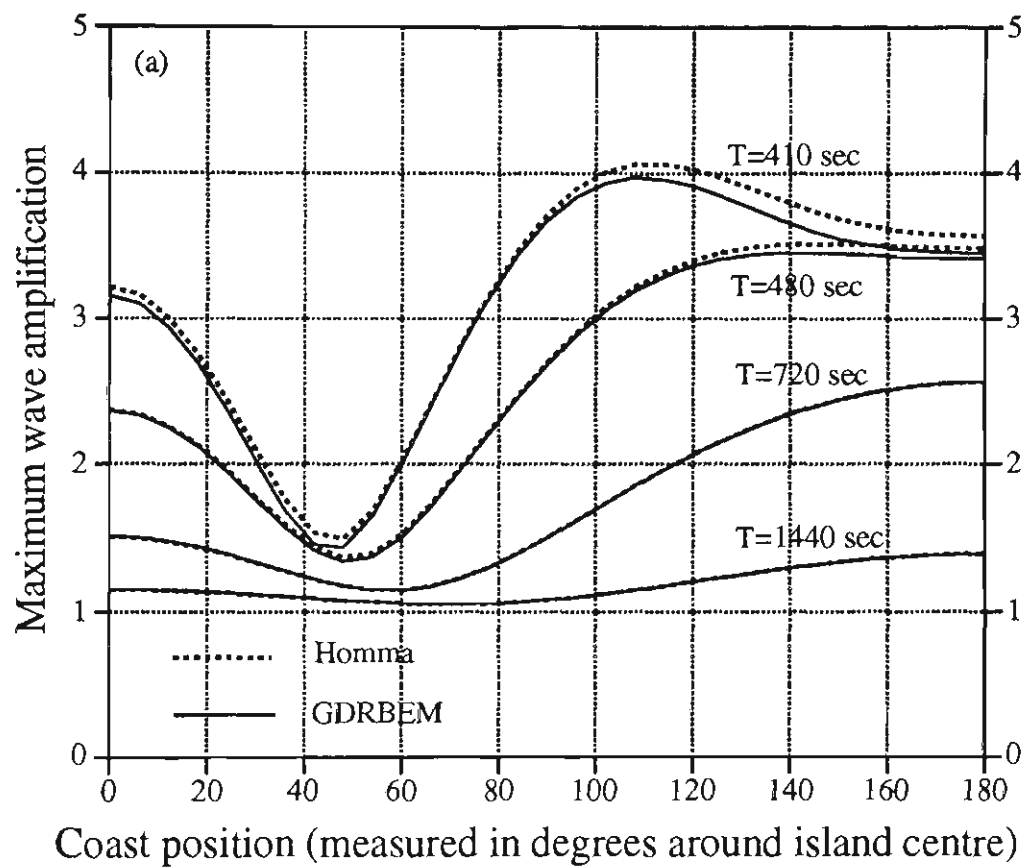


Figure 4.2: Comparison between Homma's solution and the GDRBEM solution for four periods:  $T = 1440$  sec,  $720$  sec,  $480$  sec and  $410$  sec.

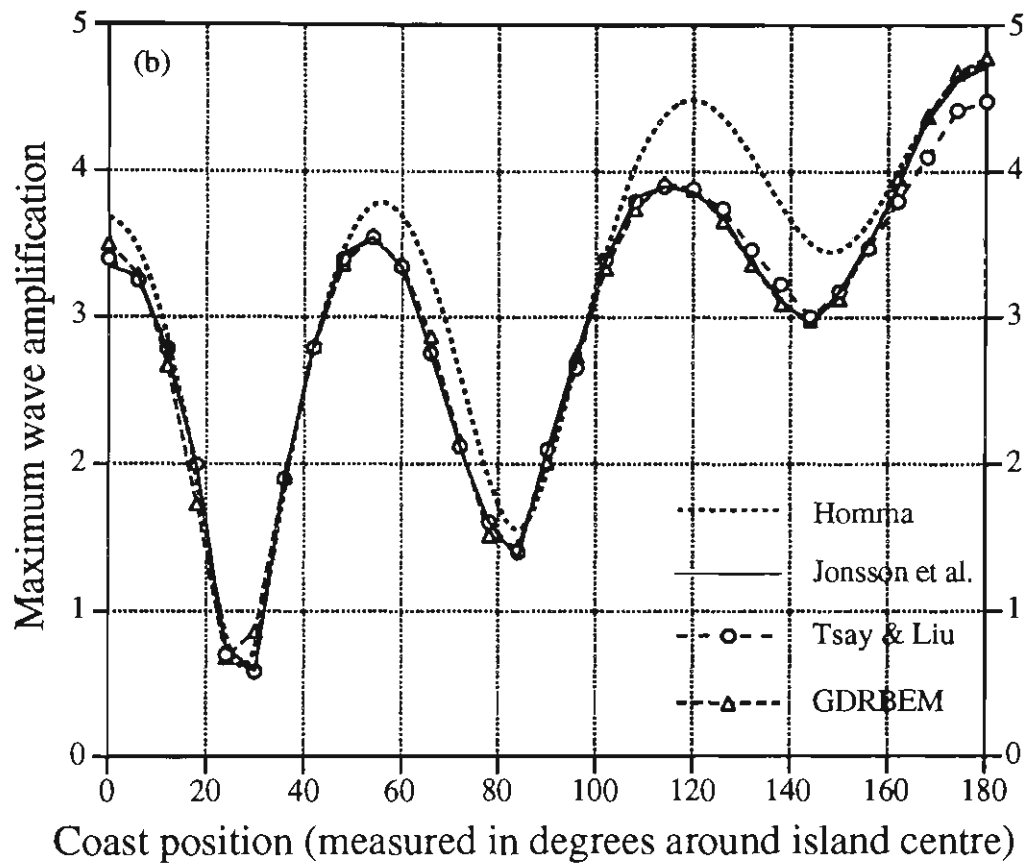


Figure 4.3: Comparison among various solutions for the period  $T = 240$  sec.



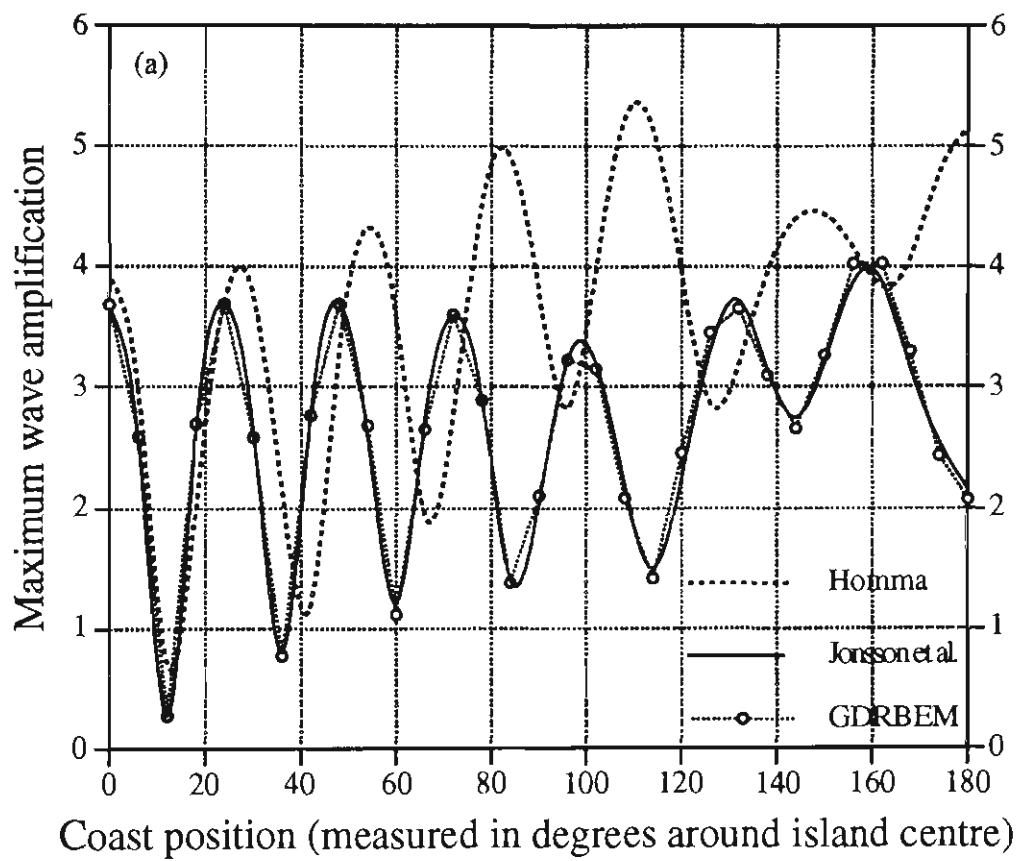


Figure 4.4: Comparison among various solutions for the period  $T = 120$  sec.

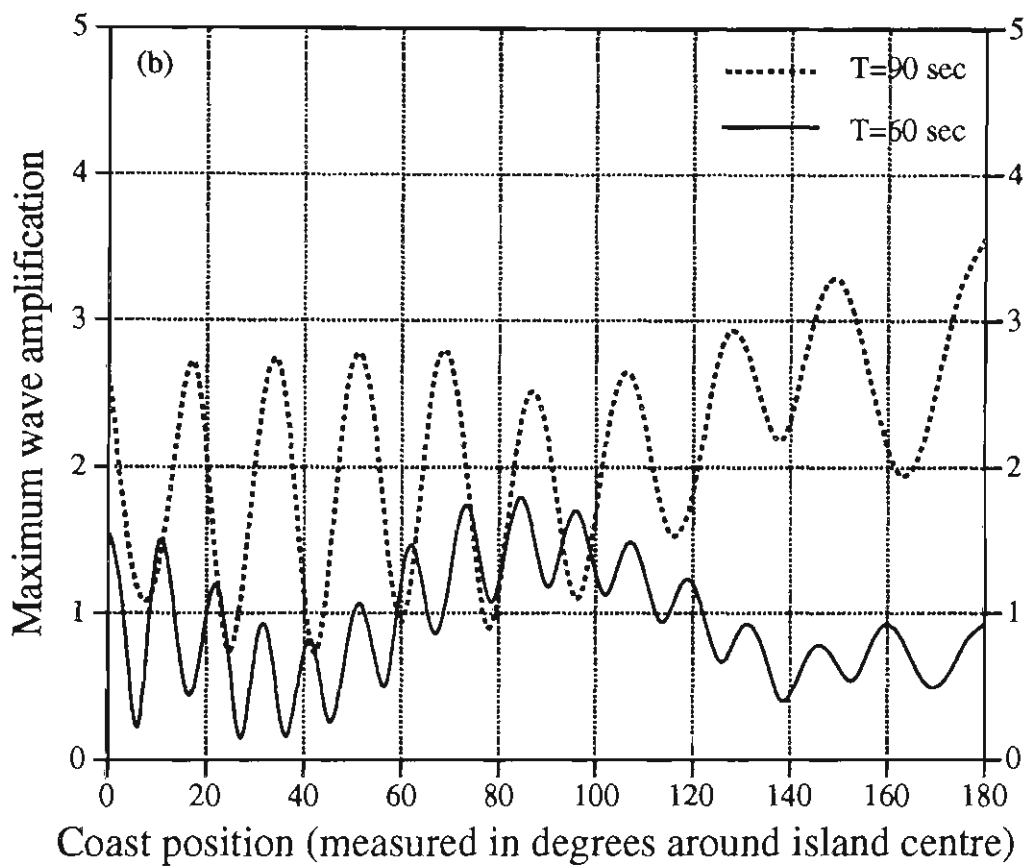


Figure 4.5: Two GDRBEM solutions (interpolation curves) for very short waves.

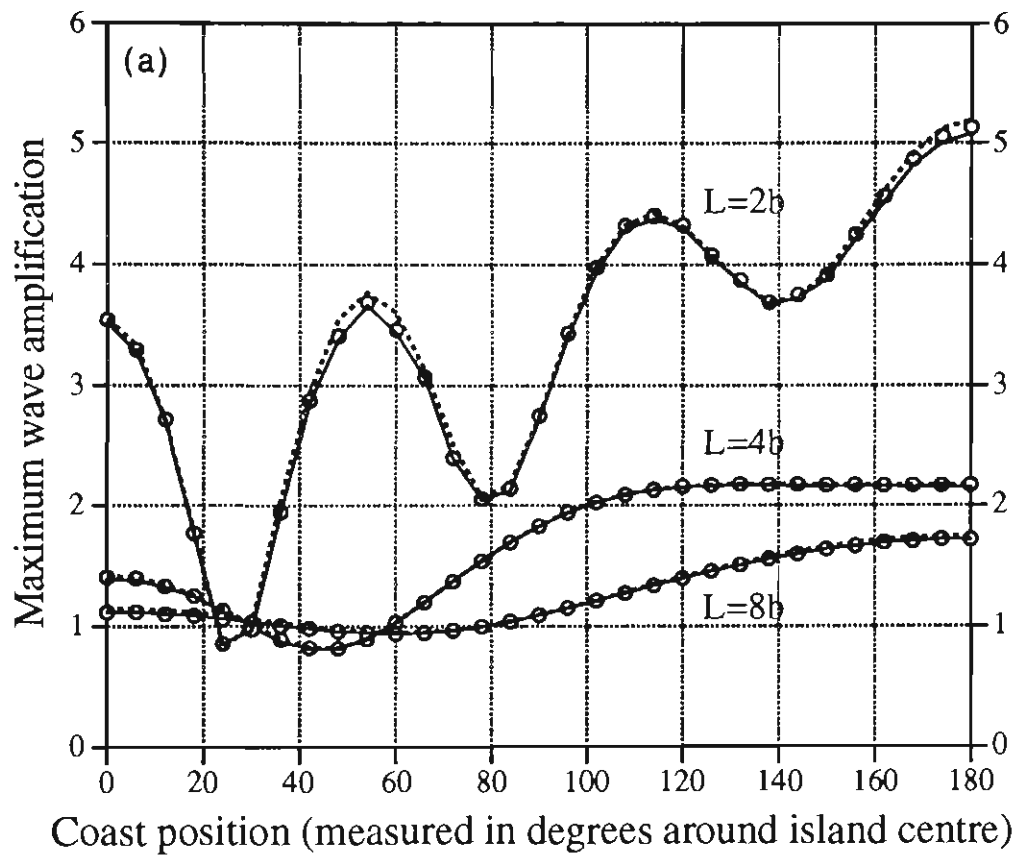


Figure 4.6: Comparison among Zhang & Zhu's (1994a) analytical solution (dotted line), the GDRBEM solution based on the MSWE (solid line) and the GDRBEM solution based on the shallow-water equation (circles): Hawaii ( $b/a=1.67$ ).

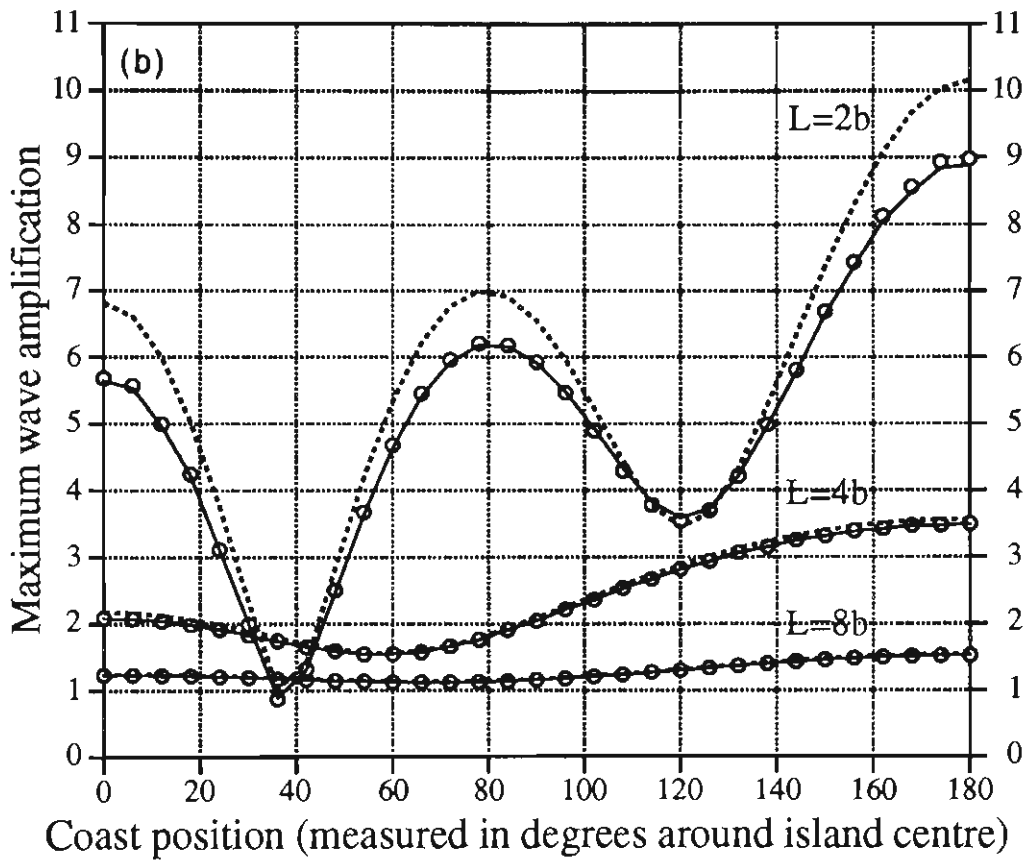


Figure 4.7: Comparison among Zhang & Zhu's (1994a) analytical solution (dotted line), the GDRBEM solution based on the MSWE (solid line) and the GDRBEM solution based on the shallow-water equation (circles): Oahu ( $b/a=4$ ).

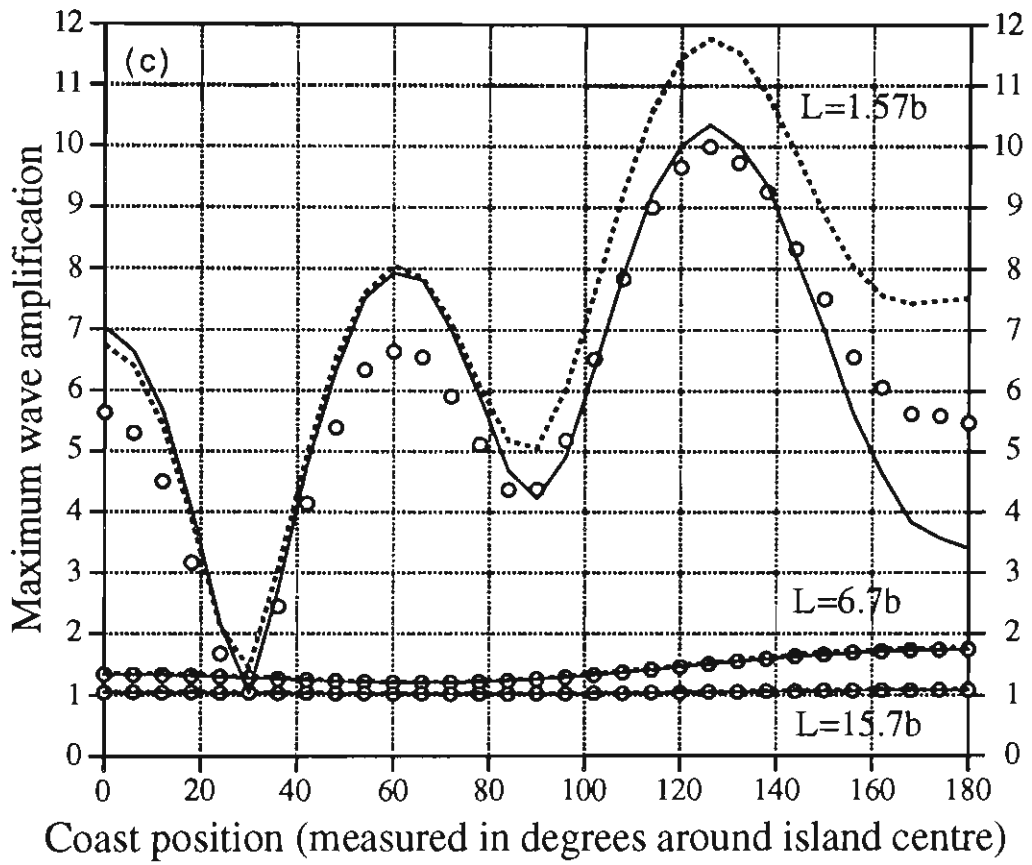


Figure 4.8: Comparison among Zhang & Zhu's (1994a) analytical solution (dotted line), the GDRBEM solution based on the MSWE (solid line) and the GDRBEM solution based on the shallow-water equation (circles): Small ( $b/a=4.65$ ).

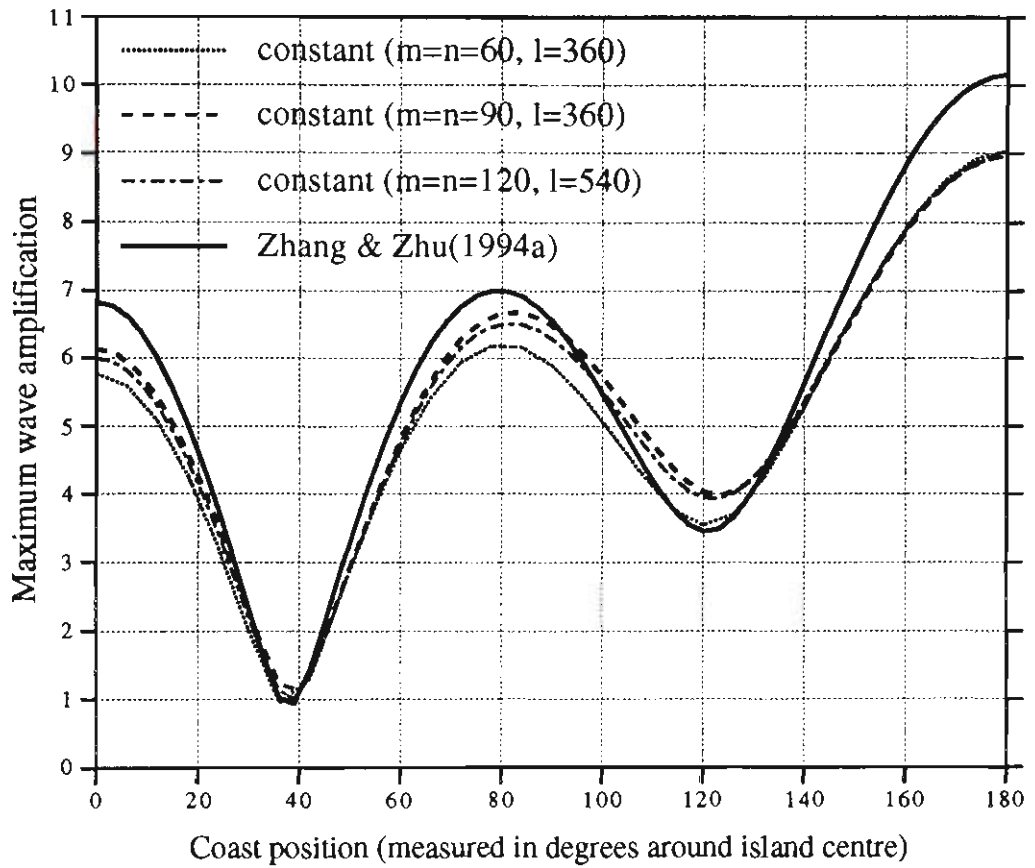


Figure 4.9: Comparison among Zhang & Zhu's (1994a) analytical solution and various GDRBEM solutions based on the shallow-water equation in the case of  $L = 2b$  for the island Oahu: constant elements;

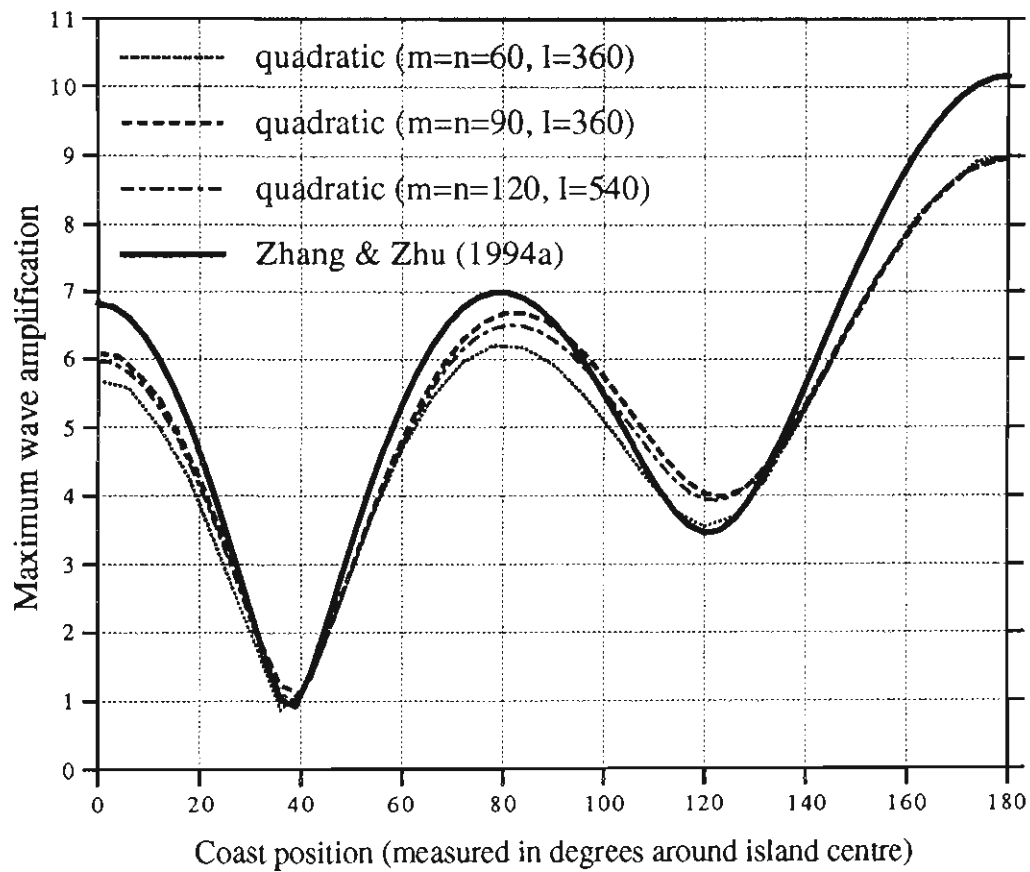


Figure 4.10: Comparison among Zhang & Zhu’s (1994a) analytical solution and various GDRBEM solutions based on the shallow-water equation in the case of  $L = 2b$  for the island Oahu: quadratic elements.

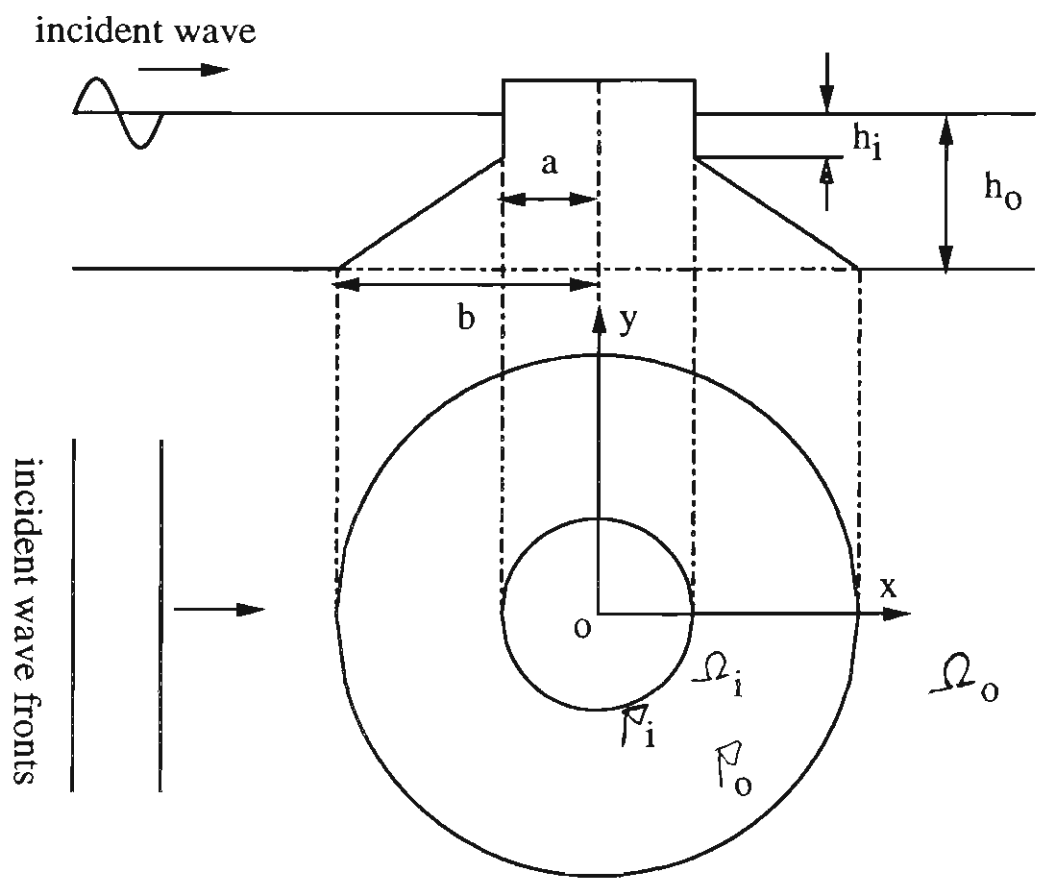


Figure 4.11: This is the Hawaii island with a cylindrical top.



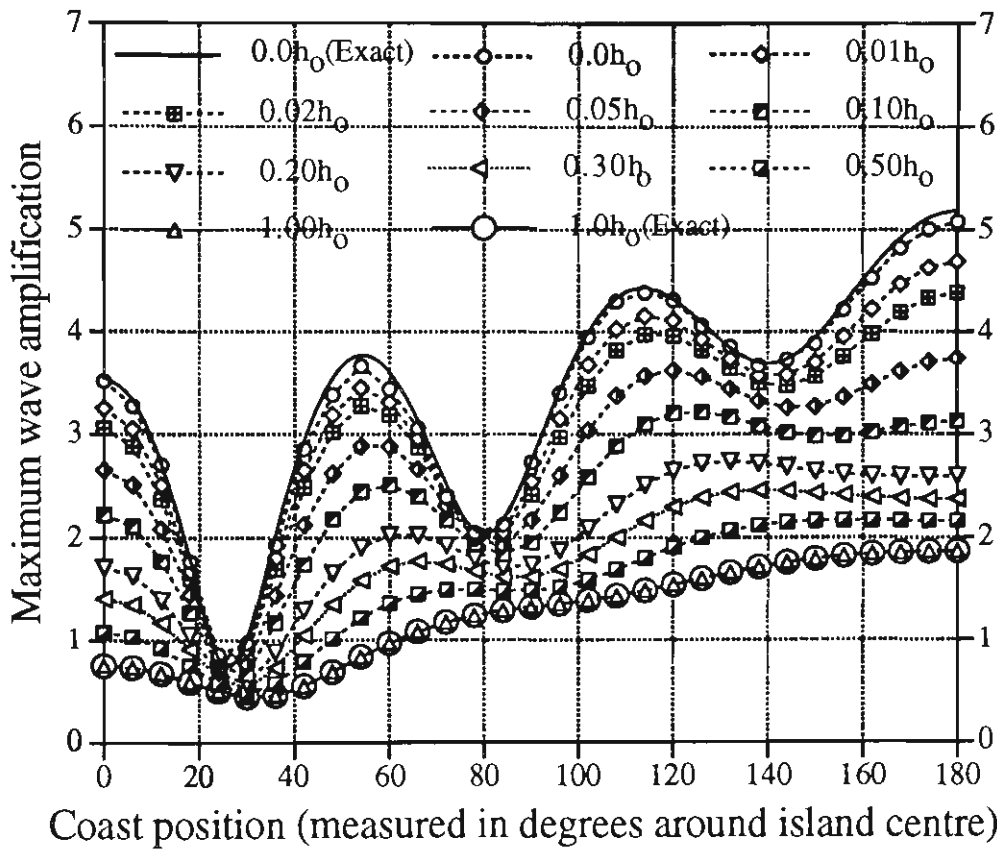


Figure 4.12: Comparison among zero-water solutions and various nonzero-water solutions, including two analytical solutions from Zhang & Zhu (1994a) and from MacCamy & Fuchs (1954) for two limiting cases.

# Chapter 5

## A weakly nonlinear wave model: PDRBEM

In this chapter, the linear GDRBEM wave model is extended to a weakly-nonlinear wave model, called perturbation dual reciprocity boundary element model (PDRBEM). By using the perturbation method, the time-dependent nonlinear Boussinesq equations are transformed into three time-independent linear equations in section 5.1, where no approximation for the seabed slope  $\nabla h$  is used. The three linear equations are then solved sequentially by means of the linear GDRBEM described in section 5.2. In section 5.3, we show that the formula for calculating the run-ups of weakly-nonlinear waves is different from that for linear waves. In order to verify our weakly-nonlinear PDRBEM model, thirteen cases of wave run-ups around a vertical cylinder are tested in section 5.4 and four cases of wave run-ups around a conical island are tested in section 5.5.

### 5.1 Governing equations

As illustrated in Figure 2.2-2.3, we consider the weakly nonlinear refraction and diffraction of a plane monochromatic incident wave by an island standing on a seabed

of otherwise constant water depth,  $h_o$ . Cartesian coordinates with the  $(x, y)$ -plane in the quiescent free surface and  $z$  positive upward are chosen. Since the monochromatic incident waves in the deep ocean can be generally regarded as linear waves, the corresponding potential can be expressed as

$$\begin{aligned}\zeta_{inc}(x, y, t) &= \eta^I(x, y)e^{-i\omega t} = Ae^{i[k_o r \cos(\theta - \theta^I) - \omega t]}, \\ &= A \sum_{n=0}^{\infty} \epsilon_n J_n(k_o r) \cos n(\theta - \theta^I) e^{-i\omega t},\end{aligned}\quad (5.1.1)$$

with  $A$  being the incident wave amplitude,  $\omega$  the angular frequency,  $k_o$  the wave number in constant-depth ( $h_o$ ) water,  $\theta^I$  the angle of incidence with respect to the  $x$  axis, and  $\epsilon_n$  the Jacobi symbol ( $\epsilon_n = 1$  for  $n=0$  and  $\epsilon_n = 2$  for  $n \neq 0$ ). The waves may be diffracted and reflected by the island and may also be refracted because of the change of water depth as they approach the island.

Let  $\zeta(x, y, t)$  be the water surface elevation and  $\bar{\mathbf{u}}(x, y, t) = (u, v)$  the depth-averaged horizontal velocity vector. The following dimensionless quantities

$$\begin{aligned}(x', y') &= \frac{1}{L}(x, y), \quad \zeta' = \frac{\zeta}{A}, \quad t' = \frac{\sqrt{gh_o}}{L}t, \\ h' &= \frac{h}{h_o}, \quad u' = \frac{h_o}{A\sqrt{gh_o}}u, \quad v' = \frac{h_o}{A\sqrt{gh_o}}v, \quad \omega' = \frac{L}{\sqrt{gh_o}}\omega,\end{aligned}\quad (5.1.2)$$

are introduced with  $L$  being the wave length. For convenience the primes will be dropped from here now. If the scale of the water depth is small in comparison with the horizontal length scale and the wave amplitude is small compared with the water depth, i.e.

$$\mu^2 = (h_o/L)^2 \ll 1, \quad \epsilon = A/h_o \ll 1, \quad (5.1.3)$$

$\bar{\mathbf{u}}$  and  $\zeta$  may satisfy the so-called Boussinesq equations in dimensionless variables

(Peregrine 1967)

$$\begin{cases} \bar{\mathbf{u}}_t + \nabla \zeta = -\epsilon(\bar{\mathbf{u}} \cdot \nabla)\bar{\mathbf{u}} + \mu^2 \frac{h}{2} \nabla[\nabla \cdot (h\bar{\mathbf{u}}_t)] - \mu^2 \frac{h^2}{6} \nabla(\nabla \cdot \bar{\mathbf{u}}_t), \\ \zeta_t + \nabla \cdot (h\bar{\mathbf{u}}) = -\epsilon \nabla \cdot (\zeta \bar{\mathbf{u}}), \end{cases} \quad (5.1.4)$$

where two small parameters,  $\epsilon$  and  $\mu^2$ , are assumed to be of the same order.

If we assume that  $\bar{\mathbf{u}}$  and  $\zeta$  are harmonic, they can be written as the following perturbation series

$$\begin{cases} \bar{\mathbf{u}} = \bar{\mathbf{u}}_0(x, y)e^{-i\omega t} + \mu^2 \bar{\mathbf{u}}_1(x, y)e^{-i\omega t} + \epsilon \bar{\mathbf{u}}_2(x, y)e^{-i2\omega t}, \\ \zeta = \eta_0(x, y)e^{-i\omega t} + \mu^2 \eta_1(x, y)e^{-i\omega t} + \epsilon \eta_2(x, y)e^{-i2\omega t}. \end{cases} \quad (5.1.5)$$

Then by substituting (5.1.5) into (5.1.4) and sorting out terms of the same order, the following three groups of equations are obtained

$$\begin{cases} -i\omega \bar{\mathbf{u}}_0 + \nabla \eta_0 = 0, \\ -i\omega \eta_0 + \nabla \cdot (h\bar{\mathbf{u}}_0) = 0, \end{cases} \quad (5.1.6)$$

$$\begin{cases} -i\omega \bar{\mathbf{u}}_1 + \nabla \eta_1 = -i\omega \frac{h}{2} \nabla[\nabla \cdot (h\bar{\mathbf{u}}_0)] + i\omega \frac{h^2}{6} \nabla(\nabla \cdot \bar{\mathbf{u}}_0), \\ -i\omega \eta_1 + \nabla \cdot (h\bar{\mathbf{u}}_1) = 0, \end{cases} \quad (5.1.7)$$

$$\begin{cases} -i2\omega \bar{\mathbf{u}}_2 + \nabla \eta_2 = -(\bar{\mathbf{u}}_0 \cdot \nabla)\bar{\mathbf{u}}_0, \\ -i2\omega \eta_2 + \nabla \cdot (h\bar{\mathbf{u}}_2) = -\nabla \cdot (\eta_0 \bar{\mathbf{u}}_0), \end{cases} \quad (5.1.8)$$

after  $O(\epsilon^2, \mu^4, \epsilon\mu^2)$  terms are ignored. From (5.1.5), the scattered wave field is given by

$$\zeta^s(x, y, t) = \eta_0^s(x, y)e^{-i\omega t} + \mu^2 \eta_1^s(x, y)e^{-i\omega t} + \epsilon \eta_2^s(x, y)e^{-i2\omega t}, \quad (5.1.9)$$

with

$$\eta_0^s = \eta_0 - \eta^I, \quad \eta_1^s = \eta_1, \quad \eta_2^s = \eta_2.$$

And the reflecting boundary condition along  $\Gamma_i$  is

$$h\bar{\mathbf{u}} \cdot \mathbf{n} = 0, \quad (5.1.10)$$

which is equivalent to

$$h\bar{\mathbf{u}}_i \cdot \mathbf{n} = 0, \quad i = 0, 1, 2. \quad (5.1.11)$$

We now simplify the equations (5.1.6)-(5.1.8). Firstly, eliminating  $\bar{\mathbf{u}}_0$  in (5.1.6), we get the first-order governing equation

$$\nabla \cdot (h\nabla\eta_0) + \omega^2\eta_0 = 0, \quad (5.1.12)$$

which is the well-known linear long-wave equation. The corresponding boundary condition (5.1.11) along the coastline  $\Gamma_i$  is equivalent to

$$h\frac{\partial\eta_0}{\partial\mathbf{n}} = 0. \quad (5.1.13)$$

In addition, a far-field radiation condition must be specified to ensure that the first-order scattered waves  $\eta_0^s(x, y)$  behaves as outgoing waves propagating away from the island. Sommerfeld (1949) gave the radiation condition as

$$\lim_{r \rightarrow \infty} \sqrt{r} \left( \frac{\partial\eta_0^s}{\partial r} - i\omega\eta_0^s \right) = 0, \quad r = \sqrt{x^2 + y^2}. \quad (5.1.14)$$

Secondly, eliminating  $\bar{\mathbf{u}}_1$  in (5.1.7), we have

$$\begin{aligned} & \nabla \cdot (h\nabla\eta_1) + \omega^2\eta_1 \\ = & i\omega\nabla \cdot \left[ -\frac{h^2}{2}\nabla(\nabla \cdot (h\bar{\mathbf{u}}_0)) + \frac{h^3}{6}\nabla(\nabla \cdot \bar{\mathbf{u}}_0) \right] \\ = & i\omega\nabla \cdot \left[ -\frac{h^2}{2}\nabla(i\omega\eta_0) + \frac{h^3}{6}\nabla\left(\frac{1}{i\omega}\nabla^2\eta_0\right) \right] \\ = & \frac{\omega^2}{2}(2h\nabla h \cdot \nabla\eta_0 + h^2\nabla^2\eta_0) + \frac{1}{6}[3h^2\nabla h \cdot \nabla(\nabla^2\eta_0) + h^3\nabla^2(\nabla^2\eta_0)] \\ = & \frac{\omega^2}{2}[2h\nabla h \cdot \nabla\eta_0 + h(-\nabla h \cdot \nabla\eta_0 - \omega^2\eta_0)] + \frac{1}{6}[3h^2\nabla h \cdot \nabla(\nabla^2\eta_0) + h^3\nabla^2(\nabla^2\eta_0)] \\ = & -\frac{\omega^4}{2}h\eta_0 + \frac{\omega^2}{2}h\nabla h \cdot \nabla\eta_0 + \frac{h^2}{2}\nabla h \cdot \nabla(\nabla^2\eta_0) + \frac{h^3}{6}\nabla^2(\nabla^2\eta_0). \end{aligned} \quad (5.1.15)$$

This gives the second-order equation for  $\eta_1$ , which describes the dispersive effects, as

$$\nabla \cdot (h \nabla \eta_1) + \omega^2 \eta_1 = -\frac{\omega^4 h}{2} \eta_0 + \frac{\omega^2 h}{2} \nabla h \cdot \nabla \eta_0 + \frac{h^2}{2} \nabla h \cdot \nabla (\nabla^2 \eta_0) + \frac{h^3}{6} \nabla^2 (\nabla^2 \eta_0). \quad (5.1.16)$$

Note that

$$\begin{aligned} h \frac{\partial \eta_1}{\partial \mathbf{n}} &= i\omega [h \bar{\mathbf{u}}_1 - \frac{h^2}{2} \nabla (\nabla \cdot (h \bar{\mathbf{u}}_0)) + \frac{h^3}{6} \nabla (\nabla \cdot \bar{\mathbf{u}}_0)] \cdot \mathbf{n} \\ &= i\omega [h \bar{\mathbf{u}}_1 - \frac{h^2}{2} \nabla (i\omega \eta_0) + \frac{h^3}{6} \nabla (\frac{1}{i\omega} \nabla^2 \eta_0)] \cdot \mathbf{n} \\ &= i\omega [h \bar{\mathbf{u}}_1 - \frac{h^2}{2} i\omega \nabla \eta_0 + \frac{h^3}{6} \frac{1}{i\omega} \nabla (\nabla^2 \eta_0)] \cdot \mathbf{n}, \end{aligned}$$

The boundary condition (5.1.11) along the coastline  $\Gamma_i$  is equivalent to

$$h \frac{\partial \eta_1}{\partial \mathbf{n}} = \frac{h^3}{6} \frac{\partial (\nabla^2 \eta_0)}{\partial \mathbf{n}}. \quad (5.1.17)$$

As to the far-field radiation condition for the scattered wave  $\eta_1$ , the Sommerfeld radiation condition can also be applied. But, since (5.1.16) is an inhomogeneous equation in an infinite region, we have to deal with a domain integral defined on the whole infinite region if the Sommerfeld radiation condition is applied to. In order to solve equation (5.1.16) numerically in a finite computational domain, an artificial boundary  $\mathcal{B}$  must be set up and some sort of non-reflecting boundary condition along  $\mathcal{B}$  need to be imposed. Since the 1970s, there have been many different non-reflecting boundary conditions proposed. A good review article was written by Givoli (1991) on these conditions. As the Boussinesq equations are weakly nonlinear long-wave equations with a small dispersive effect, we can choose a non-reflecting boundary condition for non-dispersive waves, such as those proposed by Engquist & Majda (1977) and Halpern & Trefethen (1988). In this thesis, we choose the artificial boundary  $\mathcal{B}$  to

be a circle and therefore use the following non-reflecting boundary conditions in the polar coordinate system which was derived by Engquist & Majda (1977)

$$\frac{\partial \zeta}{\partial r} + \frac{\partial \zeta}{\partial t} + \frac{1}{2R}\zeta = 0, \quad (5.1.18)$$

where  $R$  is the radius of the circle  $\mathcal{B}$  and  $C$  is the phase velocity. In our case, this is simplified to

$$\frac{\partial \eta_1}{\partial \mathbf{n}} = \left( -\frac{1}{2R} + i\omega \right) \eta_1. \quad (5.1.19)$$

Finally, eliminating  $\bar{\mathbf{u}}_2$  in equation (5.1.8), we have

$$\begin{aligned} & \nabla \cdot (h \nabla \eta_2) + 4\omega^2 \eta_2 \\ = & -2i\omega \nabla \cdot (\eta_0 \bar{\mathbf{u}}_0) - \nabla \cdot (h(\bar{\mathbf{u}}_0 \cdot \nabla) \bar{\mathbf{u}}_0) \\ = & -2\nabla \cdot (\eta_0 \nabla \eta_0) + \frac{1}{\omega^2} \nabla h \cdot (\nabla \eta_0 \cdot \nabla) \nabla \eta_0 + \frac{1}{\omega^2} h \nabla \cdot (\nabla \eta_0 \cdot \nabla) \nabla \eta_0 \\ = & -2\nabla \eta_0 \cdot \nabla \eta_0 - 2\eta_0 \nabla^2 \eta_0 + \frac{1}{2\omega^2} \nabla h \cdot \nabla (\nabla \eta_0 \cdot \nabla \eta_0) + \frac{1}{2\omega^2} h \nabla^2 (\nabla \eta_0 \cdot \nabla \eta_0). \end{aligned}$$

Hence the second-order governing equation for the term  $\eta_2$  which describes the non-linear effects, is

$$\begin{aligned} \nabla \cdot (h \nabla \eta_2) + 4\omega^2 \eta_2 = & -2\nabla \eta_0 \cdot \nabla \eta_0 - 2\eta_0 \nabla^2 \eta_0 + \frac{1}{2\omega^2} \nabla h \cdot \nabla (\nabla \eta_0 \cdot \nabla \eta_0) \\ & + \frac{1}{2\omega^2} h \nabla^2 (\nabla \eta_0 \cdot \nabla \eta_0). \end{aligned} \quad (5.1.20)$$

As the boundary condition (5.1.10) along the coastline  $\Gamma_i$ , we have

$$h \bar{\mathbf{u}}_2 \cdot \mathbf{n} = 0, \quad (5.1.21)$$

that is,

$$\begin{aligned} h \nabla \eta_2 \cdot \mathbf{n} &= 2i\omega h \bar{\mathbf{u}}_2 \cdot \mathbf{n} - h \nabla \left( \frac{1}{2} \bar{\mathbf{u}}_0 \cdot \bar{\mathbf{u}}_0 \right) \cdot \mathbf{n} \\ &= \frac{1}{2\omega^2} h \nabla (\nabla \eta_0 \cdot \nabla \eta_0) \cdot \mathbf{n}, \end{aligned}$$

which gives

$$h \frac{\partial \eta_2}{\partial \mathbf{n}} = \frac{h}{2\omega^2} \frac{\partial(\nabla \eta_0 \cdot \nabla \eta_0)}{\partial \mathbf{n}}. \quad (5.1.22)$$

In addition, as to the far-field radiation condition for scattered wave  $\eta_2$ , the Sommerfeld radiation condition cannot be applied. A suitable far-field radiation condition for second-order scattered waves  $\eta_2$  at the second-harmonic has not been established. See Rahman & Heaps (1983) and Kriebel (1990) for the discussion on this issue. Similar to  $\eta_1$ , the corresponding non-reflecting condition for  $\eta_2$  along  $\mathcal{B}$  becomes

$$\frac{\partial \eta_2}{\partial \mathbf{n}} = \left( -\frac{1}{2R} + i2\omega \right) \eta_2. \quad (5.1.23)$$

It is worth indicating that, both the equations (5.1.16) and (5.1.20) for  $\eta_1$  and  $\eta_2$  are inhomogeneous equations with their right-hand sides containing some partial derivatives of  $\eta_0$  up to the fourth-order. All these derivatives will be approximated by using the first-order numerical solution  $\eta_0$  and therefore large errors may result in representing these higher-order derivatives. Generally, the higher the order of the derivative is, the larger the error of the approximation is. In order to minimize these errors, we need to further simplify (5.1.16) and (5.1.20). Introducing the transformation

$$\tilde{\eta}_1 = \eta_1 - \frac{h^2}{6} \nabla^2 \eta_0, \quad (5.1.24)$$



we have from the governing equation (5.1.16)

$$\begin{aligned}
& \nabla \cdot (h \nabla \tilde{\eta}_1) + \omega^2 \tilde{\eta}_1 \\
&= -\frac{\omega^4}{2} h \eta_0 + \frac{\omega^2}{2} h \nabla h \cdot \nabla \eta_0 - \frac{\omega^2 h^2}{6} \nabla^2 \eta_0 - \frac{1}{3} \nabla \cdot (h^2 \nabla h \nabla^2 \eta_0) \\
&= -\frac{\omega^4}{2} h \eta_0 + \frac{\omega^2}{2} h \nabla h \cdot \nabla \eta_0 + \frac{\omega^2 h}{6} (\nabla h \cdot \nabla \eta_0 + \omega^2 \eta_0) + \frac{1}{3} \nabla \cdot [h \nabla h (\nabla h \cdot \nabla \eta_0 + \omega^2 \eta_0)] \\
&= -\frac{\omega^4}{3} h \eta_0 + \frac{2\omega^2 h}{3} \nabla h \cdot \nabla \eta_0 + \frac{1}{3} \nabla \cdot (h \nabla h) (\nabla h \cdot \nabla \eta_0 + \omega^2 \eta_0) + \frac{h}{3} \nabla h \cdot \nabla (\nabla h \cdot \nabla \eta_0 + \omega^2 \eta_0) \\
&= -\frac{\omega^2}{3} [\omega^2 h - \nabla \cdot (h \nabla h)] \eta_0 + \left[ \omega^2 h + \frac{1}{3} \nabla \cdot (h \nabla h) \right] \nabla h \cdot \nabla \eta_0 + \frac{h}{3} \nabla h \cdot \nabla (\nabla h \cdot \nabla \eta_0),
\end{aligned}$$

Hence, the second-order governing equation (5.1.16) is transformed into

$$\begin{aligned}
\nabla \cdot (h \nabla \tilde{\eta}_1) + \omega^2 \tilde{\eta}_1 &= -\frac{\omega^2}{3} [\omega^2 h - \nabla \cdot (h \nabla h)] \eta_0 + \left[ \omega^2 h + \frac{1}{3} \nabla \cdot (h \nabla h) \right] \nabla h \cdot \nabla \eta_0 \\
&\quad + \frac{h}{3} \nabla h \cdot \nabla (\nabla h \cdot \nabla \eta_0),
\end{aligned} \tag{5.1.25}$$

which contains derivatives up to second-order only. The corresponding boundary conditions along  $\Gamma_i$  and the non-reflecting boundary conditions along  $\mathcal{B}$  now become

$$h \frac{\partial \tilde{\eta}_1}{\partial \mathbf{n}} = \frac{h}{3} \frac{\partial h}{\partial \mathbf{n}} (\nabla h \cdot \nabla \eta_0 + \omega^2 \eta_0), \tag{5.1.26}$$

and

$$\frac{\partial \tilde{\eta}_1}{\partial \mathbf{n}} = \left( -\frac{1}{2R} + i\omega \right) \tilde{\eta}_1 + f_1(h, \eta_0), \tag{5.1.27}$$

with

$$\begin{aligned}
f_1(h, \eta_0) &= \frac{h}{6} \left( \frac{1}{2R} - i\omega \right) (\nabla h \cdot \nabla \eta_0 + \omega^2 \eta_0) + \frac{\omega^2 h}{6} \frac{\partial \eta_0}{\partial \mathbf{n}} + \\
&\quad + \frac{h}{6} \frac{\partial (\nabla h \cdot \nabla \eta_0)}{\partial \mathbf{n}} + \frac{1}{6} \frac{\partial h}{\partial \mathbf{n}} (\nabla h \cdot \nabla \eta_0 + \omega^2 \eta_0).
\end{aligned} \tag{5.1.28}$$

Similarly, let

$$\tilde{\eta}_2 = \eta_2 - \frac{1}{2\omega^2} \nabla \eta_0 \cdot \nabla \eta_0, \tag{5.1.29}$$

and the governing equation (5.1.20) for the second-harmonic now becomes

$$\nabla \cdot (h \nabla \tilde{\eta}_2) + 4\omega^2 \tilde{\eta}_2 = -4\nabla \eta_0 \cdot \nabla \eta_0 - 2\eta_0 \nabla^2 \eta_0. \quad (5.1.30)$$

The corresponding boundary conditions along  $\Gamma_i$  and the non-reflecting boundary conditions along  $\mathcal{B}$ , i.e., (5.1.22) and (5.1.23), respectively become

$$h \frac{\partial \tilde{\eta}_2}{\partial \mathbf{n}} = 0, \quad (5.1.31)$$

and

$$\frac{\partial \tilde{\eta}_2}{\partial \mathbf{n}} = \left( -\frac{1}{2R} + i2\omega \right) \tilde{\eta}_2 + f_2(\eta_0), \quad (5.1.32)$$

with

$$f_2(\eta_0) = \frac{1}{2\omega^2} \left( -\frac{1}{2R} + i2\omega \right) \nabla \eta_0 \cdot \nabla \eta_0 - \frac{1}{2\omega^2} \frac{\partial}{\partial \mathbf{n}} (\nabla \eta_0 \cdot \nabla \eta_0). \quad (5.1.33)$$

These three sets of linear differential systems are now solved with the DRBEM.

## 5.2 Formation of integral equations

To solve (5.1.12), (5.1.25) and (5.1.30) together with their boundary conditions efficiently, we cast them into boundary integral equations. In this section, the integral equations corresponding to (5.1.12), (5.1.25) and (5.1.30) are given.

*The first-order solution.* Let

$$\eta^*(\xi, \mathbf{x}) = \frac{i}{4} H_0^{(1)}(\omega \rho).$$

Similar to (4.2.11), the first-order equation (5.1.12) can be transformed into the following integral equation

$$\begin{aligned}
& c_\xi h \eta_0 - \int_{\Gamma_o + \Gamma_i} \frac{\partial h}{\partial \mathbf{n}} \eta_0 \eta^* d\Gamma + h_i \int_{\Gamma_i} \eta_0 q^* d\Gamma \\
& = h_o c_\xi^{(o)} \eta^I - h_o \int_{\Gamma_o} (\eta^I q^* - q^I \eta^*) d\Gamma + \\
& + \sum_{j=1}^{n+m+l} \alpha_j^{(0)} \left[ c_\xi^{(i)} \hat{\eta}_j^{(0)} - \int_{\Gamma_o + \Gamma_i} (\hat{q}_j^{(0)} \eta^* - \hat{\eta}_j^{(0)} q^*) d\Gamma \right]. \quad (5.2.1)
\end{aligned}$$

*The second-order fundamental frequency solution.* The equation (5.1.25) for the nonlinear contribution at the fundamental frequency is

$$\nabla^2(h\tilde{\eta}_1) + \omega^2(h\tilde{\eta}_1) = R_1(x, y), \quad (5.2.2)$$

where

$$\begin{aligned}
R_1(x, y) = & \omega^2(h-1)\tilde{\eta}_1 + \nabla h \cdot \nabla \tilde{\eta}_1 + \tilde{\eta}_1 \nabla^2 h - \frac{\omega^2}{3} [\omega^2 h - \nabla \cdot (h \nabla h)] \eta_0 + \\
& + \left[ \omega^2 h + \frac{1}{3} \nabla \cdot (h \nabla h) \right] \nabla h \cdot \nabla \eta_0 + \frac{h}{3} \nabla h \cdot \nabla (\nabla h \cdot \nabla \eta_0).
\end{aligned}$$

Let  $\Omega_B$  be the domain between  $\Gamma_i$  and  $B$ . Then using DRBEM, equation (5.2.2) can be transformed into the following integral equation

$$\begin{aligned}
& c_\xi^{(B)} h \tilde{\eta}_1 - \int_{\Gamma_i + B} \left[ \frac{\partial h}{\partial \mathbf{n}} \tilde{\eta}_1 \eta^* - h \tilde{\eta}_1 q^* \right] d\Gamma + \int_B h \left( \frac{1}{2R} - i\omega \right) \tilde{\eta}_1 \eta^* d\Gamma - \\
& - \int_{\Gamma_i} \frac{h}{3} \frac{\partial h}{\partial \mathbf{n}} (\nabla h \cdot \nabla \eta_0 + \omega^2 \eta_0) \eta^* d\Gamma + \int_B h f_1(h, \eta_0) \eta^* d\Gamma \\
& = \sum_{j=1}^{n+m+l} \alpha_j^{(1)} \left[ c_\xi^{(B)} \hat{\eta}_j^{(1)} - \int_{\Gamma_i + B} (\hat{q}_j^{(1)} \eta^* - \hat{\eta}_j^{(1)} q^*) d\Gamma \right]. \quad (5.2.3)
\end{aligned}$$

where

$$c_\xi^{(B)} = \begin{cases} \frac{\alpha(\xi)}{2\pi} & \text{if } \xi \in \Gamma_i + B, \\ 1 & \text{if } \xi \in \Omega_B. \end{cases}$$

*The second-order solution for the second-harmonic.* The governing equation (5.1.30) for the second-harmonic can be rewritten as

$$\nabla^2(h\tilde{\eta}_2) + 4\omega^2(h\tilde{\eta}_2) = R_2(x, y), \quad (5.2.4)$$

where

$$R_2(x, y) = 4\omega^2(h - 1)\tilde{\eta}_2 + \nabla h \cdot \nabla \tilde{\eta}_2 + \tilde{\eta}_2 \nabla^2 h - 4\nabla \eta_0 \cdot \nabla \eta_0 - 2\eta_0 \nabla^2 \eta_0.$$

Let

$$\eta_2^*(\xi, \mathbf{x}) = \frac{i}{4} H_0^{(1)}(2\omega\rho).$$

Using DRBEM, we can transform equation (5.2.4) into

$$\begin{aligned} & c_\xi^{(\mathcal{B})} h \tilde{\eta}_2 - \int_{\Gamma_i + \mathcal{B}} \left[ \frac{\partial h}{\partial \mathbf{n}} \tilde{\eta}_2 \eta_2^* - h \tilde{\eta}_2 q_2^* \right] d\Gamma + \int_{\mathcal{B}} h \left( \frac{1}{2R} - i2\omega \right) \tilde{\eta}_2 \eta_2^* d\Gamma - \int_{\mathcal{B}} h f_2(\eta_0) \eta_2^* d\Gamma \\ &= \sum_{j=1}^{n+m+l} \alpha_j^{(2)} \left[ c_\xi^{(\mathcal{B})} \hat{\eta}_j^{(2)} - \int_{\Gamma_i + \mathcal{B}} (\hat{q}_j^{(2)} \eta_2^* - \hat{\eta}_j^{(2)} q_2^*) d\Gamma \right], \end{aligned} \quad (5.2.5)$$

where  $q_2^* = \frac{\partial \eta_2^*(\xi, \mathbf{x})}{\partial \mathbf{n}}$ .

Equations (5.2.1)-(5.2.5) involve boundary integrals only, after appropriate discretization and approximation to all derivatives of  $\eta_0$ ,  $\tilde{\eta}_1$  and  $\tilde{\eta}_2$ , a linear system of algebraic equations involving the unknown function  $\eta_0$  on  $\Gamma_i + \Gamma_o + \Omega_i$  or  $\tilde{\eta}_1$  and  $\tilde{\eta}_2$  on  $\Gamma_i + \mathcal{B} + \Omega_{\mathcal{B}}$  can be established. The details of such a system is similar to those in Appendix A.

### 5.3 Run-ups of nonlinear waves

After  $\eta_0$ ,  $\eta_1$  and  $\eta_2$  are solved numerically, the next step is to calculate the maximum wave run-up. For the linear case, we have obtained in Section 4.4 that

$$\max_t \zeta_{phys}(x, y, t) = \max_t |\zeta(x, y, t)|. \quad (5.3.1)$$

For weakly nonlinear waves, according to expression (5.1.5), the total (complex) instantaneous surface elevation is

$$\begin{aligned}
 \zeta(x, y, t) &= \eta_0(x, y)e^{-i\omega t} + \mu^2\eta_1(x, y)e^{-i\omega t} + \epsilon\eta_2(x, y)e^{-i2\omega t} \\
 &= (a_{01}(x, y) + ib_{01}(x, y))e^{-i\omega t} + (a_2(x, y) + ib_2(x, y))e^{-i2\omega t} \\
 &= (a_{01} \cos \omega t + b_{01} \sin \omega t) + i(b_{01} \cos \omega t - a_{01} \sin \omega t) + \\
 &\quad + (a_2 \cos 2\omega t + b_2 \sin 2\omega t) + i(b_2 \cos 2\omega t - a_2 \sin 2\omega t).
 \end{aligned}$$

And the physical surface elevation is the real part of this expression, that is,

$$\begin{aligned}
 \zeta_{phys}(x, y, t) &= a_{01} \cos \omega t + b_{01} \sin \omega t + a_2 \cos 2\omega t + b_2 \sin 2\omega t \\
 &= \sqrt{a_{01}^2 + b_{01}^2} \sin(\omega t + \theta_1) + \sqrt{a_2^2 + b_2^2} \sin(2\omega t + \theta_2), \quad (5.3.2)
 \end{aligned}$$

where

$$\theta_1 = \begin{cases} \tan^{-1} \frac{a_{01}}{b_{01}}, & \text{if } b_{01} > 0, \\ \frac{\pi}{2} + \tan^{-1} \frac{a_{01}}{b_{01}}, & \text{if } b_{01} < 0, \\ \frac{\pi}{2}, & \text{if } b_{01} = 0, a_{01} > 0, \\ -\frac{\pi}{2}, & \text{if } b_{01} = 0, a_{01} < 0, \end{cases}$$

and

$$\theta_2 = \begin{cases} \tan^{-1} \frac{a_2}{b_2}, & \text{if } b_2 > 0, \\ \frac{\pi}{2} + \tan^{-1} \frac{a_2}{b_2}, & \text{if } b_2 < 0, \\ \frac{\pi}{2}, & \text{if } b_2 = 0, a_2 > 0, \\ -\frac{\pi}{2}, & \text{if } b_2 = 0, a_2 < 0. \end{cases}$$

Also in contrast to the linear case, the relationship (5.3.1) does not hold for the nonlinear case. In fact, since

$$\begin{aligned}
 |\eta(x, y, t)|^2 &= (a_{01} \cos \omega t + b_{01} \sin \omega t + a_2 \cos 2\omega t + b_2 \sin 2\omega t)^2 + \\
 &\quad + (b_{01} \cos \omega t - a_{01} \sin \omega t + (b_2 \cos 2\omega t - a_2 \sin 2\omega t))^2 \\
 &= a_{01}^2 + b_{01}^2 + a_2^2 + b_2^2 + \\
 &\quad + 2(a_{01} \cos \omega t + b_{01} \sin \omega t)(a_2 \cos 2\omega t + b_2 \sin 2\omega t) + \\
 &\quad + 2(b_{01} \cos \omega t - a_{01} \sin \omega t)(b_2 \cos 2\omega t - a_2 \sin 2\omega t) \\
 &= a_{01}^2 + b_{01}^2 + a_2^2 + b_2^2 + \\
 &\quad + 2(a_{01}a_2 + b_{01}b_2) \cos \omega t + 2(a_{01}b_2 - b_{01}a_2) \sin \omega t, \quad (5.3.3)
 \end{aligned}$$

we have

$$\begin{aligned}
 \max_t |\eta(x, y, t)|^2 &= a_{01}^2 + b_{01}^2 + a_2^2 + b_2^2 + \\
 &\quad + 2\sqrt{(a_{01}a_2 + b_{01}b_2)^2 + (a_{01}b_2 - b_{01}a_2)^2} \\
 &= \left( \sqrt{a_{01}^2 + b_{01}^2} + \sqrt{a_2^2 + b_2^2} \right)^2. \quad (5.3.4)
 \end{aligned}$$

Hence

$$\max_t |\zeta(x, y, t)| = \sqrt{a_{01}^2 + b_{01}^2} + \sqrt{a_2^2 + b_2^2}, \quad (5.3.5)$$

which is not the same as (5.3.2). Thus, to obtain run-ups of the nonlinear waves in this thesis, we need to calculate the maximum value

$$\max_t \left( \sqrt{a_{01}^2 + b_{01}^2} \sin(\omega t + \theta_1) + \sqrt{a_2^2 + b_2^2} \sin(2\omega t + \theta_2) \right).$$

Note that, the periods of  $\sin(\omega t + \theta_1)$  and  $\sin(2\omega t + \theta_2)$  are  $\frac{2\pi}{\omega}$  and  $\frac{\pi}{\omega}$ , respectively, the period of  $\zeta_{phys}(x, y, t)$  is  $\frac{2\pi}{\omega}$  and the maximum value of  $\zeta_{phys}(x, y, t)$  must appear in the interval  $[0, \frac{2\pi}{\omega}]$ . Numerically, we can easily find out the maximum value in  $[0, \frac{2\pi}{\omega}]$ .

### 5.4 Numerical examples

To test the PDRBEM model, we calculated wave amplification around coastlines for both a vertical cylinder and a circular conical island and compared our results with experimental data, linear theoretical solutions and other numerical solutions. For simplicity, the incident angle  $\theta^I$  of the incident waves is taken to be  $0^\circ$  and all the variables are now referred back to dimensional quantities.

Table 5.1. Parameters in Kriebel's (1990, 1992a) experiments.							
cases	$k_o$	$k_o a$	$k_o h_o$	$L/h_o$	$\mu^2$	$\epsilon$	$k_o H$
1	1.668	0.271	0.750	8.378	0.0143	0.0880	0.132
2						0.1187	0.178
3						0.1433	0.215
4	1.895	0.308	0.853	7.366	0.0184	0.0498	0.085
5						0.0803	0.137
6						0.1067	0.182
7						0.1465	0.250
8						0.1735	0.296
9	2.302	0.374	1.036	6.065	0.0272	0.0589	0.122
10						0.0989	0.205
11						0.1380	0.286
12						0.1858	0.385
13						0.1940	0.402

#### 5.4.1 Diffraction around a vertical cylinder

For wave diffraction on a vertical cylinder, there have been many experiments conducted for various cylinders and incident waves. However most of them only concerned wave forces rather than wave run-ups. Data from wave run-up experiments are somewhat limited, only found in Laird (1955), Nagai (1973), Chakrabarti & Tam (1975) and Raman & Venkatanarsaiah (1976). The cylinders studied in these literature are usually small and the waves are usually linear waves with very small amplitudes anyway.

Recently, Kriebel (1990, 1992a) developed a nonlinear diffraction theory for wave-structure interaction to the second order where a set of experimental data of nonlinear wave run-ups was presented and compared with his second-order diffraction theoretical solutions. According to Kriebel (1990, 1992a), a total of 22 experiments were carried out in a wave basin at the University of Florida Coastal and Oceanographic Engineering Laboratory, in which wave run-up was measured for steep regular waves passing a fixed vertical cylinder with a radius,  $a$ , of 16.25 cm in a water depth,  $h_o$ , of 45 cm. The water depth ranged from nearly-deep water with  $L/h_o = 2.478$  to nearly shallow water with  $L/h_o = 8.378$ . And  $k_o H$  values ranged from 0.085 to 0.806. Since the governing equations used in this thesis are the Boussinesq equations which are based on the assumption of shallow water depth and the requirement that the nonlinearity  $\epsilon = k_o A$  be small, only cases 1 to 13 shall be examined as the water depth ranged from shallow water with  $L/h_o = 8.378$  to near shallow water with  $L/h_o = 6.065$  and the nonlinearity  $\epsilon$  ranged from 0.0498 to 0.1940, see Table 5.1.

As the cylinder can be regarded as a special conical island, the toe  $\Gamma_o$  of the cylinder and the coastline  $\Gamma_i$  are coincident. In our calculation, the artificial boundary



$\mathcal{B}$  is taken to be a circle of radius  $R = 8a$ . For all the 13 cases, 16 quadratic elements (with 32 boundary nodes) are used in each of the two boundary circles  $\Gamma_i$  and  $\mathcal{B}$  and 72 internal collocation points are evenly distributed on six inner circles, the radius of which are  $r_j = a + c_j(R - a)$  with  $c_j$  being 0.10, 0.26, 0.42, 0.58, 0.70 and 0.86 for  $j = 1, \dots, 6$  respectively. The results of the wave run-ups by experiments (Kriebel 1992a), the linear diffraction theory (MacCamy & Fuchs 1954), Kriebel's second-order diffraction theory (Kriebel 1990, 1992a) and the present PDRBEM numerical model are presented in Figure 5.1 to Figure 5.13.

First of all, as expected, the first-order solutions,  $\eta_0(x, y)$ , of the PDRBEM for all 13 cases agree with the linear diffraction theoretical solutions (MacCamy & Fuchs 1954) very well. For clarity, all these first-order solutions are not graphed in these figures.

Secondly, as shown in Figure 5.1 to Figure 5.13, the dispersive and nonlinear contribution from the PDRBEM model are significant. It can be seen that, at the front side ( $\theta = 180^\circ$ ) of the cylinder, the linear diffraction theory badly underestimates the maximum wave run-ups in all cases with measured run-ups exceeding the linear theory by 13-78% and by 46% on average. In contrast, measured run-ups exceed the PDRBEM solution by up to 16% but by only 7% on average. Furthermore, the run-up distributions around the circumference are also poorly predicted by linear diffraction theory whereas the agreements between the measured run-ups and the PDRBEM run-ups are excellent in all thirteen cases. Especially, for cases 2-5 and 9-13, the measured run-up profile is almost exactly replicated over all angular positions by the current PDRBEM model.

Finally, we notice that the present PDRBEM solutions, in some cases, show an

improvement over Kriebel's (1990,1992a) second-order diffraction theory. Kriebel's second-order model consistently underestimated the run-ups for cases 8, 10, 11, 12 and 13 with steep waves whereas our model gives a good prediction. It is believe that this is due to different radiation boundary conditions in Kriebel's and our model. Hence, at large nonlinearities, our model performs better.

In addition, as shown in Table 5.1, all 13 cases correspond to three different wavenumbers. The corresponding linear (MacCamy & Fuchs 1954) and weakly-nonlinear solutions of the wave run-ups for these four wavenumbers are separately graphed in Figure 5.14 to Figure 5.16. In each group, although the amplitudes of all the cases are different, the linear solutions are the same since they correspond to the same wavenumber. However, as we can see from the weakly-nonlinear solutions in all the three graphs, as the amplitude of the incident waves increases, the maximum wave run-up increases.

#### 5.4.2 Combined refraction and diffraction on a conical island

We now apply the PDRBEM model to the combined wave refraction and diffraction on a conical island. Up to now, only two published experimental data on run-up of periodic waves around conical islands are reported by Provis (1975) and Liu *et al.* (1994). Provis' experiments were conducted in a small basin (5.55 m wide and 5.80 m long). The base diameter of the island was 3 m and the slope was 1:10. The water depth in the constant-depth region in the experiments was 0.15 m. Provis reported large discrepancies between his experimental data and theoretical results predicted by Smith & Sprinks (1975). Sprinks & Smith (1983) pointed out later that because of the relatively small size of the wave basin and the shallow-water depth, the viscous

damping and standing waves between the wave generator and the island contaminated the experimental results. In addition, in order to reduce the nonlinear effect, the wave amplitudes were kept as small as possible, the incident wave typically having a amplitude of 0.00005 m. Provis' experments are inappropriate for testing our PDRBEM model.

Table 5.2. The parameters in the experiments used by Liu *et al.* (1994).

cases	$a$	$b$	$h_o$	$A$	$T$	$\epsilon$	$\mu^2$
1	0.468 m	1.65 m	0.2955 m	0.00250 m	4.5 sec	0.00846	0.00149
2	0.468 m	1.65 m	0.2955 m	0.00085 m	2.5 sec	0.00288	0.00483
3	0.878 m	1.65 m	0.1930 m	0.00285 m	3.0 sec	0.01477	0.00219
4	0.862 m	1.65 m	0.1970 m	0.00235 m	2.5 sec	0.01193	0.00322

We chose the experiments reported by Liu *et al.* (1994) as numerical examples to test our PDRBEM model. The experiments were performed at the National Defence Academy (NDA), Japan. They were carried out in a small basin with 7 m width and 11 m length. The base diameter of the island was 3.3 m and the slope was 1:4. The water depth in the constant-depth region in the experiments was 0.1930 m to 0.2955 m. These conditions together with the parameters of the incident waves are tabulated in Table 5.2.

In our numerical computation, for all these four cases the artificial boundary  $\mathcal{B}$  is taken to be the toe,  $\Gamma_o$ , of the island. In addition, 20 quadratic elements (with 40 boundary nodes) are used in each of the two boundary circles  $\Gamma_i$  and  $\Gamma_o$  and 72 internal collocation points are evenly distributed on six inner circles where their

radius are  $r_j = a + c_j(b - a)$  with  $c_j$  being 0.10, 0.26, 0.42, 0.58, 0.70 and 0.86 for  $j = 1, \dots, 6$ , respectively.

In Figure 5.17-5.20, the maximum run-ups are shown for experimental data, linear theory (Zhang & Zhu 1994a) based on the linear shallow-water equation, the time-marching finite difference scheme for the nonlinear shallow-water equations (Liu *et al.* 1994) and the present PDRBEM based on the Boussinesq equations. As we can see from Table 5.2, the nonlinearity is weakest in cases 1 and 2 while the dispersive effects are weakest in cases 1 and 3. For cases 1 and 3 all the different theories lie close together. For case 1 there is an excellent comparison with experimental results while for case 3 there is some variation between the experimental results and theory near the  $120^\circ$  region.

In cases 2 and 4, for which dispersion is important, Liu *et al.* (1994) results diverge significantly from the other results. This is due to the fact no dispersive terms are present in the nonlinear shallow-water equations. The present PDRBEM method does extremely well in case 2 while there is some divergence between all the theories and the experimental results near  $\theta = 0^\circ$  for case 4.

Significant unexplained differences between the PDRBEM solutions and experimental data are observed in both cases 3 and 4. These are the cases in which the nonlinear effects are largest so perhaps neglected higher-order nonlinear terms are the cause of these variations.

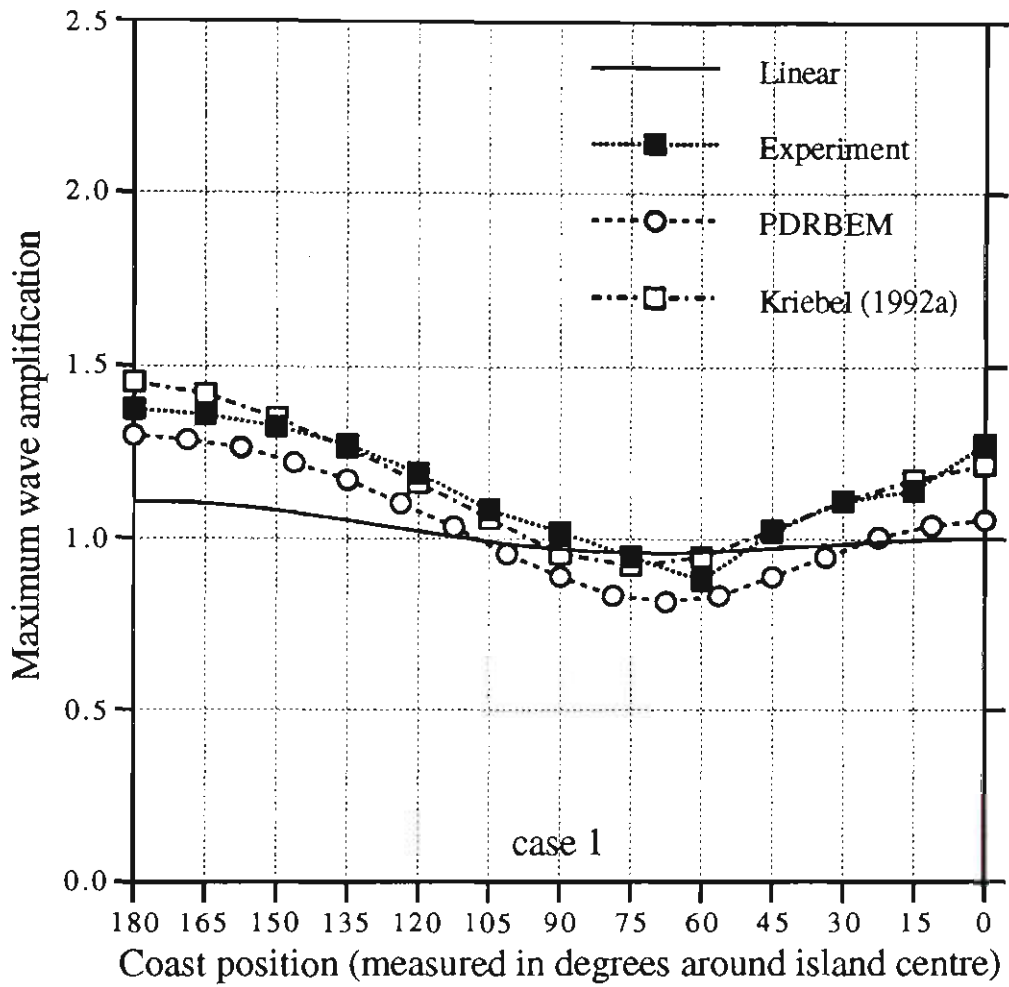


Figure 5.1: Comparison among the experimental data (Kriebel 1990 and 1992a), linear run-ups, the second order diffraction run-ups and the present weakly-nonlinear run-ups for case 1 of cylindrical island.

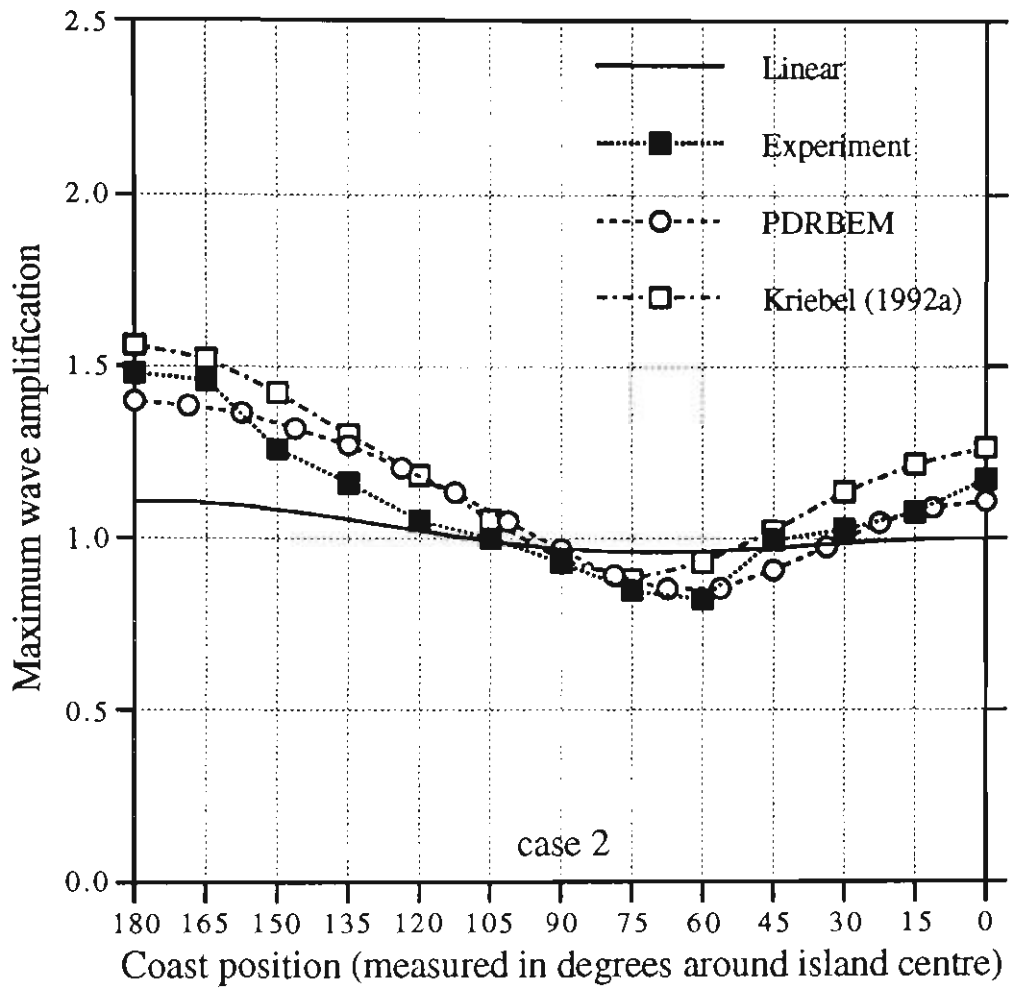


Figure 5.2: Comparison among the experimental data (Kriebel 1990 and 1992a), linear run-ups, the second order diffraction run-ups and the present weakly-nonlinear run-ups for case 2 of cylindrical island.

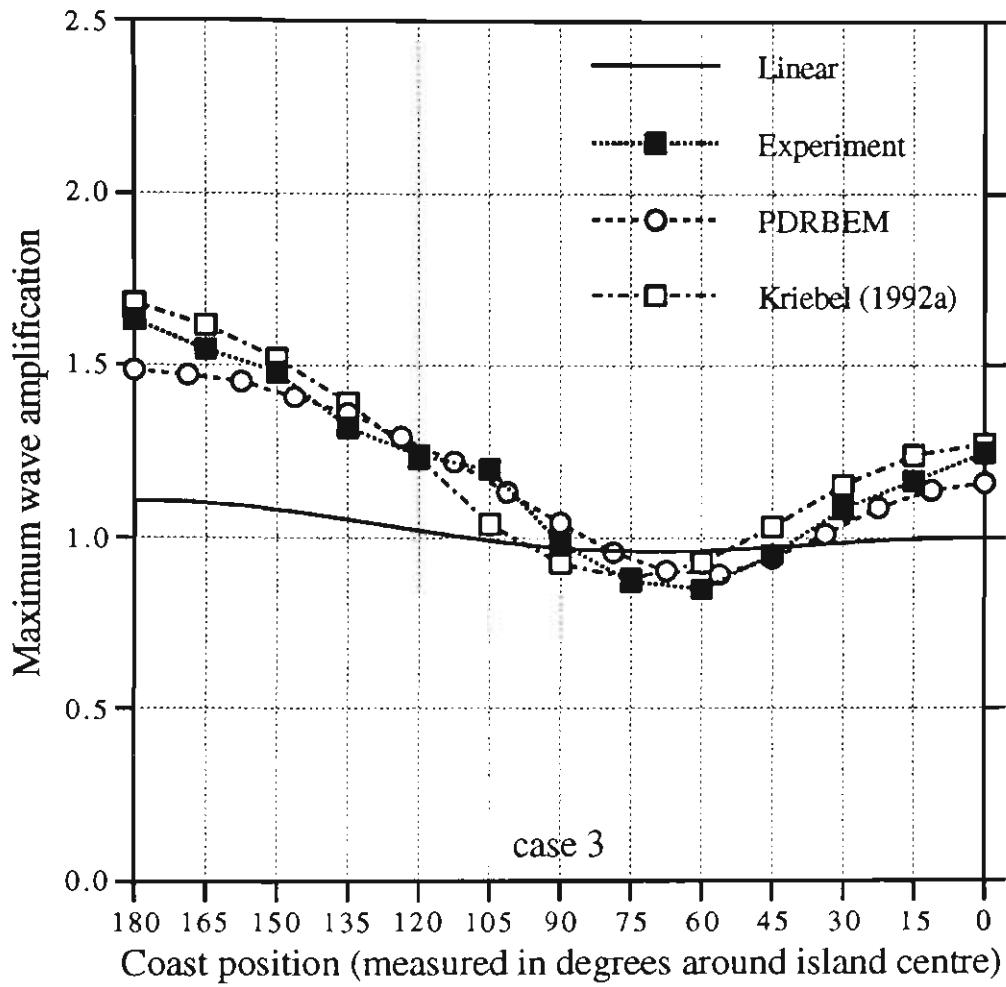


Figure 5.3: Comparison among the experimental data (Kriebel 1990 and 1992a), linear run-ups, the second order diffraction run-ups and the present weakly-nonlinear run-ups for case 3 of cylindrical island.

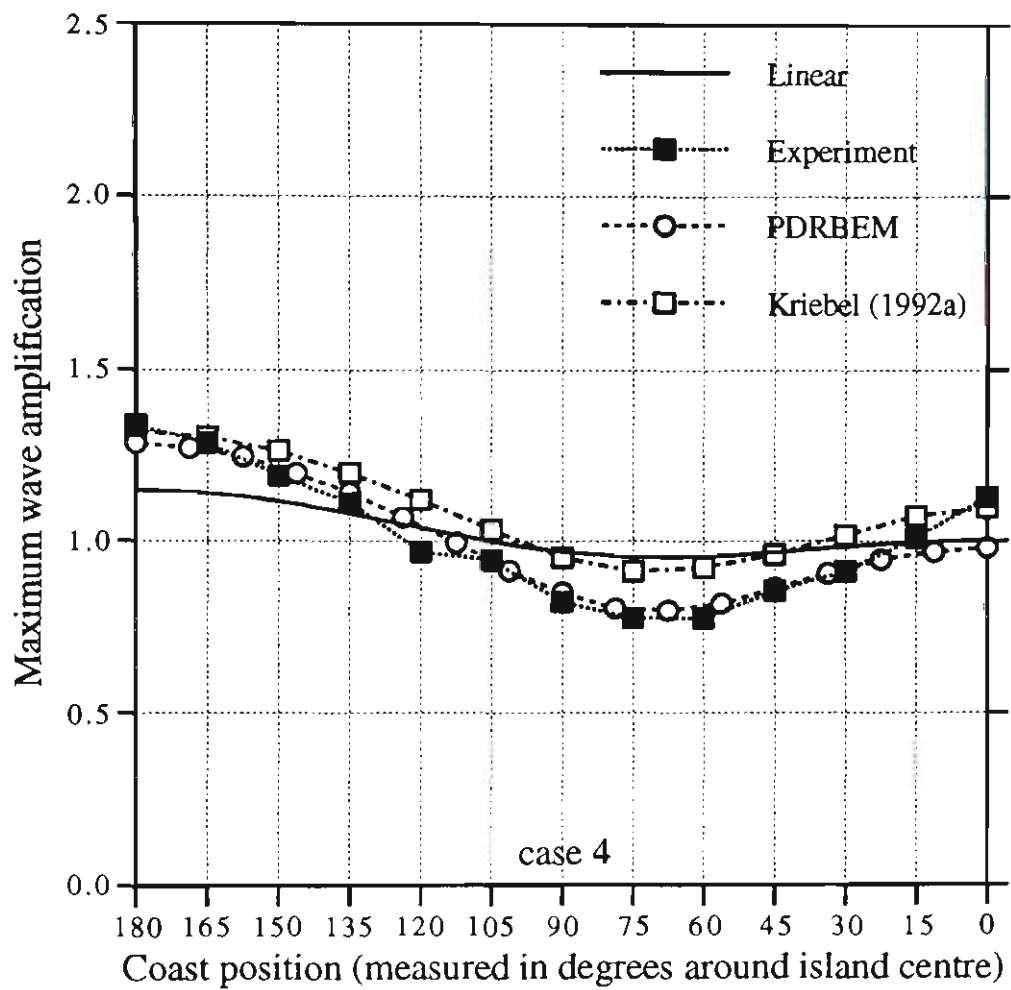


Figure 5.4: Comparison among the experimental data (Kriebel 1990 and 1992a), linear run-ups, the second order diffraction run-ups and the present weakly-nonlinear run-ups for case 4 of cylindrical island.



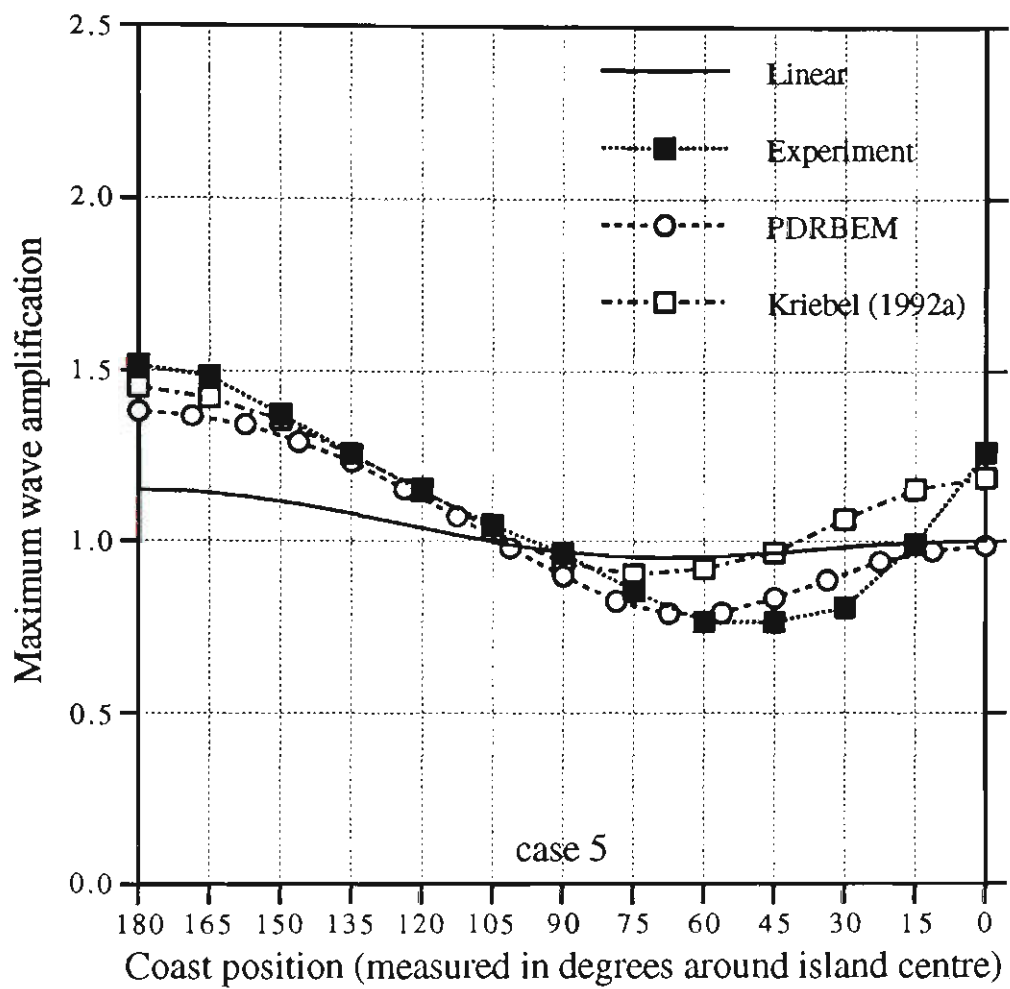


Figure 5.5: Comparison among the experimental data (Kriebel 1990 and 1992a), linear run-ups, the second order diffraction run-ups and the present weakly-nonlinear run-ups for case 5 of cylindrical island.

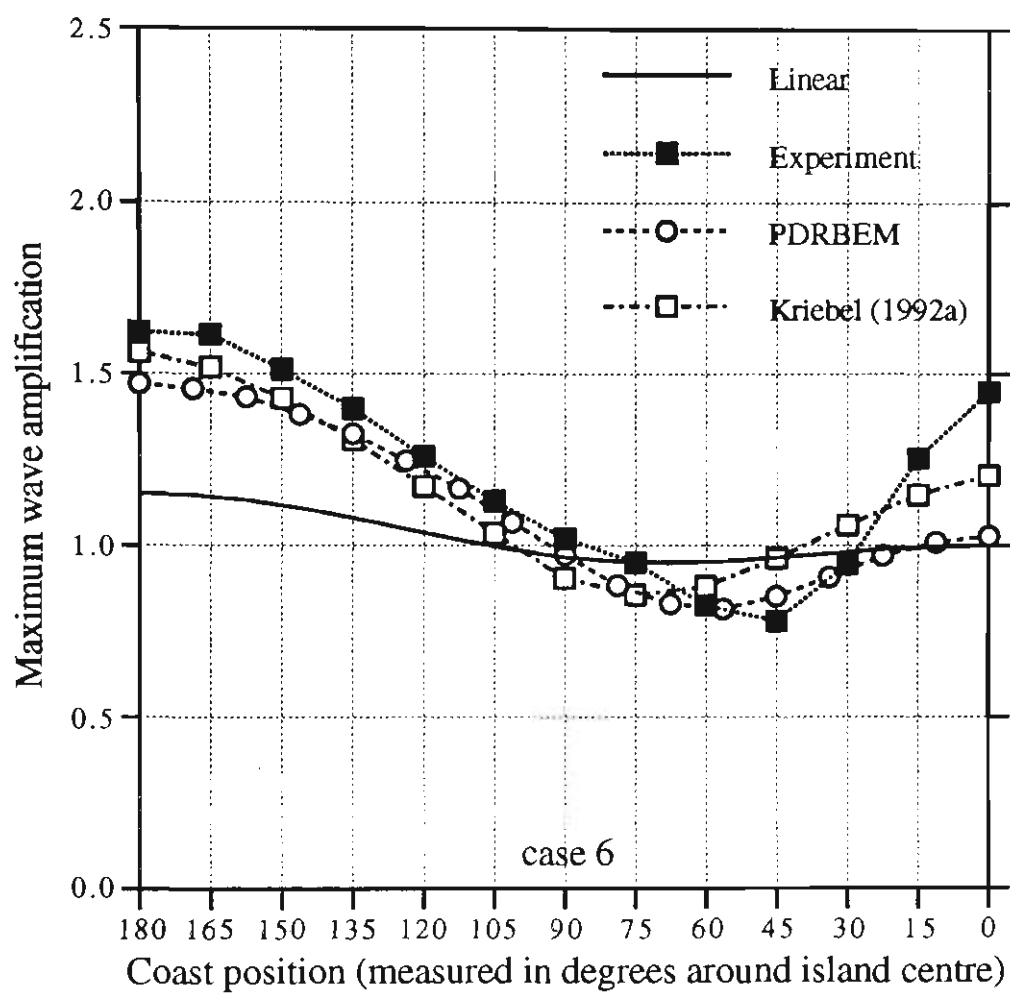


Figure 5.6: Comparison among the experimental data (Kriebel 1990 and 1992a), linear run-ups, the second order diffraction run-ups and the present weakly-nonlinear run-ups for case 6 of cylindrical island.

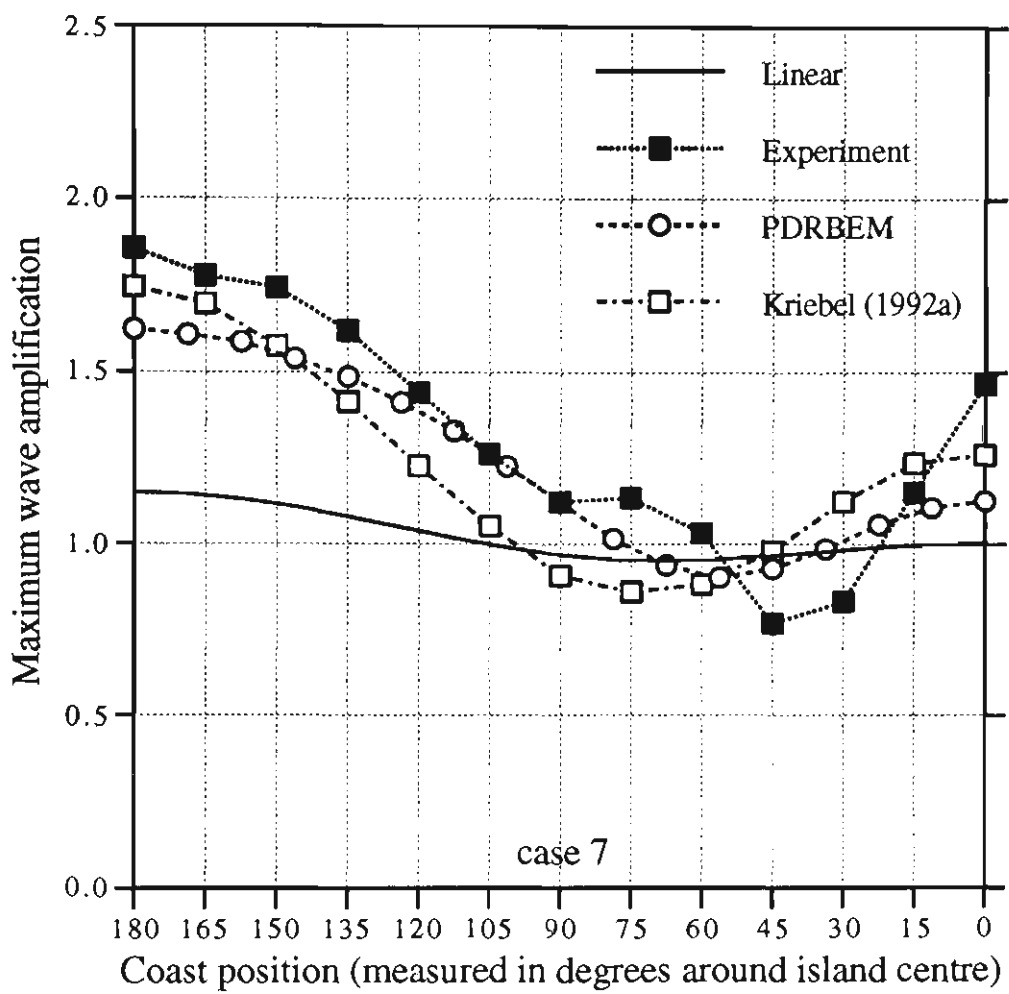


Figure 5.7: Comparison among the experimental data (Kriebel 1990 and 1992a), linear run-ups, the second order diffraction run-ups and the present weakly-nonlinear run-ups for case 7 of cylindrical island.

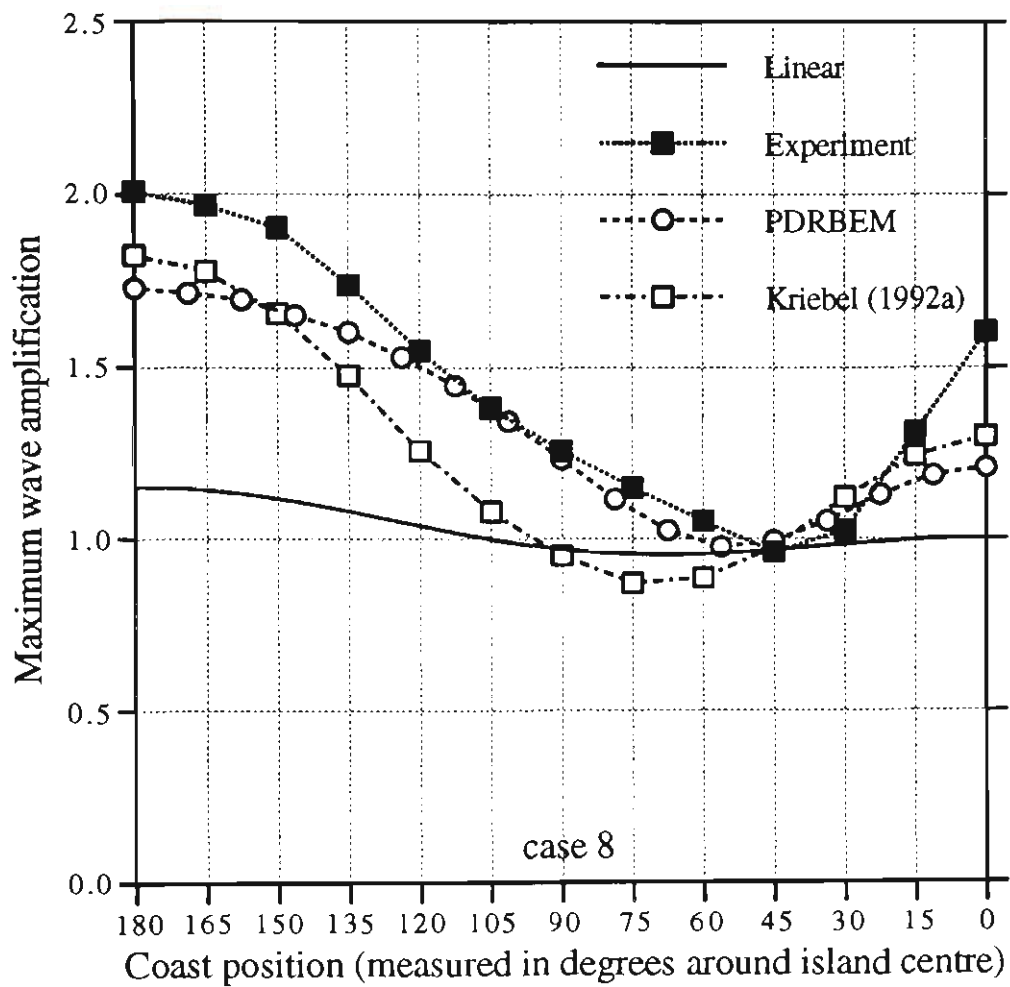


Figure 5.8: Comparison among the experimental data (Kriebel 1990 and 1992a), linear run-ups, the second order diffraction run-ups and the present weakly-nonlinear run-ups for case 8 of cylindrical island.

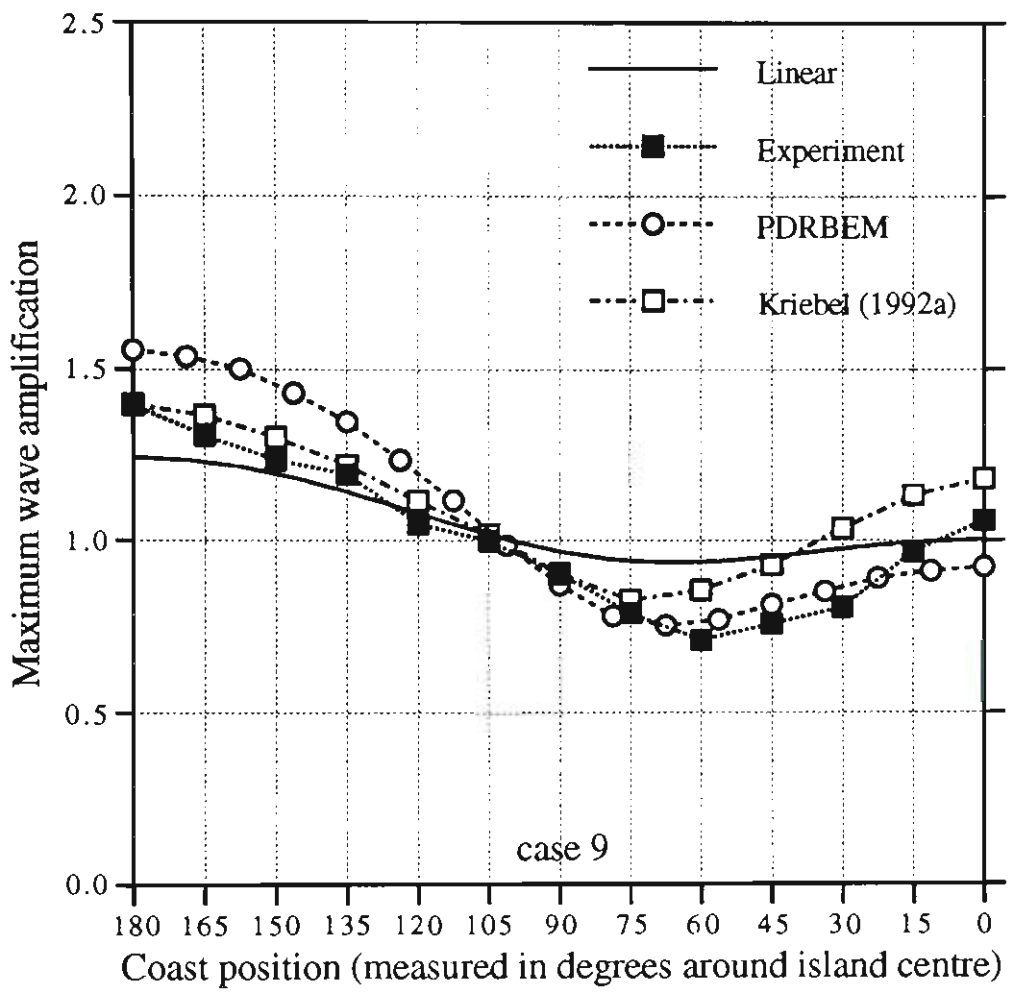


Figure 5.9: Comparison among the experimental data (Kriebel 1990 and 1992a), linear run-ups, the second order diffraction run-ups and the present weakly-nonlinear run-ups for case 9 of cylindrical island.

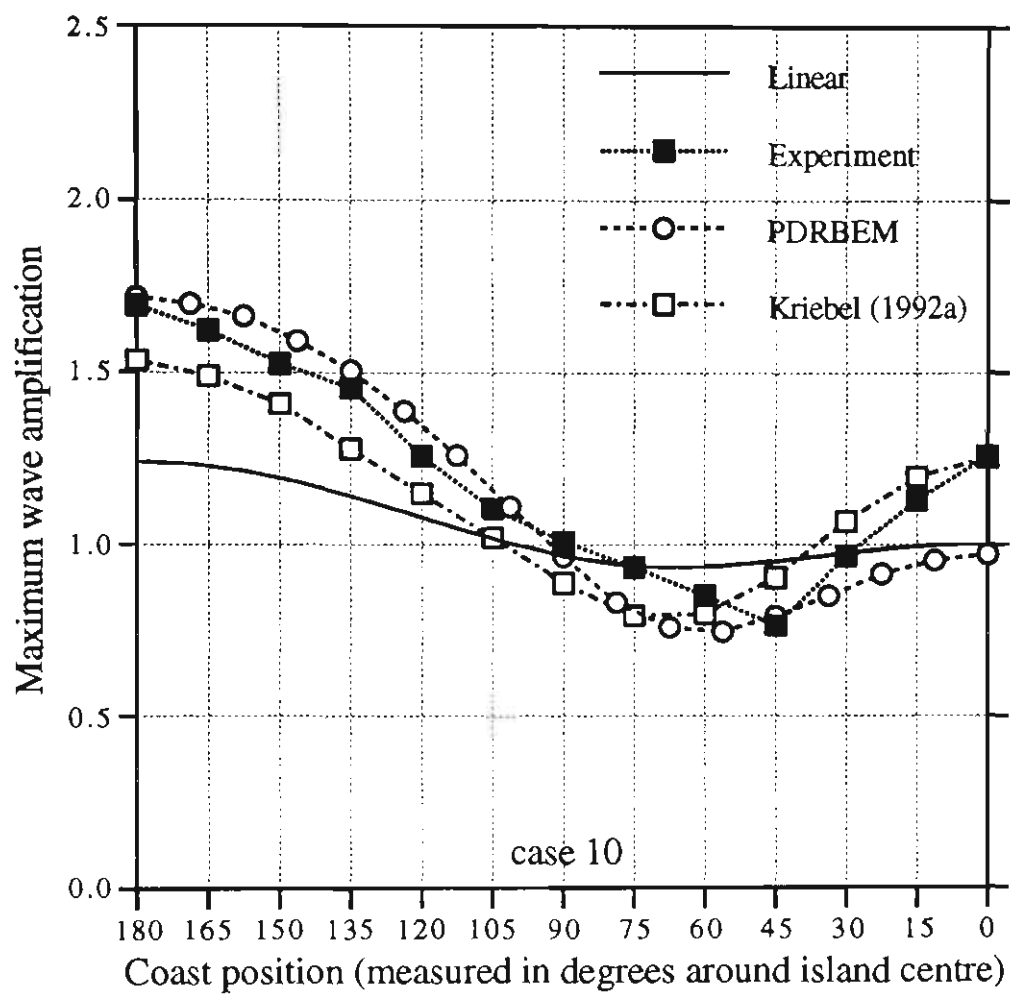


Figure 5.10: Comparison among the experimental data (Kriebel 1990 and 1992a), linear run-ups, the second order diffraction run-ups and the present weakly-nonlinear run-ups for case 10 of cylindrical island.

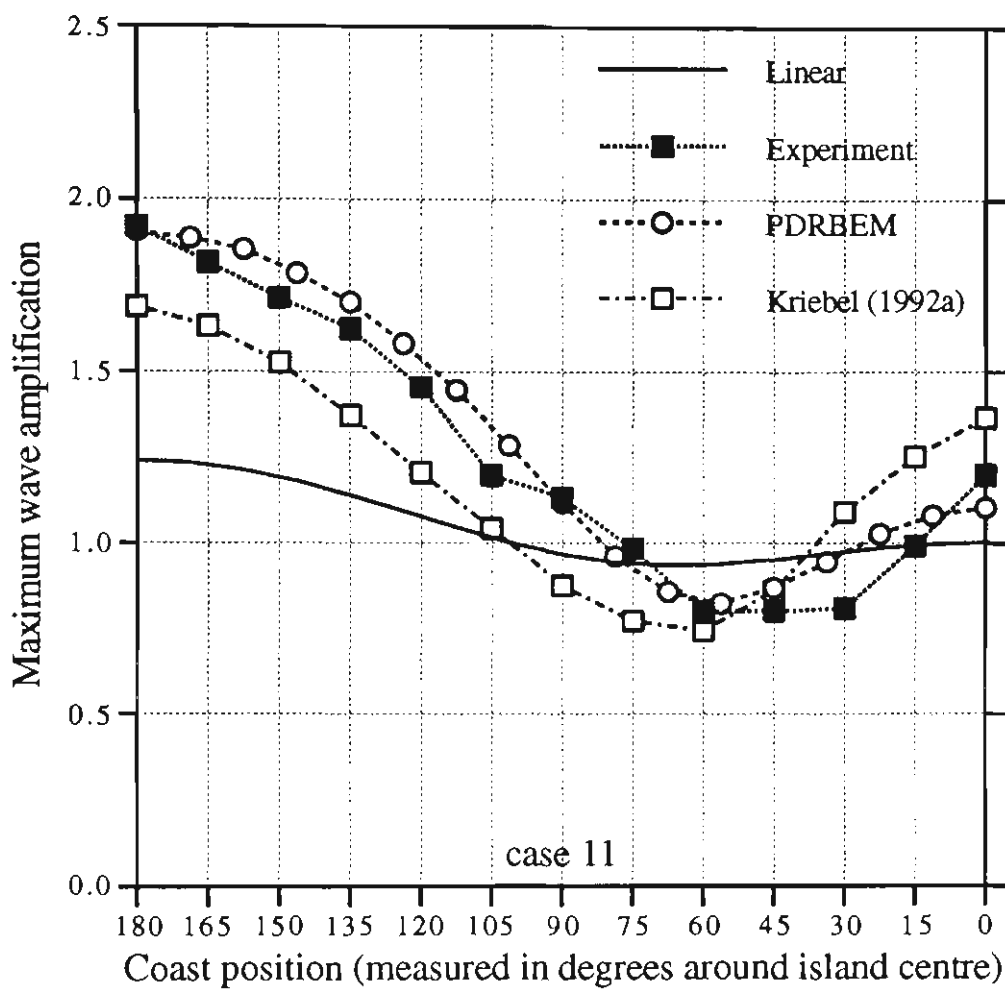


Figure 5.11: Comparison among the experimental data (Kriebel 1990 and 1992a), linear run-ups, the second order diffraction run-ups and the present weakly-nonlinear run-ups for case 11 of cylindrical island.

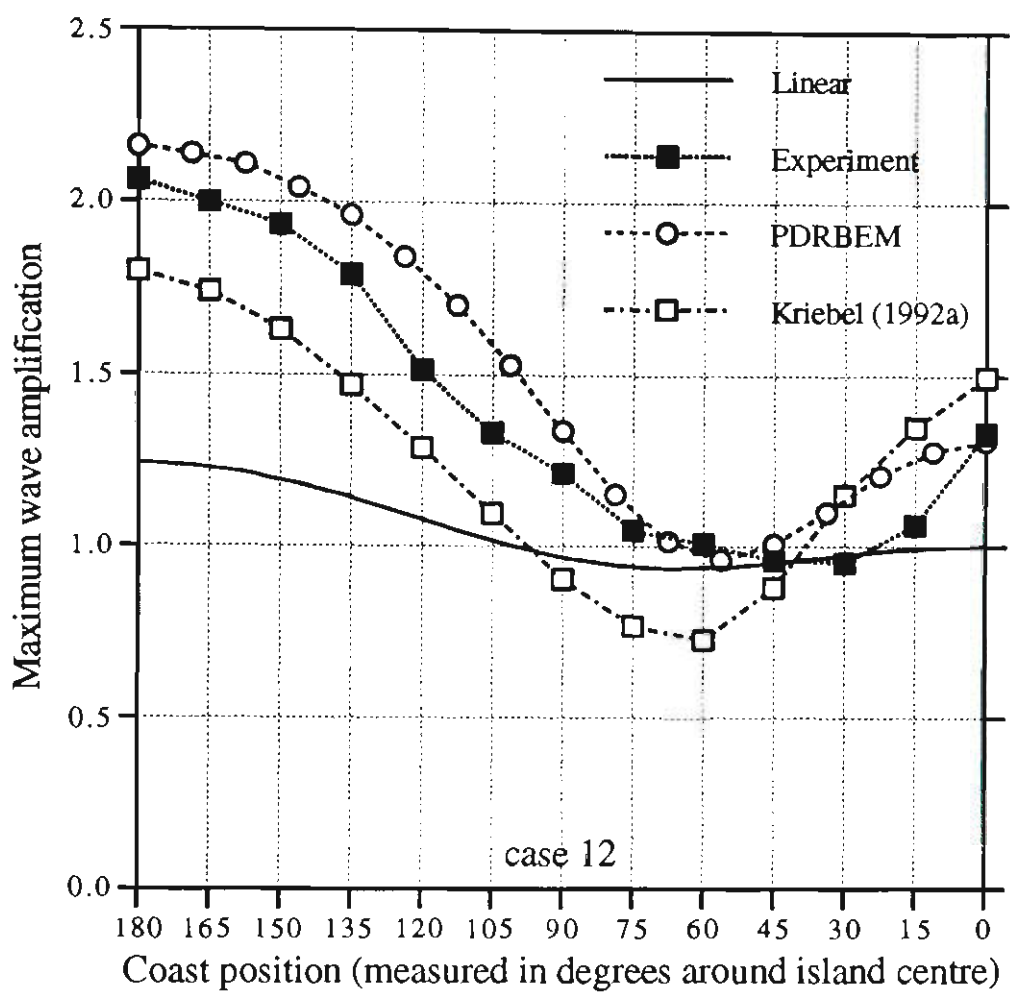


Figure 5.12: Comparison among the experimental data (Kriebel 1990 and 1992a), linear run-ups, the second order diffraction run-ups and the present weakly-nonlinear run-ups for case 12 of cylindrical island.



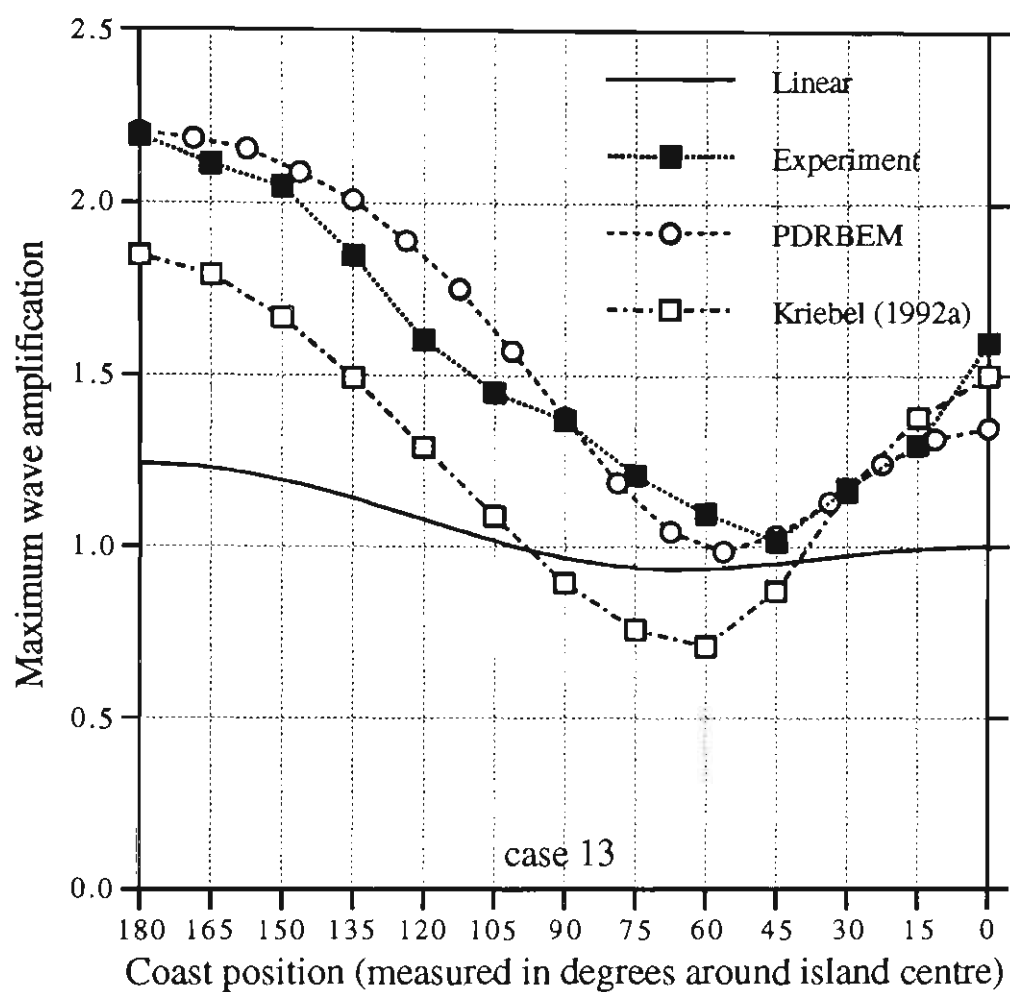


Figure 5.13: Comparison among the experimental data (Kriebel 1990 and 1992a), linear run-ups, the second order diffraction run-ups and the present weakly-nonlinear run-ups for case 13 of cylindrical island.

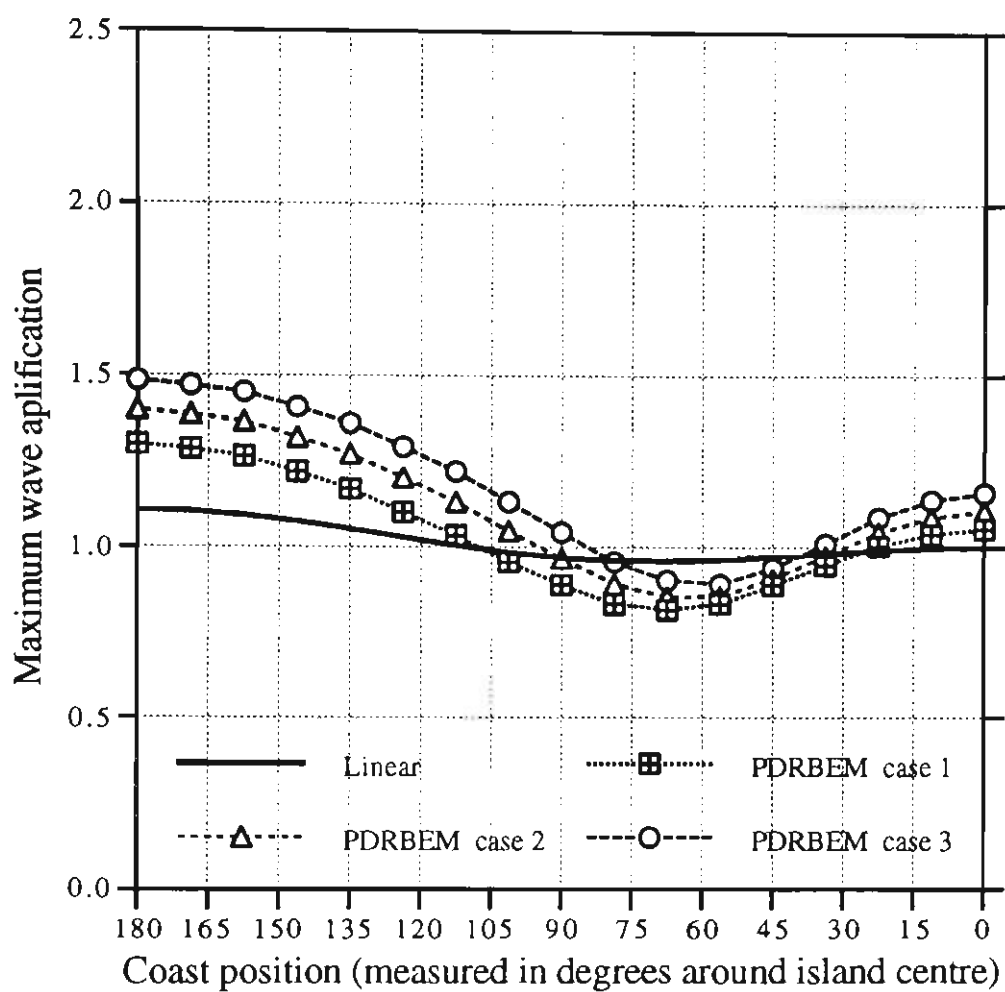


Figure 5.14: Comparison between the linear diffraction run-ups and the present weakly-nonlinear run-ups for cases 1-3 of cylindrical island.

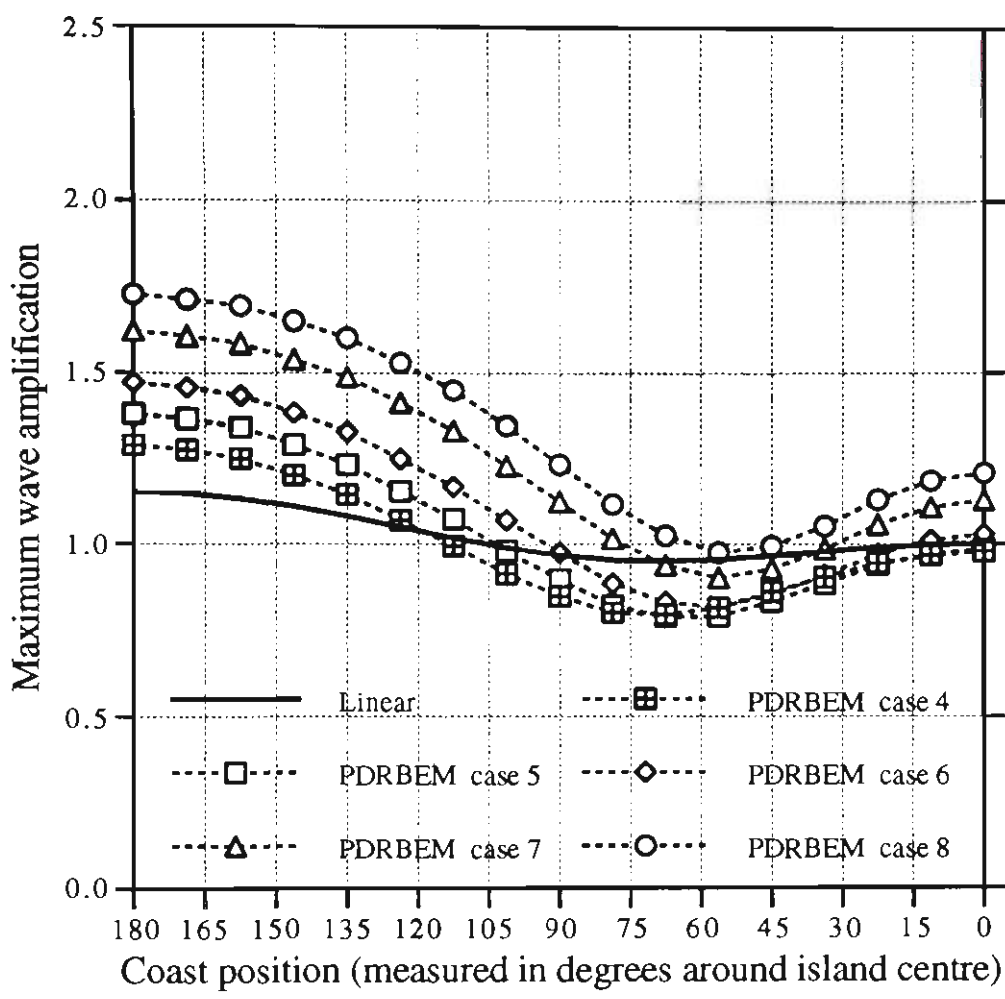


Figure 5.15: Comparison between the linear diffraction run-ups and the present weakly-nonlinear run-ups for cases 4-8 of cylindrical island.

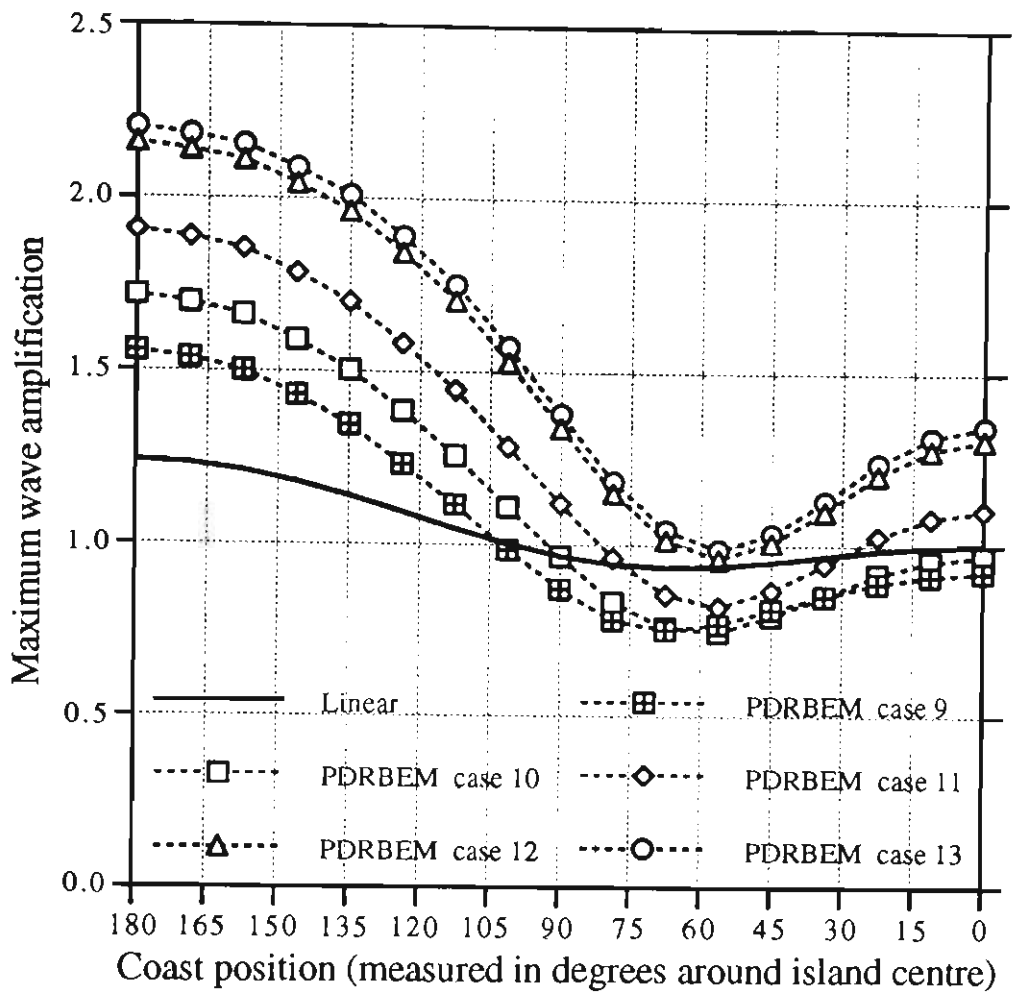


Figure 5.16: Comparison between the linear diffraction run-ups and the present weakly-nonlinear run-ups for cases 9-13 of cylindrical island.

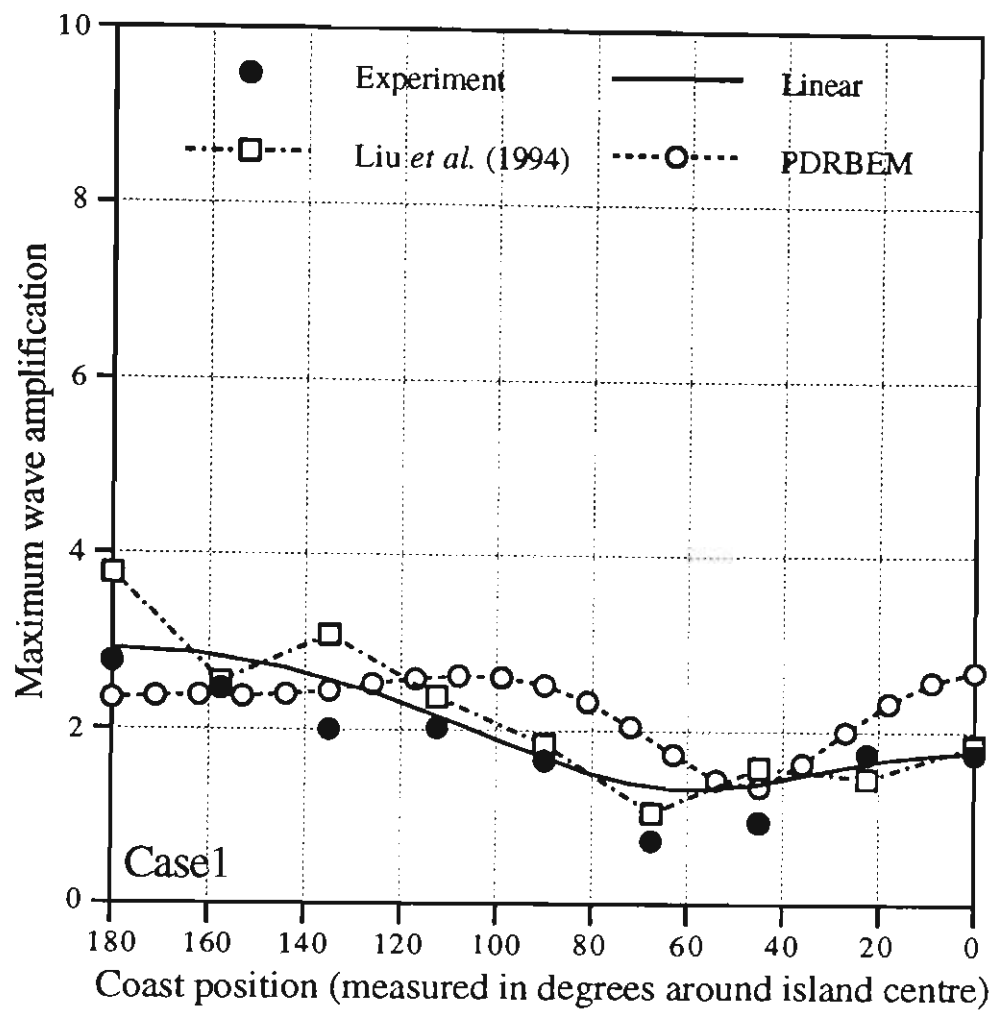


Figure 5.17: Comparison among the experimental data, the linear analytical run-ups (Zhang & Zhu 1994a), the nonlinear shallow-water run-ups (Liu *et al.* 1994) and the PDRBEM run-ups for case 1 of conical island.

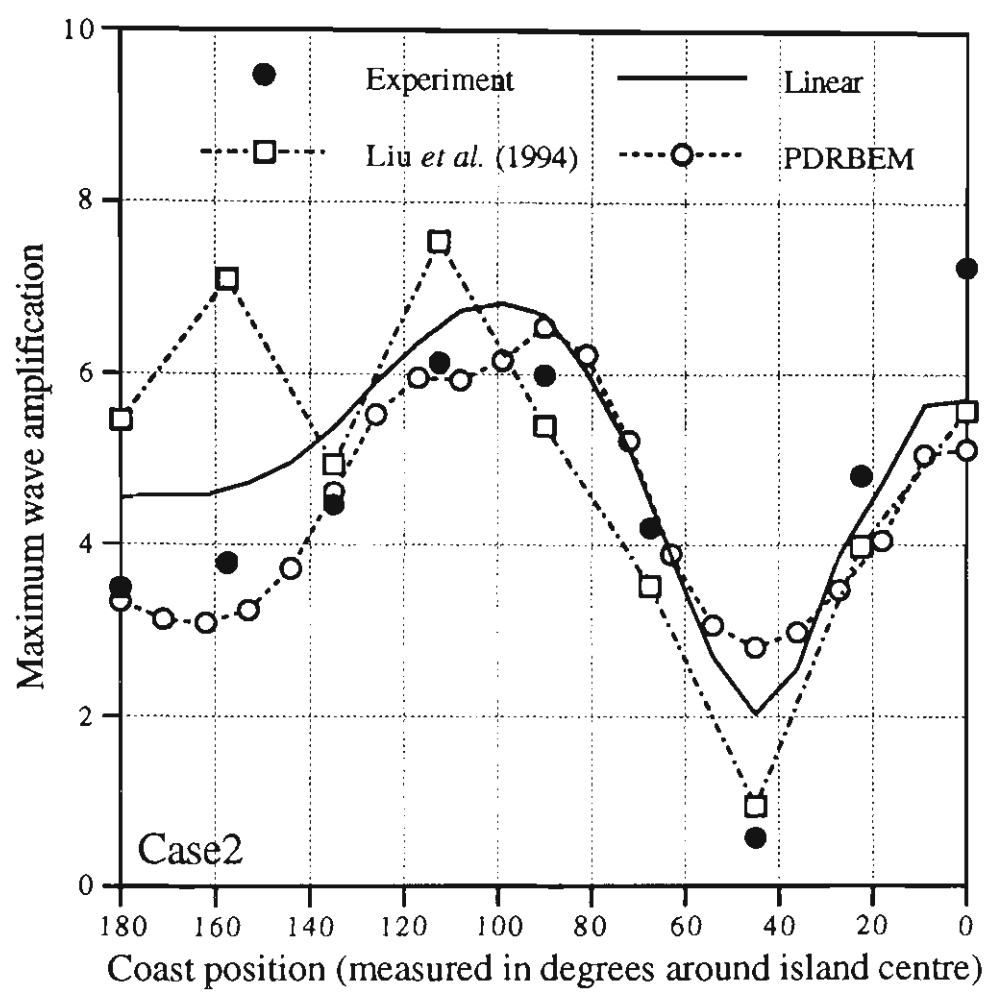


Figure 5.18: Comparison among the experimental data, the linear analytical run-ups (Zhang & Zhu 1994a), the nonlinear shallow-water run-ups (Liu *et al.* 1994) and the PDRBEM run-ups for case 2 of conical island.

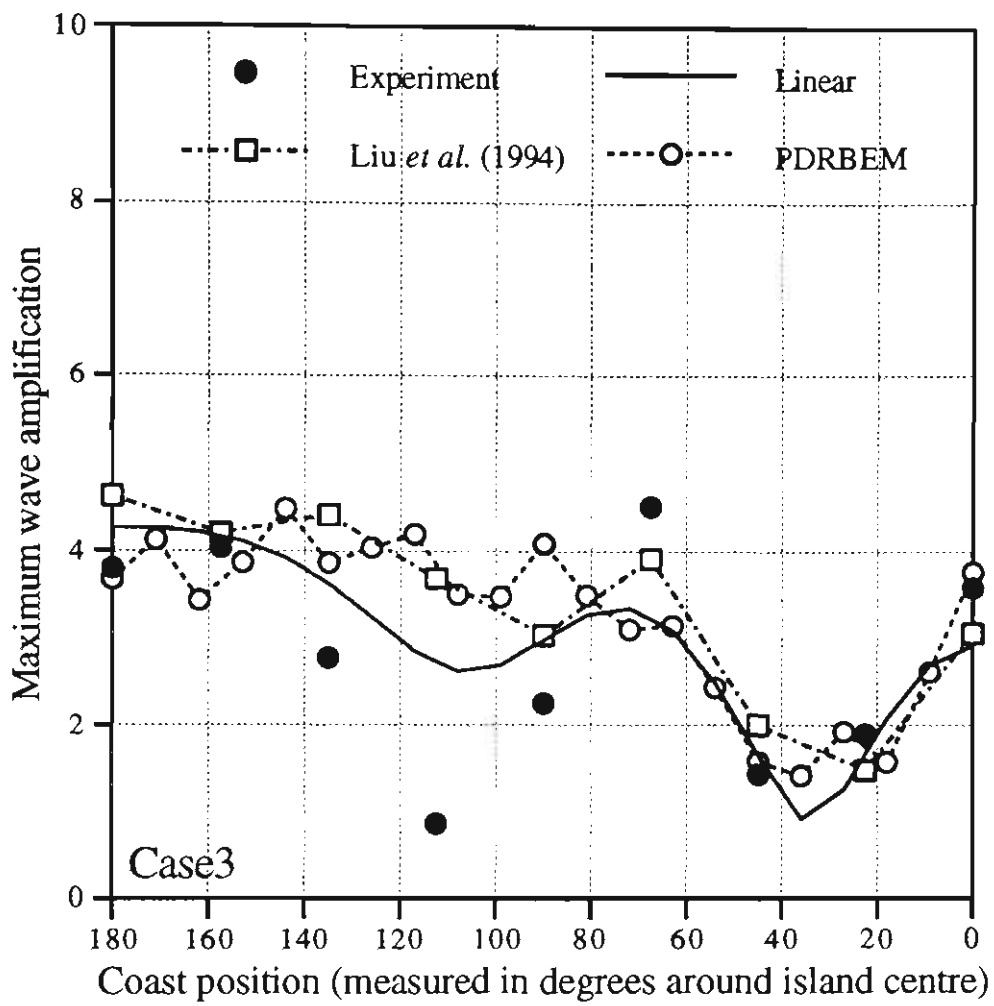


Figure 5.19: Comparison among the experimental data, the linear analytical run-ups (Zhang & Zhu 1994a), the nonlinear shallow-water run-ups (Liu *et al.* 1994) and the PDRBEM run-ups for case 3 of conical island.

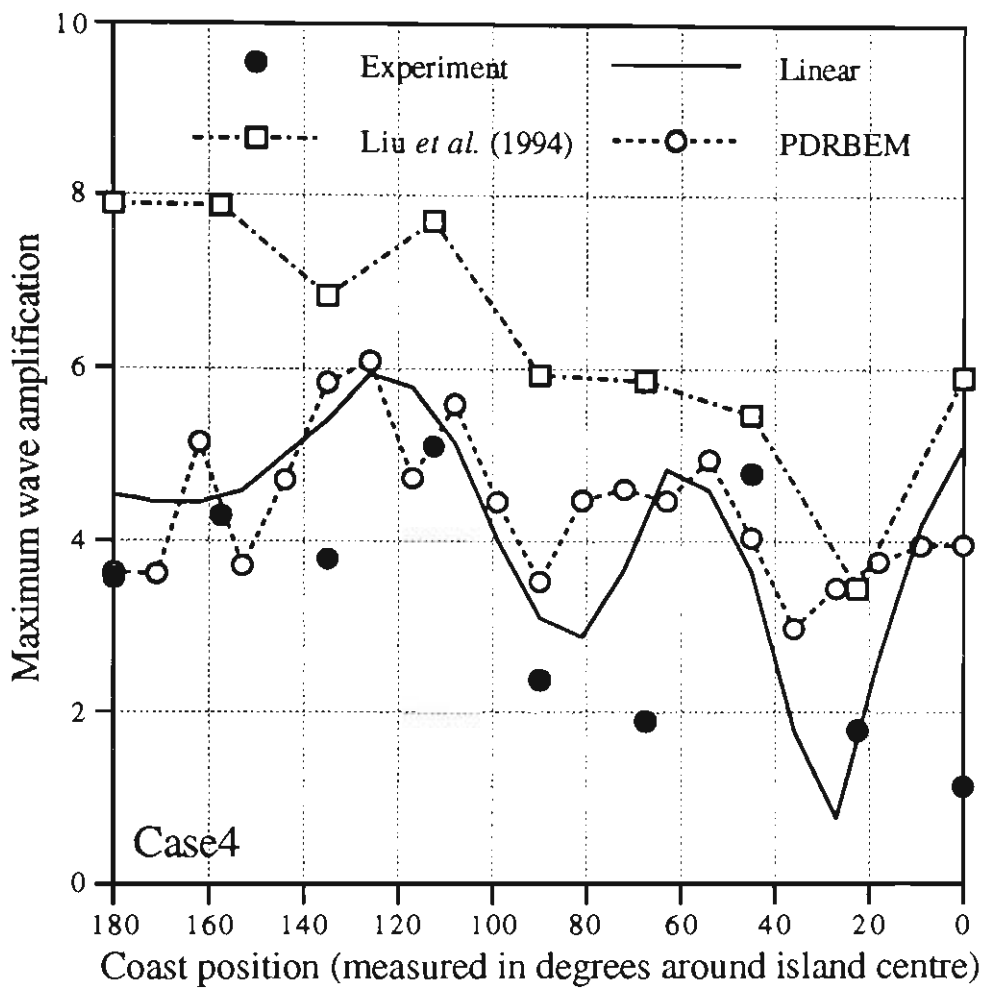


Figure 5.20: Comparison among the experimental data, the linear analytical run-ups (Zhang & Zhu 1994a), the nonlinear shallow-water run-ups (Liu *et al.* 1994) and the PDRBEM run-ups for case 4 of conical island.



# Chapter 6

## Conclusions

Firstly, a general numerical model for wave refraction and diffraction problems, based on the MSWE, has been presented in Chapter 4. The model is an extension to that in Zhu (1993a) with the assumption that the water depth must be nonzero everywhere within the computational domain being completely removed. Numerical results of the run-ups for both Homma's paraboloidal island and three Hawaiian islands have been calculated and compared with previous analytical solutions and numerical solutions. The comparison shows the GDRBEM model is very accurate for long waves (tsunami waves). It is numerically very efficient in comparison with models based on finite elements too. Using the new model, we were able to examine the interaction between the diffraction and refraction effects. It is shown that the diffraction effect is significantly enhanced when there is a combined diffraction and refraction than when there is just diffraction alone.

Then, in Chapter 5 of this thesis, a new numerical model, called the PDRBEM, is also presented for wave diffraction and refraction governed by the Boussinesq equations. To validate this new model, wave diffraction by a vertical cylinder has been calculated and the maximum wave runups around the cylinder have been compared

with experimental results and linear solutions. It is shown that, for water depth ranging from shallow water to near-deep water, the nonlinear effect of the new model for steep waves with the steepness ( $k_o H$ ) ranging from 0.2 to 0.53 is significant. Then, the model is applied to the combined wave diffraction and refraction by a conical island. The nonlinear and linear wave runups around the conical island are calculated and commented upon.

The PDRBEM model is useful for a number of reasons. Firstly it is more accurate than linear models when the wave steepness is large enough for nonlinear effects to be important. Moreover, since frequency decomposition has been used and the time-dependent governing equations have been transformed into three time-independent linear equations, our model does not require time-marching. Also, the dimensionality in our model has been reduced by one because of the application of DRBEM. Hence our model is much more computationally efficient than other numerical schemes which include nonlinear effects.

# Appendix A

## Numerical discretization

Equation (4.2.11) can be discretized by dividing the boundary curves,  $\Gamma_o$  and  $\Gamma_i$  into a finite number of small sections, on each of which, the unknown function is replaced by an interpolation function, resulting the integration on each of these “elements” being carried out either analytically or numerically. Constant elements are the simplest interpolation when the unknown function is assumed to be constant across each element.

If the constant boundary elements are used, the discretized form of equation (4.2.11) is then

$$\begin{aligned}
 & c_\xi G(\xi) \eta(\xi) - \sum_{k=1}^{n+m} \left( \frac{\partial G}{\partial \mathbf{n}} \eta \right) |_{\mathbf{x}_k} g_{\xi k} + G_i \sum_1^n \eta |_{\mathbf{x}_k} h_{\xi k} - G_i \sum_1^n q |_{\mathbf{x}_k} g_{\xi k} \\
 = & \sum_{j=1}^{n+m+l} \alpha_j \left[ c_\xi^{(i)} \hat{\eta}_j(\xi) + \sum_{k=1}^{n+m} \hat{\eta}_j |_{\mathbf{x}_k} h_{\xi k} - \sum_{k=1}^{n+m} \hat{q}_j |_{\mathbf{x}_k} g_{\xi k} \right] - \\
 & - G_o \left[ -c_\xi^{(o)} \eta^{(I)}(\xi) + \sum_{k=n+1}^{n+m} \eta^{(I)} |_{\mathbf{x}_k} h_{\xi k} - \sum_{k=n+1}^{n+m} q^{(I)} |_{\mathbf{x}_k} g_{\xi k} \right], \quad (\text{A.0.1})
 \end{aligned}$$

where

$$g_{\xi k} = \int_{e_k} \eta^*(\xi, \mathbf{x}) d\Gamma, \quad h_{\xi k} = \int_{e_k} q^*(\xi, \mathbf{x}) d\Gamma. \quad (\text{A.0.2})$$

After placing the source point  $\xi$  in equation (A.0.1) at all  $n + m + l$  collocation points

$\mathbf{x}_j$ , one obtains a linear system of order  $n + m + l$  as

$$\begin{aligned}
 & [\mathbf{C} - (\mathbf{G}_i + \mathbf{G}_o)\mathbf{G}_n]\mathbf{U} + \mathbf{G}_i(\mathbf{H}_i\mathbf{U} - \mathbf{G}_i\mathbf{Q}) \\
 = & \left[ (\mathbf{C}^{(i)} + \mathbf{H}_i + \mathbf{H}_o)\hat{\mathbf{U}} - (\mathbf{G}_i + \mathbf{G}_o)\hat{\mathbf{Q}} \right] \mathbf{F}^{-1}\mathbf{R} + \\
 & + \mathbf{G}_o[(\mathbf{C}^{(o)} - \mathbf{H}_o)\mathbf{U}^{(I)} + \mathbf{G}_o\mathbf{Q}^{(I)}],
 \end{aligned} \tag{A.0.3}$$

where

$$\begin{aligned}
 \mathbf{C} &= \text{diag}(0.5G|_{\mathbf{x}_1}, \dots, 0.5G|_{\mathbf{x}_n}, G|_{\mathbf{x}_{n+1}}, \dots, G|_{\mathbf{x}_{nml}}), \\
 \mathbf{G}_n &= \text{diag}\left(\frac{\partial G}{\partial \mathbf{n}}|_{\mathbf{x}_1}, \dots, \frac{\partial G}{\partial \mathbf{n}}|_{\mathbf{x}_{nm}}, \underbrace{0, \dots, 0}_l\right), \\
 \mathbf{C}^{(o)} &= \text{diag}(\underbrace{0, \dots, 0}_n, \underbrace{0.5, \dots, 0.5}_m, \underbrace{0, \dots, 0}_l), \\
 \mathbf{C}^{(i)} &= \text{diag}(\underbrace{0.5, \dots, 0.5}_n, \underbrace{0.5, \dots, 0.5}_m, \underbrace{1, \dots, 1}_l), \\
 \mathbf{U} &= (\eta|_{\mathbf{x}_1}, \dots, \eta|_{\mathbf{x}_{nml}})^T, \\
 \mathbf{Q} &= (q|_{\mathbf{x}_1}, \dots, q|_{\mathbf{x}_{nm}}, \underbrace{0, \dots, 0}_l)^T, \\
 \mathbf{U}^{(I)} &= (\eta^{(I)}|_{\mathbf{x}_1}, \dots, \eta^{(I)}|_{\mathbf{x}_{nml}})^T, \\
 \mathbf{Q}^{(I)} &= (q^{(I)}|_{\mathbf{x}_1}, \dots, q^{(I)}|_{\mathbf{x}_{nm}}, \underbrace{0, \dots, 0}_l)^T, \\
 \hat{\mathbf{U}} &= \begin{bmatrix} \hat{\eta}_{11} & \dots & \hat{\eta}_{1nml} \\ \vdots & \ddots & \vdots \\ \hat{\eta}_{nml1} & \dots & \hat{\eta}_{nml\ nml} \end{bmatrix},
 \end{aligned}$$

$$\hat{\mathbf{Q}} = \begin{bmatrix} \hat{q}_{11} & \dots & \hat{q}_{1\underline{nm}l} \\ \vdots & \ddots & \vdots \\ \hat{q}_{\underline{nm}1} & \dots & \hat{q}_{\underline{nm}\underline{nm}l} \\ 0 & \dots & 0 \\ \vdots & \ddots & \vdots \\ 0 & \dots & 0 \end{bmatrix}_{\underline{nm}l \times \underline{nm}l}$$

with  $\underline{nm} = n + m$ ,  $\underline{nm}l = n + m + l$ , and  $\hat{\eta}_{ij}$  and  $\hat{q}_{ij}$  being the values of  $\hat{\eta}_j$  and  $\hat{q}_j$  on point  $\mathbf{x}_i$ , respectively, and

$$\begin{aligned} \mathbf{H}_i &= \begin{bmatrix} h_{11} & \dots & h_{1n} & 0 & \dots & 0 & 0 & \dots & 0 \\ \vdots & \ddots & \vdots & \vdots & \ddots & \vdots & \vdots & \ddots & \vdots \\ h_{\underline{nm}l1} & \dots & h_{\underline{nm}ln} & 0 & \dots & 0 & 0 & \dots & 0 \end{bmatrix}_{\underline{nm}l \times \underline{nm}l}, \\ \mathbf{H}_o &= \begin{bmatrix} 0 & \dots & 0 & h_{1n+1} & \dots & h_{1\underline{nm}} & 0 & \dots & 0 \\ \vdots & \ddots & \vdots & \vdots & \ddots & \vdots & \vdots & \ddots & \vdots \\ 0 & \dots & 0 & h_{\underline{nm}ln+1} & \dots & h_{\underline{nm}l\underline{nm}} & 0 & \dots & 0 \end{bmatrix}_{\underline{nm}l \times \underline{nm}l}, \\ \mathbf{G}_i &= \begin{bmatrix} g_{11} & \dots & g_{1n} & 0 & \dots & 0 & 0 & \dots & 0 \\ \vdots & \ddots & \vdots & \vdots & \ddots & \vdots & \vdots & \ddots & \vdots \\ g_{\underline{nm}l1} & \dots & g_{\underline{nm}ln} & 0 & \dots & 0 & 0 & \dots & 0 \end{bmatrix}_{\underline{nm}l \times \underline{nm}l}, \\ \mathbf{G}_o &= \begin{bmatrix} 0 & \dots & 0 & g_{1n+1} & \dots & g_{1\underline{nm}} & 0 & \dots & 0 \\ \vdots & \ddots & \vdots & \vdots & \ddots & \vdots & \vdots & \ddots & \vdots \\ 0 & \dots & 0 & g_{\underline{nm}ln+1} & \dots & g_{\underline{nm}l\underline{nm}} & 0 & \dots & 0 \end{bmatrix}_{\underline{nm}l \times \underline{nm}l}. \end{aligned}$$

Furthermore, according to Partridge & Brebbia (1989), we can express  $\mathbf{R}$  as

$$\mathbf{R} = [\mathbf{K}^2 \mathbf{G} + \nabla^2 \mathbf{G} + (\mathbf{G}_x \mathbf{F}_x + \mathbf{G}_y \mathbf{F}_y) \mathbf{F}^{-1}] \mathbf{U} \quad (\text{A.0.4})$$

with

$$\begin{aligned}
 \mathbf{F}_x &= \left[ \frac{\partial f_j}{\partial x} \Big|_{\mathbf{x}_i} \right]_{\underline{nm}l \times \underline{nm}l}, \\
 \mathbf{F}_y &= \left[ \frac{\partial f_j}{\partial y} \Big|_{\mathbf{x}_i} \right]_{\underline{nm}l \times \underline{nm}l}, \\
 \mathbf{G} &= \text{diag}(G|_{\mathbf{x}_1}, \dots, G|_{\mathbf{x}_{\underline{nm}l}}), \\
 \mathbf{G}_x &= \text{diag}\left(\frac{\partial G}{\partial x} \Big|_{\mathbf{x}_1}, \dots, \frac{\partial G}{\partial x} \Big|_{\mathbf{x}_{\underline{nm}l}}\right), \\
 \mathbf{G}_y &= \text{diag}\left(\frac{\partial G}{\partial y} \Big|_{\mathbf{x}_1}, \dots, \frac{\partial G}{\partial y} \Big|_{\mathbf{x}_{\underline{nm}l}}\right), \\
 \nabla^2 G &= \text{diag}(\nabla^2 G|_{\mathbf{x}_1}, \dots, \nabla^2 G|_{\mathbf{x}_{\underline{nm}l}}), \\
 \mathbf{K}^2 &= \text{diag}(k_o^2 - k^2|_{\mathbf{x}_1}, \dots, k_o^2 - k^2|_{\mathbf{x}_n}, \underbrace{0, \dots, 0}_m, k_o^2 - k^2|_{\mathbf{x}_{\underline{nm}+1}}, \dots, k_o^2 - k^2|_{\mathbf{x}_{\underline{nm}l}}).
 \end{aligned}$$

So finally, equation (A.0.3) becomes

$$[\mathbf{C} - (\mathbf{G}_i + \mathbf{G}_o)\mathbf{G}_n + G_i\mathbf{H}_i - \mathbf{S}]\mathbf{U} - G_i\mathbf{G}_i\mathbf{Q} = G_o[(\mathbf{C}^{(o)} - \mathbf{H}_o)\mathbf{U}^{(I)} + \mathbf{G}_o\mathbf{Q}^{(I)}] \quad (\text{A.0.5})$$

with

$$\mathbf{S} = \left[ (\mathbf{C}^{(i)} + \mathbf{H}_i + \mathbf{H}_o)\hat{\mathbf{U}} - (\mathbf{G}_i + \mathbf{G}_o)\hat{\mathbf{Q}} \right] \mathbf{F}^{-1} \left[ \mathbf{K}^2\mathbf{G} + \nabla^2\mathbf{G} + (\mathbf{G}_x\mathbf{F}_x + \mathbf{G}_y\mathbf{F}_y) \mathbf{F}^{-1} \right].$$

By denoting

$$\mathbf{T} = \mathbf{C} - (\mathbf{G}_i + \mathbf{G}_o)\mathbf{G}_n + G_i\mathbf{H}_i - \mathbf{S}, \quad \mathbf{W} = -G_i\mathbf{G}_i, \quad \mathbf{P} = G_o(\mathbf{C}^{(o)} - \mathbf{H}_o), \quad \mathbf{V} = G_o\mathbf{G}_o,$$

equation (A.0.5) can be rewritten into a real linear system

$$\begin{aligned}
 & \begin{pmatrix} \mathbf{T}_r & -\mathbf{T}_i \\ \mathbf{T}_i & \mathbf{T}_r \end{pmatrix} \begin{pmatrix} \text{Re}\mathbf{U} \\ \text{Im}\mathbf{U} \end{pmatrix} + \begin{pmatrix} \mathbf{W}_r & -\mathbf{W}_i \\ \mathbf{W}_i & \mathbf{W}_r \end{pmatrix} \begin{pmatrix} \text{Re}\mathbf{Q} \\ \text{Im}\mathbf{Q} \end{pmatrix} \\
 &= \begin{pmatrix} \mathbf{P}_r & -\mathbf{P}_i \\ \mathbf{P}_i & \mathbf{P}_r \end{pmatrix} \begin{pmatrix} \text{Re}\mathbf{U}^{(I)} \\ \text{Im}\mathbf{U}^{(I)} \end{pmatrix} + \begin{pmatrix} \mathbf{V}_r & -\mathbf{V}_i \\ \mathbf{V}_i & \mathbf{V}_r \end{pmatrix} \begin{pmatrix} \text{Re}\mathbf{Q}^{(I)} \\ \text{Im}\mathbf{Q}^{(I)} \end{pmatrix}
 \end{aligned}$$

with

$$\begin{aligned} \mathbf{T} &= \mathbf{T}_r + i\mathbf{T}_i, \quad \mathbf{W} = \mathbf{W}_r + i\mathbf{W}_i, \\ \mathbf{P} &= \mathbf{P}_r + i\mathbf{P}_i, \quad \mathbf{V} = \mathbf{V}_r + i\mathbf{V}_i. \end{aligned}$$

If other type of boundary elements are used, the corresponding discretized forms of equation (4.2.11) will be slightly different.

## Appendix B

### $G(x, y)$ and its derivatives for nonzero water depth

Since

$$G(x, y) = \frac{g}{2k} \tanh kh \left( 1 + \frac{2kh}{\sinh 2kh} \right) \quad (\text{B.0.1})$$

is an implicit function with  $k(x, y)$  being implicitly defined by the dispersion relation:

$$gk \tanh kh = \omega^2, \quad (\text{B.0.2})$$

the calculation of the partial derivatives  $G_x$ ,  $G_y$ ,  $G_n$  and  $\nabla^2 G$  is now quite involved.

For simplicity, let  $L(x, y) = k(x, y)h(x, y)$ . Using the dispersion relation, i.e.,

$$L \tanh L = \frac{\omega^2 h}{g}$$

or

$$k = \frac{\omega^2}{g \cdot \tanh L},$$



we have the following fundamental relationships:

$$\begin{aligned}
 L_x &= \frac{\omega^2/g}{\tanh L + L/\cosh^2 L} h_x \\
 &= \frac{gk\omega^2}{g\omega^2 - h\omega^4 + hg^2k^2} h_x \\
 &= C_1 h_x,
 \end{aligned} \tag{B.0.3}$$

$$\begin{aligned}
 k_x &= \frac{\omega^2 - 1/\tanh^2 L}{g \tanh^2 L} L_x \\
 &= \left( \frac{\omega^2}{g} - \frac{gk^2}{\omega^2} \right) C_1 h_x \\
 &= C_1 C_2 h_x,
 \end{aligned} \tag{B.0.4}$$

$$\begin{aligned}
 L_{xx} &= C_1 h_{xx} + \frac{g\omega^2 k_x (g\omega^2 - h\omega^4 + hg^2k^2) - gk\omega^2 (-\omega^4 h_x + g^2k^2 h_x + 2g^2khk_x)}{(g\omega^2 - h\omega^4 + hg^2k^2)^2} h_x \\
 &= C_1 h_{xx} + \frac{g\omega^2 C_1 C_2 - C_1 (-\omega^4 + g^2k^2 + 2g^2khC_1 C_2)}{g\omega^2 - h\omega^4 + hg^2k^2} (h_x)^2 \\
 &= C_1 h_{xx} + \frac{gk\omega^2 C_1 C_2 - C_1 k (-g\omega^2 C_2 + 2g^2khC_1 C_2)}{k(g\omega^2 - h\omega^4 + hg^2k^2)} (h_x)^2 \\
 &= C_1 h_{xx} + C_1^2 \cdot 2C_2 \frac{g\omega^2 - h\omega^4}{k(g\omega^2 - h\omega^4 + hg^2k^2)} (h_x)^2 \\
 &= C_1 h_{xx} + C_1^2 C_3 (h_x)^2,
 \end{aligned} \tag{B.0.5}$$

$$\begin{aligned}
 k_{xx} &= C_1 C_2 h_{xx} + C_1^2 C_2 C_3 (h_x)^2 + C_1 \frac{-2gkk_x}{\omega^2} h_x \\
 &= C_1 C_2 h_{xx} + C_1^2 C_2 \left( C_3 - \frac{2gk}{\omega^2} \right) (h_x)^2 \\
 &= C_1 C_2 h_{xx} + C_4 (h_x)^2,
 \end{aligned} \tag{B.0.6}$$

where

$$C_1 = \frac{gk\omega^2}{g\omega^2 - h\omega^4 + hg^2k^2}, \quad C_2 = \frac{\omega^2}{g} - \frac{gk^2}{\omega^2},$$

$$C_3 = 2C_2 \frac{g\omega^2 - h\omega^4}{k(g\omega^2 - h\omega^4 + hg^2k^2)}, \quad C_4 = C_1^2 C_2 (C_3 - \frac{2gk}{\omega^2}).$$

So, from (B.0.3) to (B.0.6), we have

$$\begin{aligned} G_x &= \frac{g}{2} \left\{ \left( -\frac{h}{k} k_x \right) \left[ \frac{\omega^2}{gk^2h} + \left( 1 - \frac{\omega^4}{g^2k^2} \right) \right] + 2 \left( \frac{1}{k} L_x \right) \left( 1 - \frac{\omega^2h}{g} \right) \left( 1 - \frac{\omega^4}{g^2k^2} \right) \right\} \\ &= \frac{g}{2} \left\{ \left( -\frac{h}{k} k_x \right) T_1 + 2 \left( \frac{1}{k} L_x \right) T_2 \right\} \\ &= \frac{gC_1}{2k} (2T_2 - C_2 T_1 h) h_x \end{aligned} \quad (\text{B.0.7})$$

with

$$\begin{aligned} T_1 &= \frac{\omega^2}{gk^2h} - \frac{\omega^4}{g^2k^2} + 1, \\ T_2 &= \left( 1 - \frac{\omega^2h}{g} \right) \left( 1 - \frac{\omega^4}{g^2k^2} \right). \end{aligned}$$

Similarly, we also have

$$G_y = \frac{gC_1}{2k} (2T_2 - C_2 T_1 h) h_y, \quad (\text{B.0.8})$$

$$G_n = \frac{gC_1}{2k} (2T_2 - C_2 T_1 h) h_n. \quad (\text{B.0.9})$$

Next, we have

$$\nabla^2 G = \frac{g}{2} \left\{ S_1 T_1 - \frac{h}{k} k_x S_2 + S_3 T_2 + \frac{2}{k} L_x S_4 \right\},$$

where

$$\begin{aligned} S_1 &= \frac{\partial}{\partial x} \left( -\frac{h}{k} k_x \right), & S_2 &= \frac{\partial T_1}{\partial x}, \\ S_3 &= 2 \frac{\partial}{\partial x} \left( \frac{1}{k} L_x \right), & S_4 &= \frac{\partial T_2}{\partial x}. \end{aligned}$$

By simple differentiation, we obtain

$$\begin{aligned}
 S_1 &= -\left[\frac{1}{k}k_x h_x - \frac{h}{k^2}k_x^2 + \frac{h}{k}k_{xx}\right], \\
 S_2 &= \frac{\omega^2}{gk^3}\left[\left(\frac{2\omega^2}{g} - \frac{1}{h}\right)k_x - \frac{1}{h^2}L_x\right], \\
 S_3 &= 2\left(\frac{1}{k}L_{xx} - \frac{1}{k^2}L_x k_x\right), \\
 S_4 &= \frac{\omega^2}{g}\left(\frac{\omega^4}{g^2 k^2} - 1\right)h_x + \frac{2\omega^4}{g^2 k^3}\left(1 - \frac{\omega^2 h}{g}\right)k_x.
 \end{aligned}$$

Note that in (B.0.1), there is a symmetry in  $x, y$  as far as derivatives are concerned, so formulae for  $G_y$  and  $G_{yy}$  are similar. The Laplacian of  $G(x, y)$  takes the form

$$\begin{aligned}
 \nabla^2 G &= \frac{g}{2} \left\{ \frac{2T_2}{k} \nabla^2 L - \frac{T_1 h}{k} \nabla^2 k + \left[ \frac{T_1 h}{k^2} - \frac{\omega^2 h}{gk^4} \left( \frac{2\omega^2}{g} - \frac{1}{h} \right) \right] |\nabla k|^2 \right. \\
 &\quad + \left[ \frac{\omega^2}{ghk^4} - \frac{2T_2}{k^2} + \frac{4\omega^4}{g^2 k^4} \left( 1 - \frac{\omega^2 h}{g} \right) \right] \nabla L \cdot \nabla k \\
 &\quad \left. + \frac{2\omega^2}{gk} \left( \frac{\omega^4}{g^2 k^2} - 1 \right) \nabla L \cdot \nabla h - \frac{T_1}{k} \nabla k \cdot \nabla h \right\}.
 \end{aligned}$$

Noticing that

$$\begin{aligned}
 \nabla^2 L &= C_1^2 C_3 |\nabla h|^2 + C_1 \nabla^2 h, \\
 \nabla^2 k &= C_4 |\nabla h|^2 + C_1 C_2 \nabla^2 h, \\
 |\nabla k|^2 &= C_1^2 C_2^2 |\nabla h|^2, \\
 \nabla L \cdot \nabla k &= C_1^2 C_2 |\nabla h|^2, \\
 \nabla L \cdot \nabla h &= C_1 |\nabla h|^2, \\
 \nabla k \cdot \nabla h &= C_1 C_2 |\nabla h|^2,
 \end{aligned}$$

we have

$$\nabla^2 G = \frac{g}{2} (C_5 \nabla^2 h + C_6 |\nabla h|^2) \tag{B.0.10}$$

with

$$\begin{aligned}
 C_5 &= \frac{C_1}{k}(2T_2 - C_2 T_1 h), \\
 C_6 &= \frac{2T_2}{k} C_1^2 C_3 - \frac{T_1}{k} C_4 h + \frac{2\omega^2}{gk} \left( \frac{\omega^4}{g^2 k^2} - 1 \right) C_1 \\
 &\quad - \frac{T_1}{k} C_1 C_2 + \frac{h}{k^2} C_1^2 C_2^2 \left[ T_1 - \frac{\omega^2}{gk^2} \left( \frac{2\omega^2}{g} - \frac{1}{h} \right) \right] \\
 &\quad + \frac{2}{k^2} C_1^2 C_2 \left[ \frac{\omega^2}{2ghk^2} - T_2 + \frac{2\omega^4}{g^2 k^2} \left( 1 - \frac{\omega^2 h}{g} \right) \right].
 \end{aligned}$$

# Appendix C

## $G(x, y)$ and its derivatives for zero water depth

Unlike all the derivatives worked out in Appendix B, which are relatively straightforward although the derivation was quite involved and tedious, care must be taken when the water depth becomes zero as some limiting processes must be taken and they can be quite subtle.

On  $\Gamma_i$ , since  $h(x, y) = 0$ ,  $G(x, y)$  is singular. So we need to derive the asymptotic formulae for  $G$  and its partial derivatives and directional derivative along  $\Gamma_i$ .

Firstly, after a great deal of mathematical manipulations, we can obtain these limits as

$$\begin{array}{ll}
 \lim_{h \rightarrow 0} G = 0, & \lim_{h \rightarrow 0} k^2 G = \omega^2, \\
 \lim_{h \rightarrow 0} \frac{1}{k} = 0, & \lim_{h \rightarrow 0} kL = \frac{\omega^2}{g}, \\
 \lim_{h \rightarrow 0} \frac{1}{k} L_x = \frac{1}{2} h_x, & \lim_{h \rightarrow 0} \frac{1}{k} L_y = \frac{1}{2} h_y, \\
 \lim_{h \rightarrow 0} \frac{h}{k} k_x = -\frac{1}{2} h_x, & \lim_{h \rightarrow 0} \frac{h}{k} k_y = -\frac{1}{2} h_y, \\
 \lim_{h \rightarrow 0} \frac{1}{k^3} L_{xx} = -\frac{g}{4\omega^2} h_x^2, & \lim_{h \rightarrow 0} \frac{1}{k^3} L_{yy} = -\frac{g}{4\omega^2} h_y^2, \\
 \lim_{h \rightarrow 0} \frac{1}{k^5} k_{xx} = \frac{3g^2}{4\omega^4} h_x^2, & \lim_{h \rightarrow 0} \frac{1}{k^5} k_{yy} = \frac{3g^2}{4\omega^4} h_y^2.
 \end{array}$$

As a consequence, we have

$$\lim_{h \rightarrow 0} T_1 = 2, \quad \lim_{h \rightarrow 0} T_2 = 1 \quad (\text{C.0.1})$$

$$\lim_{h \rightarrow 0} \frac{C_1}{k} = \frac{1}{2}, \quad \lim_{h \rightarrow 0} C_2 h = -1 \quad (\text{C.0.2})$$

$$\lim_{h \rightarrow 0} C_5 = 2, \quad \lim_{h \rightarrow 0} C_6 = -\frac{8\omega^2}{3g}. \quad (\text{C.0.3})$$

Then we can find

$$\begin{aligned} \lim_{h \rightarrow 0} G_x &= gh_x|_{\Gamma_i}, & \lim_{h \rightarrow 0} G_y &= gh_y|_{\Gamma_i}, \\ \lim_{h \rightarrow 0} G_{\mathbf{n}} &= gh_{\mathbf{n}}|_{\Gamma_i}, & \lim_{h \rightarrow 0} \nabla^2 G &= (g\nabla^2 h - \frac{4\omega^2}{3}|\nabla h|^2)|_{\Gamma_i}. \end{aligned}$$

## Appendix D

### Particular solutions used in DRBEM

Consider the following Helmholtz equation

$$\nabla^2 u + k^2 u = f(x, y, t, u, u_x, u_y), \quad (x, y) \in \Omega. \quad (\text{D.0.1})$$

If DRBEM is used to solve (D.0.1) with the right-hand side approximated by a series of RBFs with the form

$$f = \sum_{j=0}^s \alpha_j r^j, \quad (\text{D.0.2})$$

then a particular solution of the equation

$$\frac{d^2 \hat{u}_j}{dr^2} + \frac{1}{r} \frac{d\hat{u}_j}{dr} + k^2 \hat{u}_j = r^j \quad (\text{D.0.3})$$

is needed for  $j = 0, 1, \dots, s$ , where  $r$  is the distance between a source point  $\mathbf{x}$  and a field point  $\xi$  in DRBEM.

It is easy to see that  $\hat{u}_0(r) = 1/k^2$ . If  $j \geq 1$ , according to Zhu (1993b),  $\hat{u}_j$  is given by

$$\hat{u}_j(r) = -\frac{\pi}{2} J_0(kr) \int_0^r t^{j+1} Y_0(kt) dt + \frac{\pi}{2} Y_0(kr) \int_0^r t^{j+1} J_0(kt) dt, \quad (\text{D.0.4})$$

where  $J_0(kr)$  and  $Y_0(kr)$  are the Bessel functions of the first and second kinds of zeroth order, respectively. The first integral in (D.0.4) can be evaluated by using a recursion formula

$$I_{j+1}(Y_0(kr)) = \int_0^r t^{j+1} Y_0(kt) dt = \frac{r^j}{k} \left[ r Y_1(kr) + \frac{j}{k} Y_0(kr) \right] - \frac{j^2}{k^2} I_{j-1}(Y_0(kr)), \quad (\text{D.0.5})$$

where

$$I_1(Y_0(kr)) = \frac{r}{k} Y_1(kr), \quad (\text{D.0.6})$$

and

$$I_0(Y_0(kr)) = r \left\{ Y_0(kr) + \frac{\pi}{2} \left[ \hat{H}_0(kr) Y_1(kr) - \hat{H}_1(kr) Y_0(kr) \right] \right\}, \quad (\text{D.0.7})$$

with  $\hat{H}_0$  and  $\hat{H}_1$  being the Struve's functions (Abramowitz & Stegun, 1965) of zeroth and first order, respectively. The evaluation of the second integral  $I_{j+1}(J_0(kr))$  in (D.0.4) is similar.

Further, by differentiating  $\hat{u}_j(r)$  with respect to the boundary normal  $\mathbf{n}$ , we have

$$\frac{\partial \hat{u}_j(r)}{\partial \mathbf{n}} = \frac{\partial \hat{u}_j(r)}{\partial r} \frac{\partial r}{\partial \mathbf{n}}, \quad (\text{D.0.8})$$

where

$$\frac{\partial \hat{u}_0(r)}{\partial r} = 0, \quad (\text{D.0.9})$$

$$\frac{\partial \hat{u}_j(r)}{\partial r} = \frac{\pi}{2} k J_1(kr) I_{j+1}(Y_0(kr)) - \frac{\pi}{2} k Y_1(kr) I_{j+1}(J_0(kr)). \quad (\text{D.0.10})$$



# Appendix E

## Publications of the author

1. H.-W. Liu, The space  $\tilde{S}_2^1 \left( \Delta_{mn}^{(2)} \right)$  of bivariate periodic spline functions (in Chinese), *Numerical Mathematics A Journal of Chinese Universities* **12**(1990), 335-341. **Math Review:** 92a: 41007.
2. H.-W. Liu, Double-periodic spline space  $\tilde{S}_2^1 \left( \Delta_{mn}^{(2)} \right)$  (in Chinese), *Journal of Xiangan University* **12**(1990), 19-26. **Math Review:** 92d: 65024.
3. H.-W. Liu, Interpolation and approximation by double periodic quadratic splines (in Chinese), *Math Numer. Sinica* **14**(1992), 152-156.
4. H.-W. Liu, The double periodic spline space  $\tilde{S}_k^1 \left( \Delta_{mn}^{(1)} \right)$  with degree  $k \geq 4$  on type-1 triangulation, *CALCOLO* **29**(1992), 269-289. **Math Review:** 95c:65014.
5. H.-W. Liu, Point-evaluation interpolation and approximation by double periodic quadratic splines (in Chinese), *Numerical Mathematics A Journal of Chinese Universities* **15**(1993), 195-206. **Math Review:** Author Index-1995, 797.

6. H.-W. Liu, An integral representation of bivariate splines and the dimension of quadratic spline spaces over stratified triangulation (in Chinese), *Acta Mathematica Sinica* **37**(1994), 534-543. **Math Review:** Author Index-1996, 861.
  
7. H.-W. Liu, A note on the recurrence relations of multivariate truncated powers and box splines, *Numerical Mathematics A Journal of Chinese Universities*(English series) **3**(1994), 10-17. **Math Review:** 95f: 65028.
  
8. H.-W. Liu, An identity of quadratic spline function in space  $\tilde{S}_2^1 \left( \bar{\Delta}_{mn}^{(2)} \right)$  (in Chinese), *Journal of Guangxi University for Nationalities* **1**(1995), 25-29.
  
9. H.Y. Yu, S. Shu and H.-W. Liu, The monotonicity of partial sum sequence on harmonic series (in Chinese), *Journal of Guangxi University for Nationalities* **1**(1995), 46-49.
  
10. H.-W. Liu and S. Shu, Double periodic quadratic spline space  $\tilde{S}_2^1 \left( \bar{\Delta}_{mn}^{(2)} \right)$  over the irregular type-2 triangulation (in Chinese), *Guangxi Sciences* **3**(1996), 8-11.
  
11. H.-W. Liu, The dimension of cubic spline space over stratified triangulation, *Journal of Mathematical Research and Exposition* **16**(1996), 199-208. **Math Review:** 97c: 65029.
  
12. H.-W. Liu and D.-X. He, A bivariate  $C^1$  B-spline finite element for rectangular

plate bending problems (in Chinese), *Journal of Guangxi University for Nationalities* **3**(1997), 77-86.

13. D. Hong and H.-W. Liu and Ram Mohapatra, Optimal triangulations and smoothness conditions for bivariate splines, in *Approximation theory IX, Vol. 2: Computational Aspects* (eds. C.K. Chui, L.L. Schumaker), (Vanderbilt University Press, Nashville, 1998) 129-136. **Math Review:** 00k: 41002.

14. S.-P. Zhu and H.-W. Liu, On the application of the multiquadric bases in conjunction with the LTDRM method to solve nonlinear diffusion equations, *Applied Mathematics and Computation* **96**(1998), 161-175. **Math Review.**

15. S.-P. Zhu, H.-W. Liu and X.-P. Lu, A combination of LTDRM and ATPS in solving linear diffusion problems, *Engineering Analysis with Boundary Elements* **21**(1998), 285-289.

16. H.-W. Liu and D. Hong, Some smoothness conditions and conformality conditions for bivariate quartic and quintic splines, *CALCOLO* **36**(1999), 43-61.

17. D. Hong and H.-W. Liu, Some new formulation of smoothness conditions and conformality conditions for bivariate cubic splines, *Computers and Mathematics with Application* **40**(2000), 117-125.

18. H.-W. Liu, An expansion of bivariate spline functions, *Journal of the Australian*

*Mathematical Society, Ser. B* **41** (2000), 527-541.

19. S.-P. Zhu, H.-W. Liu and K. Chen, A general DRBEM model for wave refraction and diffraction, *Engineering Analysis with Boundary Elements* **24**(2000), 377-390.

20. S.-P. Zhu, H.-W. Liu and T.R. Marchant, An efficient numerical model for diffraction and refraction of weakly nonlinear waves, in: *Proceeding of the Fourteenth Engineering Mechanics Conference of the American Society of Civil Engineers*(CDROM EM2000), SPZHU.PDF, Austin, Texas, 2000.

21. H.-W. Liu, W.-J. Huang and D.-Q. Cao, Some bivariate  $C^1$  spline finite elements, in: *Proc. of the 7th Int. Conf. on Computer Aided Design and Computer Graphics, Vol.1*, August 22-24, 2001, Kunming, China, p116.

22. H.-W. Liu and D. Hong, The bivariate  $C^1$  cubic spline space over even stratified triangulations, *Journal of Computational Analysis and Applications* **4**(2002), xx-xx.

23. H.-W. Liu and S.-P. Zhu, Dual reciprocity boundary element method for magnetohydrodynamic channel flows, *Journal of the Australian Mathematical Society, Ser. B* **43**(2002), xx-xx.

24. H.-W. Liu and Y.-Z. Huang, A kind of Lagrange interpolation by bivariate spline space with boundary conditions  $S_2^{1,1}(\bar{\Delta}_{mn}^{(2)})$ , *Guangxi Science*, to appear.

25. H.-W. Liu, S.-P. Zhu and T.R. Marchant, The PDRBEM model for weakly nonlinear wave runups around islands, *Journal of Fluid Mechanics*, accepted in principle.

# Bibliography

Abbott, M.B., Petersen, H.M. & Skovgaard, O. 1978 On the numerical modelling of short waves in shallow water. *J. Hydraulic Research* **16**, 173-204.

Abbott, M.B., McCowan, A.D. & Warren, I.R. 1984 Accuracy of short-wave numerical models. *J. Hydraulic Eng.* **110**, 1287-1301.

Abramowitz, M. & Stegun, I. 1965 *Handbook of Mathematical Functions. With formulas, graphs, and mathematical tables.* Dover Publ., New York.

Allesandri, C.A. & Tralli, A. 1991 A spline based approach for avoiding domain integrations in the BEM. *Computers and Structures* **41**, 859-868.

Au, M.C. & Brebbia, C.A. 1983 Diffraction of water waves for vertical cylinders using boundary elements. *Appl. Math. Modelling* **7**, 106-114.

Bascom, W. 1964 *Waves and beaches: the dynamics of the ocean surface.* Garden City, NY: Doubleday & Co., Inc.

- Beji, S. & Nadaoka, K. 1997 A time-dependent nonlinear mild-slope equation for water waves, *Proc. R. Soc. Lond. A* **453**, 319-332.
- Bettess, P. & Zienkiewicz, O.C. 1977 Diffraction and refraction of surface waves using finite and infinite elements. *Int. J. Numer. Methods in Engng.* **2**, 1271.
- Berkhoff, J.C.W. 1972 Computation of combined refraction-diffraction, *13th Int. Conf. Coastal Engineering*, Vancouver, pp. 471-490.
- Berkhoff, J.C.W. 1976 Mathematical models for simple harmonic linear water waves, wave diffraction and refraction, Delft Hydraulic Laboratory, Pub. No.163.
- Booij, N. 1981 *Gravity waves on water with non-uniform depth and current*, Doctoral thesis, Technical University of Delft, The Netherlands.
- Booij, N. 1983 A note on the accuracy of the mild-slope equation, *Coastal Engineering* **7**, 191-203.
- Boussinesq, J. 1872 Theorie des ondes et des remous qui se propagent le long d'un canal rectangulaire horizontal, en communiquant au liquide contenu dans ce canal des vitesses sensiblement pareilles de la surface au fond. *Journal de Mathematique pures et Appliquees, deuxieme serie* **17**, 55-108.

Bridges, T.R. & Wrobel, L.C. 1996 A dual reciprocity formulation for elasticity problems with body forces using augmented thin plate splines, *Communications in Numerical Methods in Engineering* **12**, 209-220.

Chakrabarti, S.K. & Tam, W.A. 1975 Wave height distribution around vertical cylinder. *J. WatWay, Harbors Coastal Eng. Div. ASCE* **101**, 225-230.

Chamberlain, P.G. & Porter, D. 1995 The modified mild-slope equation, *J. Fluid Mech.* **291**, 393-407.

Chen, C.S. & Rashed, Y.F. 1998 Evaluation of thin plate spline based particular solutions for Helmholtz-type operators for the DRM, *Mechanics Research Communications* **25**, 195-201.

Chen, H.S. & Mei, C.C. 1974 Oscillations and wave forces in a man-made harbor in the open sea, TR No. 190. Ralph M. Parsons Laboratory, Dept. Civil Engng., MIT.

Dingemans, M.W. 1997 *Water Wave Propagation over Uneven Bottoms, Part 2 - Non-linear Wave Propagation*. World Scientific.

Duchon, J. 1977 Spline minimizing rotation-invariant seminorms in Sobolev space, in *Constructive Theory of Functions of Several Variables*, Lecture Notes in Mathematics, Vol. **571**, Springer-Verlag, Berlin.



Eckart, C. 1952 The propagation of gravity waves from deep to shallow water. *National Bureau of Standards*, Circular **20**, 165-173.

Engquist, E. & Majda, A. 1977 Absorbing boundary conditions for the numerical simulation of waves. *Math. Comp.* **31**, 629-651.

Givoli, D. 1991 Non-reflecting boundary conditions. *Journal of Computational Physics* **94**, 1-29.

Golberg, M.A. 1978 *Solution Methods for Integral Equations: Theory and Applications*, Plenum Press, New York.

Golberg, M.A. 1994 The method of fundamental solutions for Poisson's equation, in *Betech IX*, Computational Mechanics Publications, Southampton.

Golberg, M.A. 1995 The numerical evaluation of particular solutions in the DRM - a review, *Boundary Element Communications* **6**, 99-106.

Golberg, M.A. & Chen C.S. 1997 *Discrete projection methods for integral equations*. Computational Mechanics Publications, Southampton.

Golberg, M.A., Chen C.S. & Karur, S. 1996 Improved multiquadric approximation for partial differential equations, *Engineering Analysis with*

*Boundary Elements* 18, 9-17.

González, F.I. 1999 Tsunamii, *Scientific American*, May issue.

Halpern L. & Trefethen, L.N. 1988 Wide-angle one-way wave equations. *J. Acoust Soc. Amer.* 84, 1397-1404.

Homma, S. 1950 On the behaviour of seismic sea waves around circular island. *Geophysical Magazine* 21, 199-208.

Houston, J.R. 1981 Combined refraction and diffraction of short waves using the finite element method. *Applied Ocean Research* 3, 163-170.

Hwang, L.-S. & Tuck, E. O. 1970 On the oscillations of harbours of arbitrary shape. *J. Fluid Mech.* 42, 447-464.

Itagaki, M. & Brebbia, C.A. 1993 Generation of higher order fundamental solutions to the two-dimensional modified Helmholtz equation, *Engineering Analysis with Boundary Elements* 11, 87-90.

Jonsson, I.G. 1979 The general wave equation and the refraction approximation. *ISVA, Techn. Univ. of Denmark, Progress Report* 49, 11-20.

- Jonsson, I.G. 1981 Booij's current-wave equation and the ray approximation. *ISVA, Techn. Univ. of Denmark, Progress Report* **54**, 7-20.
- Jonsson, I.G. & Skovgaard, O. 1979 A mild slope equation and its application to tsunami calculations. *Marine Geodesy* **2**, 41-58.
- Jonsson, I.G., Skovgaard, O. & Brink-Kjaer, O. 1976 Diffraction and refraction calculations for waves incident on an island. *Journal of Marine Research* **34**, 469-496.
- Kirby, J.T. 1984 Surface wave-current interaction over slowly varying topography. *J. Geophys. Res.* **89**, 745-747.
- Kriebel, D.L. 1990 Nonlinear wave interaction with a vertical circular cylinder, part I: diffraction theory. *Ocean Engineering* **17**, 345-377.
- Kriebel, D.L. 1992a Nonlinear wave interaction with a vertical circular cylinder, part II: wave runup. *Ocean Engineering* **19**, 75-99.
- Kriebel, D.L. 1992b Nonlinear wave runup on large circular cylinders. *Proceedings Civil Engineering in the Oceans Conference*, College Station, Texas, pp.173-187.

Laird, A.D.K. 1955 A model study of wave action on a cylindrical island. *Trans. Am. Geophys. Union* **36**, 279-285.

Lautenbacher, C.C. 1970 Gravity wave refraction by islands. *J. Fluid Mech.* **41**, 655-672.

Liu, H.-W., Zhu, S.-P. & Marchant, T.R. 2000 A perturbation DRBEM model for weakly nonlinear wave run-ups around islands, submitted.

Liu, P.L.-F., Cho, Y.-S., Briggs, M.J., Kanoglu, U. & Synolakis, C.E. 1995 Runup of solitary waves on a circular island. *J. Fluid Mech.* **302**, 259-285.

Liu, P.L.-F., Cho, Y.-S. & Fujima, K.J. 1994 Numerical solutions of three-dimensional run-up on a circular island. *Int. Symposium: Waves-Physical and Numerical Modelling*, University of British Columbia, Vancouver, Canada, pp.1031-1040.

Lozano, C. & Meyer, R.E. 1976 Leakage and response of wave trapped by round islands. *Physics of Fluids* **19**, 1075-1088.

MacCamy, R.C. & Fuchs, R.A. 1954 Wave forces on piles: a diffraction theory. *US Army Corps of Engineering, Beach Erosion Board*, Washington, DC, Tech. Mem. 69.

Madsen, P.A. & Warren, I.R. 1984 Performance of a numerical short-wave model. *Coastal Engng.* **8**, 73-93.

Madsen, P.A. & Sørensen, O.R. 1992 A new form of the Boussinesq equations with improved linear dispersion characteristics, Part 2: A slowly-varying bathymetry. *Coastal Engng.* **18**, 182-204.

Massel, S.A. 1993 Extension of mild-slope model for surface waves, *Coastal Engineering* **19**, 97-126.

Mei, C.C., 1989 *The Applied Dynamics of Ocean Surface Waves*, World Scientific, Singapore, pp. 62-66.

Mei, C.C. & LeMehaute, B. 1966 Note on the equations of long waves over an uneven bottom. *J. of Geophys. Res.* **71** 393-400.

Micchelli, C.A. 1986 Interpolation of scattered data: distance matrices and conditionally positive definite functions. *Construct. Approx.* **2**, 11-22.

Muleshkov, A.S., Golberg, M.A. & Chen, C.S. 1999 Particular solutions of Helmholtz-type operators using higher order polyharmonic splines. *Computational Mechanics* **23**, 411-419.

Nagai, S. 1973 Wave forces on structures. In *Advances in Hydroscience*,

Vol. 9 (ed. V.T. Chow), pp. 253-324. Academic Press.

Nardini, D. & Brebbia, C.A. 1982 A new approach to free vibration analysis using boundary elements. In *Boundary Element Methods in Engineering*(ed. C.A. Brebbia), Springer-Verlag.

Neves, A.C. & Brebbia, C.A. 1991 The multiple reciprocity boundary element method in elasticity: A new approach for transforming domain integrals to the boundary. *Int. J. Numer. Methods. Engng.* **31**, 709-727.

Nowak, A.J. & Brebbia, C.A. 1989 The multiple-reciprocity method. A new approach for transforming B.E.M. Domain integrals to the boundary, *Engineering Analysis with Boundary Elements* **6**, 164-168.

Nowak, A.J. & Brebbia, C.A. 1989 Solving Helmholtz equation by multiple reciprocity method, in *Computer and Experiments in Fluid flow* (eds. G.M. Carlomagno and C.A. Brebbia), Computational Mechanics Publication, Southampton, U.K.

Nowak, A.J. & Neves, A. C. 1994 *The Multiple reciprocity boundary element method*. Computational Mechanics Publications, Southampton, U.K.

Nwogu, O. 1993 An alternative form of the Boussinesq equation for nearshore wave propagation. *J. WatWay, Port, Coastal Ocean Engng.* **119**, 618-638.

Partridge, P.W. & Brebbia, C.A. 1989 Computer implementation of the BEM dual reciprocity method for the solution of Poisson type equations. *Software for Engineering Workstations* 5, 199-206.

Partridge, P.W. & Brebbia, C.A. & Wrobel, L. C. 1992 *The dual reciprocity boundary element method*. Computational Mechanics Publications, Southampton, U.K.; Boston and Elsevier Applied Science, London; New York.

Peregrine, D.H. 1967 Long waves on a beach. *J. Fluid Mech.* 27, 815-827.

Porter, D. & Staziker, D.J. 1995 Extensions of the mild-slope equation, *J. Fluid Mech.* 300, 367-382.

Poulin, S. 1997 *A Boundary Element Model for Diffraction of Water Waves on Varying Water Depth*, Doctoral thesis, Technical University of Denmark.

Powell, M.J.D. 1993 The uniform convergence of thin plate splines in two dimensions, in *Univ. of Cambridge Numer. Anal. Report DAMTP 1993/NA 16*.

Power, H. & Wrobel, L.C. 1995 *Boundary Integral Methods in Fluid Mechanics*, Computational Mechanics Publications, Southampton, UK.

- Provis, D.G. 1975 Propagation of water waves near an island. PhD Thesis, University of Essex.
- Rahman, H. & Heaps, H.S. 1983 Wave forces on offshore structures: non-linear diffraction by large cylinders. *J. Phys. Oceanogr.* **13**, 2225-2235.
- Raman, H. & Venkatanarasaiah, P. 1976 Forces due to nonlinear waves on vertical cylinders of large diameter. In *Mitteilungen*, Leichtweiss-Institut für Wasserbau, Technical University of Braunschweig, Vol. **51**, pp. 101-136.
- Rangogni, R. 1988 A simple procedure to solve the mild-slope equation using BEM and perturbation technique. *X International Conference on Boundary Element Methods*, Southampton, U.K., 331-343.
- Rygg O. 1988 Nonlinear refraction-diffraction of surface waves in intermediate and shallow water. *Coastal Engng.* **12**, 191-211.
- Smith, R. & Sprinks, T. 1975 Scattering of surface waves by a conical island. *J. Fluid Mech.* **72**, 373.
- Sommerfeld, A. 1949 *Partial Differential Equations in Physics*. Academic Press.



- Sprinks, T. & Smith, R. 1983 Scale effects in a wave-refraction experiment. *J. Fluid Mech.* **129**, 455-471.
- Svendsen, I.A. 1967 The wave equation for gravity waves in water of gradually varying depth. *ISVA, Techn. Univ. of Denmark, Basic Research Progress Report* **15**, 2-7.
- Tsay, T.-K. & Liu, P.L.-F. 1983 A finite element model for wave refraction and diffraction. *Applied Ocean Research* **5**, 30-37.
- Vastano, A.C. & Reid, R.O. 1967 Tsunami response for islands: verification of a numerical procedure, *J. Marine Research* **25**, 129-139.
- Watson, G.N. 1962 *Theory of bessel functions*, Cambridge University Press, Cambridge.
- Wei, G. & Kirby, J. T. 1995 Time-dependent numerical code for extended boussinesq equations. *J. WatWay, Port, Coastal Ocean Engng.* **121**, 251-261.
- Witting, J.M. 1984 A unified model for the evolution of nonlinear water waves. *J. Comput. Phys.* **56**, 203-236.
- Zhang, Y.L. & Zhu, S.-P. 1994a New solutions for the propagation of long water waves over variable depth. *J. Fluid Mech.* **278**, 391-406.

- Zhang, Y.L. & Zhu, S.-P. 1994b On the choice of interpolation functions used in the dual-reciprocity boundary-element method. *Engineering Analysis with Boundary Elements* **13**, 387-396.
- Zhu, S.-P. 1993a A new DRBEM model for wave refraction and diffraction. *Engineering Analysis with Boundary Elements* **12**, 261-274.
- Zhu, S.-P. 1993b, Particular solutions associated with the Helmholtz operator used in DRBEM. *Boundary Elements Abstracts* **4**, 231-233.
- Zhu, S.-P. & Liu, H.-W. 1998 On the application of the multiquadric bases in conjunction with the LTDRM method to solve nonlinear diffusion equations, *Applied Mathematics and Computation* **96**, 161-175.
- Zhu, S.-P., Liu, H.-W. & Chen, K. 2000 A general DRBEM model for wave refraction and diffraction. *Engineering Analysis with Boundary Elements* **24**, 377-390.
- Zhu, S.-P., Liu, H.-W. & Lu, X.-P. 1998 A combination of the LTDRM and the ATPS in solving linear diffusion problems, *Engineering Analysis with Boundary Elements* **21**, 285-289.
- Zhu, S.-P. & Moule, G. 1994 Numerical Calculation of Forces Induced by

Short-Crested Waves on a Vertical Cylinder of Arbitrary Cross-sections, *Ocean Engineering* **21**, 645-662.

Zhu, S.-P. & Zhang, Y.L. 1995 Scattering of long waves around a circular Island mounted on a conical shoal. *Wave Motion* **23**, 353-362.